Physics potentials with the second Hyper-Kamiokande detector in Korea

The Hyper-Kamiokande Proto-Collaboration

K. Abe[1,2], Ke. Abe[3], S. H. Ahn[†,4], H. Aihara[2,5], A. Aimi[6], R. Akutsu[7], C. Andreopoulos[8,9], I. Anghel[10], L. H. V. Anthony[8], M. Antonova[11], Y. Ashida[12], V. Aushev[13], M. Barbi[14], G. J. Barker[15], G. Barr[16], P. Beltrame[17], V. Berardi[18], M. Bergevin[19], S. Berkman[20], L. Berns[21], T. Berry[22], S. Bhadra[23], F. d. M. Blaszczyk[24], A. Blondel[25], S. Bolognesi[26], S. B. Boyd[15], A. Bravar[25], C. Bronner[2], M. Buizza Avanzini[27], F. S. Cafagna[18], R. Calland[2], S. Cao[28], S. L. Cartwright[29], M. G. Catanesi[18], C. Checchia[6], Z. Chen-Wishart[22], B. G. Cheon[†,30], M. K. Cheoun[†,31], K. Cho[†,32], J. H. Choi[33], K. Choi[34], K. Y. Choi[†,35], E. J. Chun[†,36], A. Cole[29], J. Coleman[8], G. Collazuol[6], G. Cowan[17], L. Cremonesi[37], T. Dealtry[38], G. De Rosa[39], C. Densham[9], D. Dewhurst[16], E. Drakopoulou[17], F. Di Lodovico[37], O. Drapier[27], J. Dumarchez[40], P. Dunne[41], M. Dziewiecki[42], S. Emery[26], A. Esmaili[43], A. Evangelisti[39], E. Fernández-Martinez[44,79], T. Feusels[20], A. Finch[38], G. A. Fiorentini[23], G. Fiorillo[39], M. Fitton[9], K. Frankiewicz[45], M. Friend[28], Y. Fujii[28], Y. Fukuda[46], D. Fukuda[47], K. Ganezer[48], M. Ghosh[†,49], C. Giganti[40], M. Gonin[27], N. Grant[15], P. Gumplinger[50], D. R. Hadley[15], B. Hartfiel[48], M. Hartz[2,50], Y. Hayato[1,2], K. Hayrapetyan[37], J. Hill[48], S. Hirota[12], S. Horiuchi[51], A. K. Ichikawa[12], T. Iijima[52,53], M. Ikeda[1], J. Imber[27], K. Inoue[54,2], J. Insler[55], R. A. Intonti[18], A. Ioannisian[56], T. Ishida[28], H. Ishino[47], M. Ishitsuka[57], Y. Itow[53,58], K. Iwamoto[5], A. Izmaylov[11], B. Jamieson[59], H. I. Jang[60], J. S. Jang[61], S. H. Jeon[35], K. S. Jeong[†,62], M. Jiang[12], P. Jonsson[41], K. K. Joo[63], A. Kaboth[9,22], C. Kachulis[24], T. Kajita[7,2], S. K. Kang[†,64], J. Kameda[1,2], Y. Kataoka[5], T. Katori[37], K. Kayrapetyan[37], E. Kearns[24,2], M. Khabibullin[11], A. Khotjantsev[11], C. S. Kim[†,65], H. B. Kim[†,30], H. J. Kim[†,66], J. H. Kim[35], J.-S. Kim[†,4], J. Y. Kim[63], S. B. Kim[67], S. C. Kim[†,4,68], S.-W. Kim[†,4,68], S. Y. Kim[67], T. J. Kim[†,30], W. Kim[†,66], S. King[37], Y. Kishimoto[1,2], P. Ko[†,36], T. Kobayashi[28], M. Koga[54,2], A. Konaka[50], L. L. Kormos[38], Y. Koshio[47,2], A. Korzenev[25], K. L. Kowalik[45], W. R. Kropp[69], Y. Kudenko[11,70,71], R. Kurjata[42], T. Kutter[55], M. Kuze[21], K. Kwak[†,72], E. H. Kwon[†,67], L. Labarga[44], J. Lagoda[45], P. J. J. Lasorak[37], M. Laveder[6], M. Lawe[38], J. G. Learned[34], C. H. Lee[†,62], S. J. Lee[†,73], W. J. Lee[†,67], I. T. Lim[63], T. Lindner[50], R. P. Litchfield[41], A. Longhin[6], P. Loverre[74], T. Lou[5], L. Ludovici[74], W. Ma[41], L. Magaletti[18], K. Mahn[75], M. Malek[29], L. Maret[25], C. Mariani[51], K. Martens[2], Ll. Marti[1], J. F. Martin[76], J. Marzec[42], S. Matsuno[34], E. Mazzucato[26], M. McCarthy[23], N. McCauley[8], K. S. McFarland[77], C. McGrew[78], A. Mefodiev[11], P. Mermod[25], C. Metelko[8], M. Mezzetto[6], J. Migenda[29], P. Mijakowski[45], H. Minakata[7,79], A. Minamino[80], S. Mine[69], O. Mineev[11], A. Mitra[15], M. Miura[1,2], T. Mochizuki[1], J. Monroe[22], C. S. Moon[†,66], D. H. Moon[63], S. Moriyama[1,2], T. Mueller[27], F. Muheim[17], K. Murase[81], F. Muto[52], M. Nakahata[1,2], Y. Nakajima[1], K. Nakamura[28,2], T. Nakaya[12,2], S. Nakayama[1,2], C. Nantais[76], M. Needham[17], T. Nicholls[9], Y. Nishimura[7], E. Noah[25], F. Nova[9], J. Nowak[38], H. Nunokawa[43], Y. Obayashi[2], Y. D. Oh[†,66], Y. Oh[†,66], H. M. O'Keeffe[38], Y. Okajima[21], K. Okumura[7,2], Yu. Onishchuk[13], E. O'Sullivan[82], L. O'Sullivan[29], T. Ovsiannikova[11], R. A. Owen[37], Y. Oyama[28], J. Pérez[44], M. Y. Pac[33], V. Palladino[39], J. L. Palomino[78], V. Paolone[83], H. S. Park[†,4], J. C. Park[†,84], M. G. Park[†,85], S. C. Park[†,65], W. Parker[22], S. Parsa[25], D. Payne[8], J. D. Perkin[29], C. Pidcott[29],

†Author as part of the Korean Neutrino Observatory (KNO) interest group.

E. Pinzon Guerra[23], S. Playfer[17], B. Popov[40], M. Posiadala-Zezula[86], J.-M. Poutissou[50],
A. Pritchard[8], N. W. Prouse[37], G. Pronost[1], P. Przewlocki[45], B. Quilain[12], M. Quinto[18],
E. Radicioni[18], P. N. Ratoff[38], F. Retiere[50], C. Riccio[39], B. Richards[37], E. Rondio[45], H. J. Rose[8],
C. Rott[35], S. D. Rountree[51], A. C. Ruggeri[39], A. Rychter[42], D. Ryu[†,72], R. Sacco[37], M. Sakuda[47],
M. C. Sanchez[10], E. Scantamburlo[25], M. Scott[50], S. Molina Sedgwick[37], Y. Seiya[87], T. Sekiguchi[28],
H. Sekiya[1,2], H. Seo[†,67], S. H. Seo[*,67], D. Sgalaberna[25], R. Shah[16], A. Shaikhiev[11], I. Shimizu[54],
M. Shiozawa[1,2], Y. Shitov[41,22], S. Short[37], C. Simpson[16,2], G. Sinnis[88], M. B. Smy[69,2],
S. Snow[15], J. Sobczyk[89], H. W. Sobel[69,2], D. C. Son[†,66], Y. Sonoda[1], R. Spina[18], T. Stewart[9],
J. L. Stone[24,2], Y. Suda[5], Y. Suwa[90], Y. Suzuki[2], A. T. Suzuki[3], R. Svoboda[19], M. Taani[17,52],
R. Tacik[14], A. Takeda[1], A. Takenaka[1], A. Taketa[91], Y. Takeuchi[3,2], V. Takhistov[69], H. A. Tanaka[76],
H. K. M. Tanaka[91], H. Tanaka[1,2], R. Terri[37], M. Thiesse[29], L. F. Thompson[29], M. Thorpe[9],
S. Tobayama[20], C. Touramanis[8], T. Towstego[76], T. Tsukamoto[28], K. M. Tsui[7], M. Tzanov[55],
Y. Uchida[41], M. R. Vagins[69,2], G. Vasseur[26], C. Vilela[78], R. B. Vogelaar[51], J. Walding[22], J. Walker[59],
M. Ward[9], D. Wark[16,9], M. O. Wascko[41], A. Weber[9], R. Wendell[12,2], R. J. Wilkes[92], M. J. Wilking[78],
J. R. Wilson[37], E. Won[†,73], T. Xin[10], K. Yamamoto[87], C. Yanagisawa[78], T. Yano[3], O. Yasuda[†,49],
S. Yen[50], N. Yershov[11], D. N. Yeum[67], M. Yokoyama[2,5], H. D. Yoo[†,67], J. Yoo[†,93], S. C. Yoon[†,67],
T. S. Yoon[†,85], T. Yoshida[21], I. Yu[35], M. Yu[23], J. Zalipska[45], K. Zaremba[42], M. Ziembicki[42], M. Zito[26]
and S. Zsoldos[37]

[1]*University of Tokyo, Institute for Cosmic Ray Research, Kamioka Observatory, Kamioka, Japan*
[2]*University of Tokyo, Kavli Institute for the Physics and Mathematics of the Universe (WPI), Todai Institutes
for Advanced Study, Kashiwa, Chiba, Japan*
[3]*Kobe University, Department of Physics, Kobe, Japan*
[4]*Korea Astronomy and Space Science Institute, Daejeon 34055, Korea*
[5]*University of Tokyo, Department of Physics, Tokyo, Japan*
[6]*INFN Sezione di Padova and Università di Padova, Dipartimento di Fisica, Padova, Italy*
[7]*University of Tokyo, Institute for Cosmic Ray Research, Research Center for Cosmic Neutrinos, Kashiwa,
Japan*
[8]*University of Liverpool, Department of Physics, Liverpool, United Kingdom*
[9]*STFC, Rutherford Appleton Laboratory, Harwell Oxford, and Daresbury Laboratory, Warrington, United
Kingdom*
[10]*Iowa State University, Department of Physics and Astronomy, Ames, Iowa, U.S.A.*
[11]*Institute for Nuclear Research of the Russian Academy of Sciences, Moscow, Russia*
[12]*Kyoto University, Department of Physics, Kyoto, Japan*
[13]*Kyiv National University, Department of Nuclear Physics, Kyiv, Ukraine*
[14]*University of Regina, Department of Physics, Regina, Saskatchewan, Canada*
[15]*University of Warwick, Department of Physics, Coventry, United Kingdom*
[16]*Oxford University, Department of Physics, Oxford, United Kingdom*
[17]*University of Edinburgh, School of Physics and Astronomy, Edinburgh, United Kingdom*
[18]*INFN Sezione di Bari and Università e Politecnico di Bari, Dipartimento Interuniversitario di Fisica, Bari,
Italy*
[19]*University of California, Davis, Department of Physics, Davis, California, U.S.A.*
[20]*University of British Columbia, Department of Physics and Astronomy, Vancouver, British Columbia, Canada*
[21]*Tokyo Institute of Technology, Department of Physics, Tokyo, Japan*
[22]*Royal Holloway University of London, Department of Physics, Egham, Surrey, United Kingdom*
[23]*York University, Department of Physics and Astronomy, Toronto, Ontario, Canada*
[24]*Boston University, Department of Physics, Boston, Massachusetts, U.S.A.*
[25]*University of Geneva, Section de Physique, DPNC, Geneva, Switzerland*
[26]*IRFU, CEA Saclay, Gif-sur-Yvette, France*
[27]*Ecole Polytechnique, IN2P3-CNRS, Laboratoire Leprince-Ringuet, Palaiseau, France*
[28]*High Energy Accelerator Research Organization (KEK), Tsukuba, Ibaraki, Japan*
[29]*University of Sheffield, Department of Physics and Astronomy, Sheffield, United Kingdom*
[30]*Hanyang University, Department of Physics, Seoul 04763, Korea*

[31]*Soongsil University, Origin of Matter and Evolution of Galaxy (OMEG) Institute and Department of Physics, Seoul 156-743, Korea*

[32]*Korea Institute of Science and Technology Information, Daejeon 34141, Korea*

[33]*Dongshin University, Department of Physics, Naju, Korea*

[34]*University of Hawaii, Department of Physics and Astronomy, Honolulu, Hawaii, U.S.A.*

[35]*Sungkyunkwan University, Department of Physics,Suwon 16419, Korea*

[36]*Korean Institute for Advanced Studies, Seoul, Korea*

[37]*Queen Mary University of London, School of Physics and Astronomy, London, United Kingdom*

[38]*Lancaster University, Physics Department, Lancaster, United Kingdom*

[39]*INFN Sezione di Napoli and Università di Napoli, Dipartimento di Fisica, Napoli, Italy*

[40]*Laboratoire de Physique Nucleaire et de Hautes Energies, UPMC and Universite Paris-Diderot and CNRS/IN2P3, Paris, France*

[41]*Imperial College London, Department of Physics, London, United Kingdom*

[42]*Warsaw University of Technology, Institute of Radioelectronics and Multimedia Technology, Warsaw, Poland*

[43]*Pontifícia Universidade Católica do Rio de Janeiro, Departamento de Física, Rio de Janeiro, Brazil*

[44]*University Autonoma Madrid, Department of Theoretical Physics, Madrid, Spain*

[45]*National Centre for Nuclear Research, Warsaw, Poland*

[46]*Miyagi University of Education, Department of Physics, Sendai, Japan*

[47]*Okayama University, Department of Physics, Okayama, Japan*

[48]*California State University, Department of Physics, Carson, California, U.S.A.*

[49]*Tokyo Metropolitan University, Department of Physics, Tokyo, Japan*

[50]*TRIUMF, Vancouver, British Columbia, Canada*

[51]*Virginia Tech, Center for Neutrino Physics, Blacksburg, Virginia, U.S.A.*

[52]*Nagoya University, Graduate School of Science, Nagoya, Japan*

[53]*Nagoya University, Kobayashi-Maskawa Institute for the Origin of Particles and the Universe, Nagoya, Japan*

[54]*Research Center for Neutrino Science, Tohoku University, Sendai, Japan*

[55]*Louisiana State University, Department of Physics and Astronomy, Baton Rouge, Louisiana, U.S.A.*

[56]*Yerevan Institute for Theoretical Physics and Modeling, Halabian Str. 34; Yerevan 0036, Armenia*

[57]*Tokyo University of Science, Department of Physics, Chiba, Japan*

[58]*Nagoya University, Solar-Terrestrial Environment Laboratory, Nagoya, Japan*

[59]*University of Winnipeg, Department of Physics, Winnipeg, Manitoba, Canada*

[60]*Seoyeong University, Department of Fire Safety, Gwangju, Korea*

[61]*GIST College, Gwangju Institute of Science and Technology, Gwangju 500-712, Korea*

[62]*Pusan National University, Department of Physics, Busan 46241, Korea*

[63]*Chonnam National University, Department of Physics, Gwangju, Korea*

[64]*Seoul National University of Science and Technology, School of Liberal Arts, Seoul 01811, Korea*

[65]*Yonsei University, Department of Physics and IPAP, Seoul 03722, Korea*

[66]*Kyungpook National University, Department of Physics, Daegu 41566, Korea*

[67]*Seoul National University, Department of Physics and Astronomy, Seoul 08826, Korea*

[68]*Korea University of Science and Technology, Daejeon 34113, Korea*

[69]*University of California, Irvine, Department of Physics and Astronomy, Irvine, California, U.S.A.*

[70]*National Research Nuclear University (MEPhI), Moscow, Russia*

[71]*Moscow Institute of Physics and Technology, Moscow region, Russia*

[72]*UNIST, Department of Physics, Ulsan, Korea*

[73]*Korea University, Department of Physics, Seoul 02841, Korea*

[74]*INFN Sezione di Roma, Roma, Italy*

[75]*Michigan State University, Department of Physics and Astronomy, East Lansing, Michigan, U.S.A.*

[76]*University of Toronto, Department of Physics, Toronto, Ontario, Canada*

[77]*University of Rochester, Department of Physics and Astronomy, Rochester, New York, U.S.A.*

[78]*State University of New York at Stony Brook, Department of Physics and Astronomy, Stony Brook, New York, U.S.A.*

[79]*Instituto de Física Teórica, UAM/CSIC, Madrid, Spain*

[80]*Yokohama National University, Faculty of Engineering, Yokohama, Japan*

[81]*Pennsylvania State University, Department of Physics, University Park, PA 16802, U.S.A.*

[82]*Stockholm University, Oskar Klein Centre and Department of Physics, Stockholm, Sweden*

[83]*University of Pittsburgh, Department of Physics and Astronomy, Pittsburgh, Pennsylvania, U.S.A.*

[84]*Chungnam National University, Department of Physics, Daejeon 34134, Korea*

[85]*Kyungpook National University, Department of Astronomy and Atmospheric Sciences, Daegu 41566, Korea*
[86]*University of Warsaw, Faculty of Physics, Warsaw, Poland*
[87]*Osaka City University, Department of Physics, Osaka, Japan*
[88]*Los Alamos National Laboratory, New Mexico, U.S.A.*
[89]*Wroclaw University, Faculty of Physics and Astronomy, Wroclaw, Poland*
[90]*Kyoto University, Yukawa Institute for Theoretical Physics, Kyoto, Japan*
[91]*University of Tokyo, Earthquake Research Institute, Tokyo, Japan*
[92]*University of Washington, Department of Physics, Seattle, Washington, U.S.A.*
[93]*Korea Advanced Institute of Science and Technology (KAIST), Department of Physics, Daejeon 34141, Korea*
*E-mail: sunny.seo@snu.ac.kr

....
Hyper-Kamiokande consists of two identical water-Cherenkov detectors of total 520 kt, with the first one in Japan at 295 km from the J-PARC neutrino beam with 2.5° off-axis angles (OAAs), and the second one possibly in Korea at a later stage. Having the second detector in Korea would benefit almost all areas of neutrino oscillation physics, mainly due to longer baselines. There are several candidate sites in Korea with baselines of 1000–1300 km and OAAs of 1°–3°.

We conducted sensitivity studies on neutrino oscillation physics for a second detector, either in Japan (JD × 2) or Korea (JD + KD), and compared the results with a single detector in Japan. Leptonic charge–parity (CP) symmetry violation sensitivity is improved, especially when the CP is non-maximally violated. The larger matter effect at Korean candidate sites significantly enhances sensitivities to non-standard interactions of neutrinos and mass ordering determination. Current studies indicate the best sensitivity is obtained at Mt. Bisul (1088 km baseline, 1.3° OAA). Thanks to a larger (1000 m) overburden than the first detector site, clear improvements to sensitivities for solar and supernova relic neutrino searches are expected.
....
Subject Index   C03, C04, C12, C32, C43

1. Introduction

The proposed Hyper-Kamiokande (Hyper-K or HK) experiment [1] builds upon the highly successful Super-Kamiokande (Super-K or SK) detector [2] by constructing two large water-Cherenkov detectors with 16.8 times the fiducial volume of SK to pursue a rich program of neutrino (astro)physics and proton decay. The Hyper-K design proposes the construction of two identical detectors in stages with 187 kt (fiducial mass) per detector. The first one will be constructed near the current Super-K site, 295 km away and 2.5° off-axis from the J-PARC neutrino beam used by the T2K experiment. The second one is currently under consideration to be built in Korea where the J-PARC neutrino beam is still reachable. The long-baseline neutrino program observing the J-PARC neutrino beam at Hyper-K aims for a definitive observation of CP violation (CPV) in neutrino oscillations, that may result from an irreducible phase δ_{CP} in the neutrino mixing matrix. Hyper-K will make precise measurements of δ_{CP} and other oscillation parameters, such as θ_{23} and Δm_{32}^2, and will have sufficient statistics to make "shape" tests of the three-flavor mixing paradigm. These measurements are valuable in elucidating the new physics responsible for neutrino mass and mixing and its potential connections to leptogenesis in the early universe.

Placing the second detector in Korea rather than in Japan will enhance physics sensitivities to almost all searches and measurements. In the case of proton decay it would not matter where the second detector is located since the improvement primarily depends on the detector mass. In other cases—particularly neutrino oscillation measurements using the J-PARC beam—the location of the detector is a significant factor in determining the expected benefits. In this document, we explore the possibility of placing the second detector in Korea at a baseline of 1000–1300 km; we will refer to
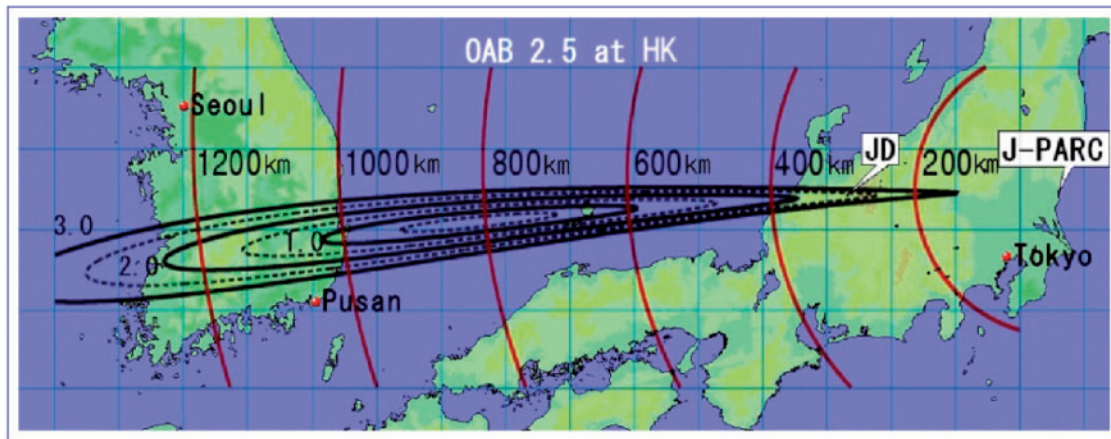
Fig. 1. Map showing the baseline and off-axis angle of the J-PARC beam in Japan and Korea [8,9].

this as T2HKK in contrast to one detector in Kamioka with 295 km baseline (T2HK). The second detector in Korea provides the opportunity for Hyper-K to probe oscillation physics at both the first and second oscillation maxima.

South Korea covers a range of angles from the axis of the J-PARC neutrino beam from 1° to 3° (see Fig. 1), which allows for tuning both the baseline and neutrino energy spectrum to maximize the physics reach of the combined two-baseline experiment. Such a configuration can improve neutrino oscillation physics sensitivities in Hyper-K in a number of ways: it can break degeneracies related to the unknown mass ordering, the mixing parameter θ_{23}, and the CP-violating phase δ_{CP}; it has better precision (especially on δ_{CP}) in important regions of the parameter space; and it can serve to mutually reduce the impact of systematic uncertainties (both known and unknown) across all measurements. It also provides an opportunity to test the preferred oscillation model in a regime not probed with existing experiments. Constraints on (or evidence of) exotic neutrino models, such as non-standard interactions with matter, are also expected to be significantly enhanced by the use of a longer baseline configuration for a second detector.

Although the use of a longer baseline in conjunction with the J-PARC beam is the primary feature distinguishing the use of a detector in Korea from a second detector at Kamioka, there are several mountains over 1 km in height that could provide suitable sites. This allows for greater overburden than the site selected for the first Hyper-K detector and would enhance the program of low-energy physics that are impacted by cosmic-ray backgrounds. This includes solar neutrinos, supernova relic neutrinos, dark matter neutrino detection studies, and neutrino geophysics. In the case of supernova neutrinos there is some benefit from the separation of detector locations.

Further enhancements are possible but not considered in this document. Recent developments in gadolinium doping of water and water-based liquid scintillators could allow for a program based on reactor neutrinos if these technologies are deployed in the detector.

There were earlier studies of a large water-Cherenkov detector in Korea using a J-PARC-based neutrino beam [3,4]. Originally, an idea for a two-baseline experiment with a second detector in Korea was discussed by several authors, pointing out possible improvements for measurements of CP violation and mass hierarchy [5–9]. Three international workshops were held in Korea and Japan in 2005, 2006, and 2007 [10]. At the time, the mixing angle of θ_{13} was not yet known, and therefore the required detector size and mass could not be determined. Now, more realistic studies and a detector design are possible due to the precisely measured value of θ_{13} [11–15,17–19].

2. The Hyper-Kamiokande experiment and the extension to Korea

In this section we present a summary of the proposed Hyper-Kamiokande experiment, with particular reference to the long-baseline neutrino oscillation physics program using the J-PARC neutrino beam. We then consider the simplest addition of an identical second detector in Korea to this configuration, focusing on practical considerations such as site selection. The physics case for a Korean detector and studies of the experiment's capability with different configurations are then considered.

2.1. J-PARC neutrino beam

The neutrino beam for Hyper-K is produced at J-PARC (Japan Proton Accelerator Research Complex), located in Tokai Village, Ibaraki prefecture on the east coast of Japan, which is 295 km from the Kamioka detector sites. The 30 GeV (kinetic energy) proton beam is extracted from the J-PARC main ring (MR) by single-turn fast extraction and transported to the production target after being deflected about 90° by 28 superconducting combined-function magnets to direct the beam toward Kamioka. The beam pulse consists of eight bunches spaced 581 ns apart to give a pulse of duration 4.2 μs. As of 2017, the repetition period of the pulses is 2.48 s. The production target is a graphite rod 26 mm in diameter and 90 cm long (corresponding to two interaction lengths). About 80% of the incoming protons interact in the target. The secondary pions (and kaons) from the target are focused by three consecutive electromagnetic horns operated by a 250 kA pulsed current. It is expected that by the time of Hyper-K, the horn currents will be increased to 320 kA. The focused pions and kaons enter a decay volume (DV) of length 96 m filled with helium gas, and decay in flight into neutrinos and charged leptons. The beam dump, which consists of graphite blocks of about 3.15 m thickness followed by iron plates of 2.5 m total thickness, is placed at the end of the DV to absorb remnant hadrons. Muon monitors (MUMONs) are placed just behind the beam dump to monitor on a spill-by-spill basis the intensity and the profile of muons with initial energy over 5 GeV which pass through the beam dump.

T2K adopted the first ever off-axis scheme to produce a narrow energy neutrino spectrum centered on the oscillation maximum to maximize the physics sensitivity. The J-PARC beam is aligned to provide a 2.5° degree off-axis beam to the Super-Kamiokande detector.

As of summer 2017, stable operation of the MR at 470 kW beam power has been achieved. The design power of the J-PARC main ring will be realized through the upgrade of the magnet power supplies, RF core, and other components. These upgrades will increase the repetition rate of the beam from 0.40 Hz to 0.77 Hz. Preparation for the upgrade has begun, and the upgrade may be completed as early as 2019. Further beam power increases will require upgrades to secondary beamline components such as the beam window, target, and horns. Upgrades primarily to the RF power supply will gradually increase the number of protons per pulse (ppp) and repetition rate further to 3.3×10^{14} p and 1/1.16 s, respectively, to reach > 1.3 MW by around 2025 before Hyper-K becomes operational.

2.2. Hyper-Kamiokande tank configuration

The Hyper-K experiment employs a ring-imaging water-Cherenkov detector technique to detect rare interactions of neutrinos and the possible spontaneous decay of protons and bound neutrons. The baseline configuration of the experiment consists of a single cylindrical tank built in the Tochibora mine at a baseline of 295 km from the J-PARC neutrino source.

A full overview of the cavern and detector design research and development, upgraded beam and near detector suite, and expected physics sensitivities can be found in the Hyper-Kamiokande Design Report [25]. A schematic view of the tank is shown in Fig. 2. The design is an upright cylindrical tank
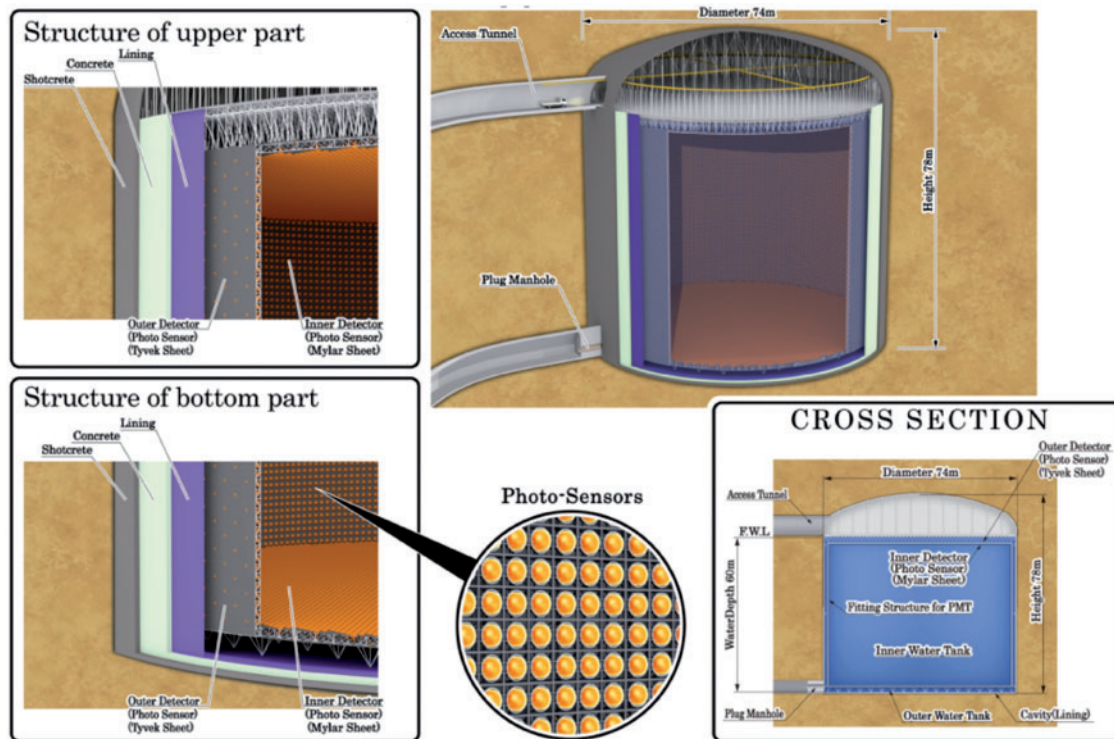
Fig. 2. Schematic view of the first tank.

with a diameter of 74 m and height of 60 m. The total (fiducial) mass of the detector is 258 (187) kt, giving a fiducial mass that is eight times larger than Super-K. The Hyper-K detector candidate site is in the Tochibora mine, which is used by the Kamioka Mining and Smelting Company, near Kamioka town in Gifu Prefecture, Japan. This is 8 km south of Super-K and 295 km away from J-PARC. The J-PARC neutrino beamline is directed so that the existing Super-Kamiokande detector in the Mozumi mine and the Hyper-K candidate site in the Tochibora mine have the same off-axis angle. The detector will lie under the peak of Nijuugo-yama, with an overburden of 650 m of rock or 1750 meters-water-equivalent (m.w.e.), at geographic coordinates N36° 21′ 20″, E137° 18′ 49″ (world geographical coordinate system), and an altitude of 514 m above sea level (a.s.l.).

The Hyper-K detector is designed to employ newly developed high-efficiency and high-resolution (timing) PMTs (Hamamatsu R12860), which will collect more photons compared to the current Super-K PMTs, and improve sensitivity to low-energy events such as neutron captures and nuclear de-excitations. This increased sensitivity contributes significantly to the major goals of the Hyper-K experiment such as clean proton decay searches via $p \rightarrow e^+ + \pi^0$ and $p \rightarrow \bar{\nu} + K^+$ decay modes and the observation of supernova electron antineutrinos. The inner detector region of the single tank is viewed by 40,000 PMTs, corresponding to a PMT density of 40% photo-cathode coverage (the same as that of Super-K). The detector will be instrumented with front-end electronics and a readout network/computer system that is capable of high-efficiency data acquisition for two successive events in which Michel electron events follow muon events with a mean interval of $2 \, \mu$s. It is also able to record data from the vast number of neutrinos that would come from a nearby supernova in a nominal time period of 10 s. Similar to Super-K, an outer detector (OD) with a layer width of 1–2 m is envisaged. In addition to enabling additional physics, this would help to constrain the external background. The photo-coverage of the OD can be sparser, and use smaller PMTs than those used for the ID.

2.3. Near and intermediate detector complex

The neutrino flux and cross-section models can be probed by data collected at near detectors, situated close enough to the neutrino production point that oscillation effects are negligible. Near detector data is extremely important to constrain uncertainties in these models.

The existing T2K ND280 detector suite comprises two detectors [26]: INGRID, which consists of 14 iron-scintillator modules in a cross pattern centered on the neutrino beam axis, and ND280, a multi-component detector at an angle of 2.5° from the beam direction. The primary purpose of the INGRID detector is to monitor the neutrino beam direction, while the off-axis detector is used to characterize the spectrum and interactions of neutrinos in the beam before oscillation. T2K has successfully applied a method of fitting to ND280 data with parametrized models of the neutrino flux and interaction cross-sections. Using the ND280 measurements, the systematic uncertainties on the parts of the models constrained by ND280 have been reduced to a typical 3% uncertainty on the Super-K (SK) predicted event rates. An upgrade of the current ND280 detector is planned before the start of Hyper-K.

Moreover, it is proposed to build a water-Cherenkov detector at ∼1–2 km, before Hyper-K becomes operational [28]. A water-Cherenkov intermediate detector can be used to measure the cross section on H_2O directly, with the same acceptance of lepton scattering angle as the far detector and with no need to account for the different target nuclei in a heterogeneous detector. Additionally, water-Cherenkov detectors have shown excellent particle identification capabilities, allowing for the detection of pure ν_μ-CC, ν_e-CC, and $NC\pi^0$ samples. The $CC\pi^0$ rate and kaon production in neutrino interactions, which are backgrounds to nucleon decay searches, can also be measured. The proposed water-Cherenkov detector will have the capability to make measurements at OAAs of 1.0°–4.0°, covering the potential OAAs of detectors in Korea.

These additional water-Cherenkov measurements are essential to achieve the low systematic errors required by Hyper-K, but are complemented by the magnetized ND280 tracking detector, which is capable of tracking particles below the Cherenkov light threshold in water and of separating neutrino and antineutrino beam components via lepton charge measurement. The design anticipates that a combination of a magnetized tracking detector such as ND280 and an "intermediate" water-Cherenkov detector will provide the greatest reduction in systematic uncertainties affecting the oscillation measurement.

2.4. T2HKK experimental configuration

The axis of the J-PARC neutrino beam emerges upwards out of the sea between Japan and Korea. The southern part of the Korean peninsula is exposed to the beam at a 1°–3° range of off-axis angles. From east to west, baselines of 1000–1300 km are possible, as shown in Fig. 1. The topography of South Korea is quite mountainous, especially in the east of the country, and provides plenty of suitable candidate sites.

The Korean rocks are in general made of granite, hard enough to build a large cavern. A search for mountains higher than 1000 m has been made to find several candidates for the Korean detector. Mountains in the national or provincial parks were not considered in the search. Six suitable sites are listed in Table 1, along with their location with respect to the J-PARC neutrino beam. The baselines and energy options of the six sites are shown in Fig. 3. All sites would provide a significant flux at the second oscillation maximum, and depending on the site it is possible to sample neutrinos from as far apart as the first and third maxima.

Table 1. Detector candidate sites with off-axis angles between 1° and 2.5°. The baseline is the distance from the production point of the J-PARC neutrino beam.

Site	Height (m)	Baseline (km)	Off-axis angle	Composition of rock
Mt. Bisul	1084	1088	1.3°	Granite porphyry, andesitic breccia
Mt. Hwangmae	1113	1141	1.9°	Flake granite, porphyritic gneiss
Mt. Sambong	1186	1169	2.1°	Porphyritic granite, biotite gneiss
Mt. Bohyun	1124	1043	2.3°	Granite, volcanic rocks, volcanic breccia
Mt. Minjuji	1242	1145	2.4°	Granite, biotite gneiss
Mt. Unjang	1125	1190	2.2°	Rhyolite, granite porphyry, quartz porphyry
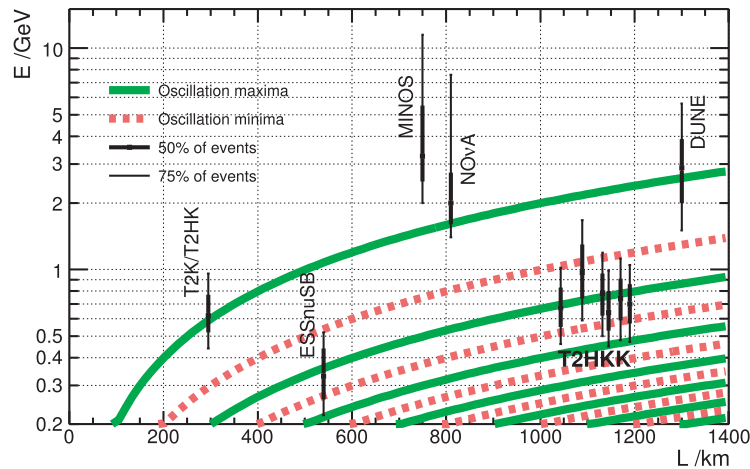
Fig. 3. Comparison of baseline and energy regime of various recent and proposed long-baseline experiments. The event rates for Kamioka and Korean sites are based on calculated fluxes, using the quasi-elastic charged-current cross section from NEUT. The ESSnuSB event rates are calculated from publicly available flux histograms [20] and the NEUT cross section. The event rates from MINOS [22], NOνA [23], and the DUNE [24] optimized design use publicly available spectra, which typically assume inclusive charged-current cross sections.

At an off-axis angle similar to that of the Kamioka site (2.5°) the neutrino interaction rate peaks at an energy of around 0.7 GeV. At this energy the second oscillation maximum occurs at a baseline of roughly 1100 km, with longer baselines corresponding to maxima for higher energies and vice versa.

The novel aspect of a detector built in Korea becomes clear if we compare it to similar long-baseline neutrino experiments. Figure 3 shows the regime of baseline (L) and neutrino energy (E) covered by recent and proposed experiments. T2HKK provides a baseline almost as long as the proposed DUNE experiment but in a similar energy band to the existing T2K experiment, which allows it to probe oscillations at the second oscillation maximum, a capability not available to any existing experiment, and only shared by the proposed ESS neutrino beam [20,21]. Furthermore, the fact that oscillations become more rapid at higher-order maxima means that the T2HKK configuration can probe more of the oscillation shape than existing experiments. It is also worth noting that a double-baseline configuration using similar fluxes and different (non-trivial) baselines within one experiment is only possible because the axis of the J-PARC beam passes below the Kamioka site. Equivalent configurations using the NuMI or proposed LBNF and ESS beamlines do not exist.
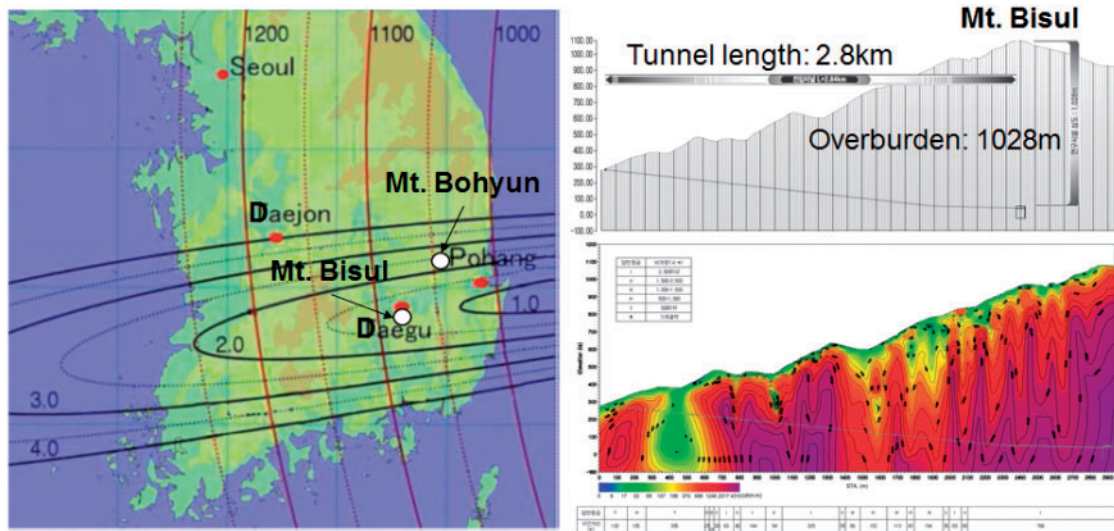
Fig. 4. Two candidate sites for the second Hyper-K detector in Korea. Mount Bisul is located near the city of Daegu at 1.3° off-axis, and Mt. Bohyun at Youngcheon at 2.3° off-axis. Mount Bisul is 1084 m high and provides excellent accessibility with an existing highway nearby. Mount Bohyun is 1124 m high and accommodates an optical telescope on the top. A detector at Bisul is expected to have ∼1000 m overburden with a slightly inclined access tunnel 2.8 km long. An electromagnetic geological survey shows excellent bedrock for the candidate site, suitable for a large cavern.

2.4.1.   Investigation of candidate sites

We can roughly partition the candidate sites into two groups. For five of the six sites the (unoscillated) interaction rate is expected to peak near or slightly below the energy of the second oscillation maximum. The exception is Mt. Bisul; at 1.3° it is much closer to the beam axis, so the typical neutrino is more energetic and the spectrum overall is broader. A detector at this site could still sample the second maximum but also sample a significant part of the first oscillation maximum and the region between the first and second oscillation maxima. Physics studies therefore treat Bisul as a distinct case.

The variation in L/E between the other sites is less substantial, and discriminating between the physics reach of each requires detailed simulations. The Bohyun site, being closest to J-PARC, is expected to provide the highest event rate after Bisul. Based on these considerations, Mt. Bisul and Mt. Bohyun are the first sites considered for more detailed investigation of their suitability.

Mount Bisul is located at Dalseong in the city of Daegu, the fourth largest city in population in South Korea, as shown in Fig. 4. Its accessibility is excellent. It takes one hour and forty minutes to get to Daegu from Seoul by the KTX (Korean bullet train). The mountain is 1084 m high and made of hard rocks: granite porphyry and andesitic breccia. A detector at Bisul is expected to have ∼1000 m overburden with a slightly inclined access tunnel and to be exposed to a 1.3° off-axis neutrino beam. The site coordinates are N35° 43′ 00″ in latitude and E128° 31′ 28″ in longitude. The baseline from J-PARC is 1088 km. A recent geological survey using a magnetotelluric method shows excellent bedrock for the candidate site, belonging to the hardest rock classes 1 or 2. Based on nearby lakes and rivers, sufficient underground water could be available in the site. The survey result obtains an estimate of ∼2.7–3.2 m³ km⁻¹ min⁻¹ underground water flow into the access tunnel through rock fractures. The expected water would be sufficient to be supplied for the detector. We find excellent access roads up to the candidate location of tunnel entrance, and easy access to electricity supply lines.
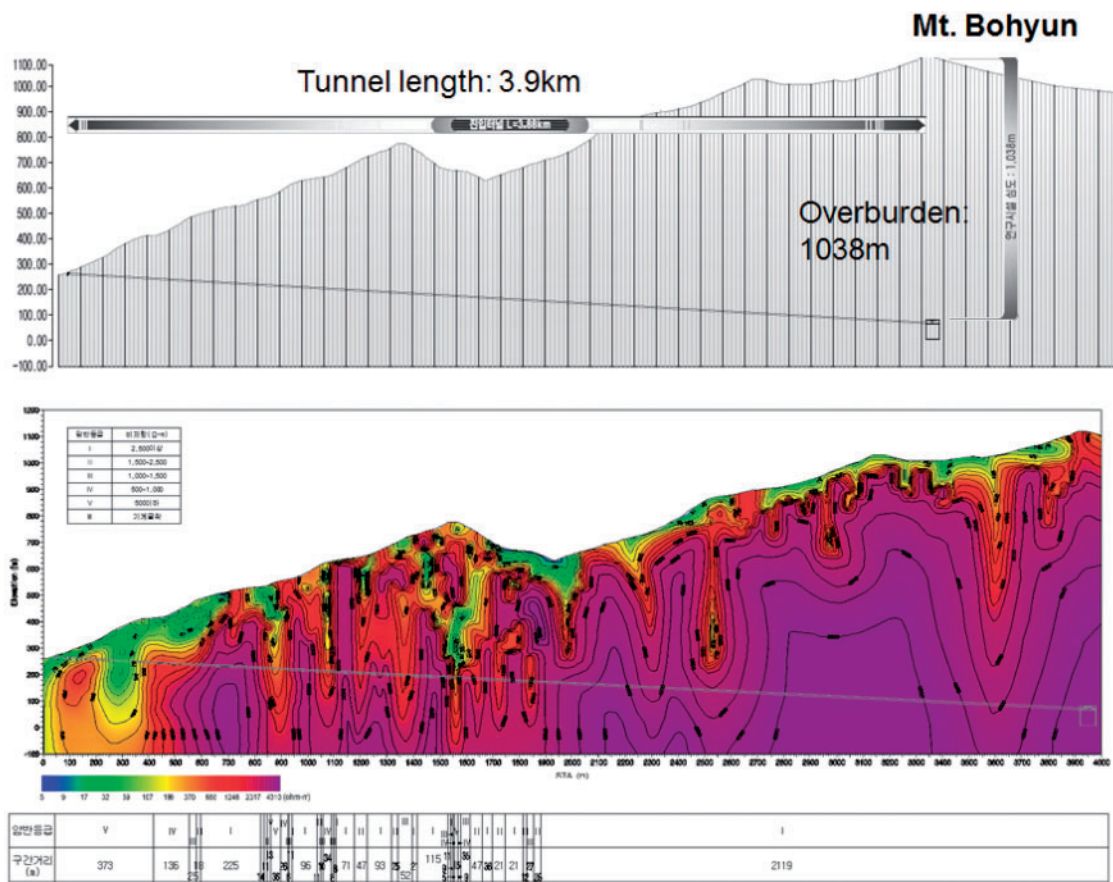
Fig. 5. Mount Bohyun as a candidate site for the second Hyper-K detector in Korea. It is 1124 m high and provides ∼1000 m overburden with a slightly inclined access tunnel that is 3.9 km long. A geological survey shows excellent bedrock for the candidate site, suitable for a large cavern.

Mount Bohyun is located at Youngcheon and is also the site of the Bohyunsan Optical Astronomy Observatory, as shown in Fig. 5. The mountain is 1124 m high and made of fairly hard rocks: granite, volcanic rocks, and volcanic breccia. It is an excellent candidate site for a large cavern. A detector at Bohyun is expected to have ∼1000 m overburden and to be exposed to a 2.3° off-axis neutrino beam. The site coordinates are N36° 09′ 47″ in latitude and E128° 58′ 26″ in longitude. The baseline from J-PARC is 1040 km. The geological survey also shows excellent bedrock for the candidate site. Based on nearby rivers, sufficient underground water is expected in the site. The survey result obtains an estimate of ∼3.7 m^3 km^{-1} min^{-1} underground water flow into the access tunnel. Its accessibility is reasonably good.

In summary, both candidate sites seem to be suitable for building a second Hyper-K detector, and can provide roughly 1000 m overburden for low-energy neutrino measurements. Investigation of the suitability of the sites for a larger cavern is already advanced, and initial estimates suggest the excavation cost in Korea would be comparatively low.

3. Physics motivation for the T2HKK configuration

In this section we explain in more detail the expected benefits of a detector sited in Korea, and why these are sufficient to make the proposal attractive despite the inevitable loss of statistics from using a longer baseline.
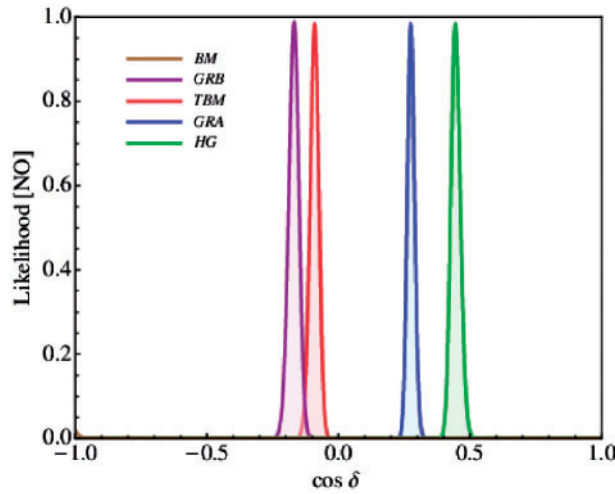
Fig. 6. The likelihood function versus $\cos\delta_{CP}$ for normal-ordering neutrino mass spectrum for different types of flavor symmetries assuming the prospective 1σ uncertainties in the determination of the neutrino mixing angles [29].

To do so, it is first worth restating the goals of the next generation of neutrino oscillation experiments. A general goal is to test the three-neutrino PMNS model. By using a different range of L/E we subject the model to a broader range of checks than existing long-baseline experiments. An example of these kinds of checks is the study of non-standard interactions (between neutrinos and normal matter), which is described in Sect. 7. Even without resorting to any particular new model, an expanded range of L/E values provides a check of the complete model used to analyze neutrino experiments. In the broadest sense, this includes the models used for systematic uncertainties, such as the modeling of neutrino fluxes and cross sections.

Assuming that the three-neutrino oscillation model is correct and the uncertainties we assign to the broader model are sensible, the primary goals of the next generation of neutrino oscillation experiments are:

- Establish the ordering of neutrino masses. That is, whether or not $m_3^2 > m_1^2$.
- Establish the existence (or not) of CP violation in the neutrino sector. That is, whether or not $\delta_{CP} = 0, \pi$.
- Make precision measurements of all oscillation parameters. Most important is to make a precision measurement of δ_{CP} (as opposed to simply determining that it is not zero or π).

The first two of these are well known, and need not be elaborated. As an example of the third goal, Fig. 6 shows the prediction of GUTs with different flavor symmetries for the value of $\cos\delta$. Four of the five models predict a sizable CP violation effect (CP conservation occurs for $\cos\delta = \pm 1$), and are only separated by precision measurement.

At the second maximum, the effect on the observed spectrum from both the CP-phase and mass hierarchy are enhanced in comparison to the Kamioka site, but the exact behavior is dependent on the site. At the Bisul site (or any hypothetical site with an off-axis angle below about $1.5°$; see Fig. 8 later in this section) the beam spectrum peaks at around $1\,\mathrm{GeV}$ with a wider energy band, making it possible to sample events from both the first and second oscillation maxima. In addition, because of the energy dependence of matter-enhancement effects, the maximum sensitivity for determining

the neutrino mass ordering is achieved by going to higher neutrino energies, so the Bisul site will provide better discrimination between normal and inverted orderings.

Alternatively, the off-axis angle can be chosen in the region of 2.5∘, to provide a similar flux (without oscillations) to that seen at Kamioka. In that case, the J-PARC neutrino beam spectrum peaks at $E_\nu = 0.6$ GeV, with a narrower energy band in the vicinity of the second oscillation maximum. With identical off-axis angles for HK and HKK, the combined analysis is essentially a ratio measurement between the two sites, which can be expected to greatly reduce the uncertainties from fluxes and cross sections.

Both alternatives sample a wider range of L/E than the Kamioka site, and this enables improved measurement resolution of the CP phase, especially near the maximally CP-violating values.

In the following section we examine the oscillation probabilities to explain the enhancements seen at various Korean sites, and how measurements at HKK would differ from the baseline HK. Following this, sensitivity studies are presented using both generic sites at a typical baseline of 1100 km and the Bisul and Bohyun sites identified above.

3.1. Neutrino oscillation probabilities

The sensitivity enhancement of a second detector in Korea can be understood by first examining the $P(\nu_\mu \to \nu_e)$ and $P(\overline{\nu}_\mu \to \overline{\nu}_e)$ probabilities. We do this by first studying the probabilities in vacuum and then the probabilities with the matter effect included. The approximate oscillation probability in vacuum is:

$$
\begin{aligned}
P(\overset{(-)}{\nu}_\mu \to \overset{(-)}{\nu}_e) \approx\ & \sin^2\theta_{23} \sin^2 2\theta_{13} \sin^2(\Delta_{31}) \\
& + \sin 2\theta_{23} \sin 2\theta_{13} \sin 2\theta_{12} \cos\theta_{13} \sin(\Delta_{31}) \sin(\Delta_{21}) \cos(\Delta_{32}) \cos\delta \\
& \mp \sin 2\theta_{23} \sin 2\theta_{13} \sin 2\theta_{12} \cos\theta_{13} \sin(\Delta_{31}) \sin(\Delta_{21}) \sin(\Delta_{32}) \sin\delta \\
& + \cos^2\theta_{13} \cos^2\theta_{23} \sin^2 2\theta_{12} \sin^2(\Delta_{21}).
\end{aligned}
\tag{1}
$$

Here, we use the shorthand $\Delta_{ji} = \frac{\Delta m_{ji}^2 L}{4E}$. The first line represents the oscillations at the atmospheric mass splitting, and this term dominates for L/E values of $\sim$500 km/1 GeV typical of accelerator-based long-baseline oscillation experiments. The fourth line gives the oscillations driven by the solar mass splitting, which are small for the L/E values of interest. The second and third lines are the CP-conserving and CP-violating parts, respectively, of the interference term. The sign of the third line flips to positive when considering antineutrinos, introducing the CP violation effect.

To understand the benefit of a second-maximum experiment, note that the CP-violating interference term depends on $\sin(\frac{\Delta m_{21}^2 L}{4E})$. Since the argument is small for the L/E values of interest, this dependence is approximately linear. Thus, for a given energy, a larger CP effect will be observed at longer baselines. This is illustrated in Fig. 7, where the intrinsic CP-driven neutrino–antineutrino probability difference is shown for baselines of 300, 900, and 1100 km.

We identify the "oscillation maxima" as points where $\frac{\Delta m_{32}^2 L}{4E} = n\pi/2$ and n is an odd integer. For a fixed baseline, the second oscillation maximum will be located at 1/3 the energy of the first oscillation maximum. Alternatively, for a fixed energy, the necessary baseline to observe the second oscillation maximum will be three times larger than the baseline needed to observe the first oscillation maximum. The neutrino flux will decrease by the ratio of the baselines squared—a factor of 1/9 in this case—which means the statistical sensitivity decreases by a factor of three. At the same time, the CP effect is around three times larger at the second oscillation maximum. The result is that CP
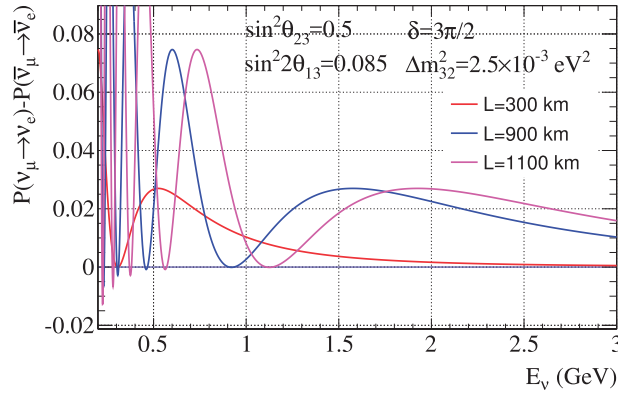
Fig. 7. The neutrino–antineutrino probability difference for $\delta = 3\pi/2$ at 300, 900, and 1100 km baselines for oscillations in vacuum. As the effects of matter are ignored here, this indicates the empirical size of "true" CP violation, driven only by δ_{CP}.

violation measurements made at the second oscillation maximum have similar sensitivity to the first maximum, despite the reduction in event rate that comes with a three-times-larger baseline.

The significant benefit for second-maxima experiments is that this near indifference of the statistical sensitivity to the baseline does not apply in relation to systematic uncertainties. Most important systematic errors are not significantly constrained by data from the oscillated neutrino beam. This can be because parameters are better constrained by a near detector in the same beamline, by other independent experiments, or perhaps by using data taken with local calibration sources. Such uncertainties do *not* grow with the baseline and as such are reduced relative to the larger CP violation effect.

Another uncertainty that potentially impacts the CP measurement is that associated with the leading atmospheric term. This dominates the overall appearance probability at the first maximum, so in a realistic case where we cannot do a perfect neutrino–antineutrino comparison, there will be some contribution to the overall uncertainty arising from our imperfect measurement of the parameters that appear in this term. But at the second maximum, where the size of the interference term is roughly as large as the leading term, the finite precision to which the latter is known has less impact. In essence, there is less "background" due to contributions that are independent of δ_{CP}. The picture is not that simple in practice, but this effectively means that correlations between oscillation parameter measurements at Kamioka and a Korean detector can be different, leading to potential synergies by having both.

When neutrinos propagate in matter, the matter potential is added to the Hamiltonian of the system, modifying the neutrino oscillation probabilities. There are few expressions of the approximate probability in matter [31–34] and one of them can be written as [31]:

$$
\begin{aligned}
P(\overset{(-)}{\nu_\mu} \to \overset{(-)}{\nu_e}) \approx\ & \sin^2\theta_{23} \sin^2 2\theta_{13} \frac{\sin^2(\Delta_{31} \mp aL)}{(\Delta_{31} \mp aL)^2} \Delta_{31}^2 \\
& + \sin 2\theta_{23} \sin 2\theta_{13} \sin 2\theta_{12} \cos\theta_{13} \frac{\sin(\Delta_{31} \mp aL)}{(\Delta_{31} \mp aL)} \Delta_{31} \frac{\sin(aL)}{aL} \Delta_{21} \cos(\Delta_{32}) \cos\delta \\
& \mp \sin 2\theta_{23} \sin 2\theta_{13} \sin 2\theta_{12} \cos\theta_{13} \frac{\sin(\Delta_{31} \mp aL)}{(\Delta_{31} \mp aL)} \Delta_{31} \frac{\sin(aL)}{aL} \Delta_{21} \sin(\Delta_{32}) \sin\delta \\
& + \cos^2\theta_{13} \cos^2\theta_{23}\ \sin^2 2\theta_{12} \frac{\sin^2(aL)}{(aL)^2} \Delta_{21}^2 .
\end{aligned}
\tag{2}
$$

The matter effect depends on $a = G_\mathrm{F}N_e/\sqrt{2}$, where G_F is Fermi's constant and N_e is the number density of electrons in the matter. The signs of the aL terms flip for antineutrinos, introducing an effect that can mimic CP violation for some experimental configurations.

From here, note that the amplitudes of the first, second, and third terms are dependent on the ratio

$$\frac{\Delta_{31}}{\Delta_{31} \mp aL} = \left(1 \mp A\right)^{-1}, \tag{3}$$

where $A = aL/\Delta_{31} = 2\sqrt{2}G_\mathrm{F}N_eE/\Delta m_{31}^2$ is directly proportional to E and inversely proportional to the signed value of Δm_{31}^2. Similarly, the vacuum oscillation phase Δ_{31} in $\sin(\Delta_{31})$ is scaled by a factor of $(1 \mp A)$. Since A is signed, this factor is less than unity for the combination of normal ordering with neutrinos or inverted ordering with antineutrinos, but greater than unity for the opposite combinations. As a result, both the amplitude of the appearance probability and the location of the oscillation maxima shift depending on the mass ordering, and can be used to determine it experimentally.

The shift in the amplitude of the probability depends only on E, and this is the reason the sensitivity of first-maxima experiments increases with L and E at fixed L/E. Among the Korean sites, it also means that a detector at Mt. Bisul will have greater sensitivity to the mass ordering than other locations.

The shift in the phase is more interesting. It also depends on energy, but when considering a fixed value of E, the physical effect will grow linearly as the baseline increases. Thus, even Korean sites at a $2.5°$ off-axis angle are more sensitive to the effect compared to Kamioka, even though the amplitude difference is not larger.

This enhanced sensitivity to the mass ordering and δ_{CP} are illustrated first in Fig. 8 and further in the following section. Figure 8 shows the oscillation probabilities as a function of energy, at a baseline of $L = 1100$ km. In the region of the first oscillation maximum above 1.2 GeV, the matter effect has separated the oscillation probabilities for normal and inverted ordering for all values of the CP phase. In the region of the second oscillation maximum, 0.5–1.2 GeV, the CP probability differences are significant, while the matter effect also affects the height and position of the oscillation maximum. The spectrum of neutrino interactions (ignoring oscillations) for a $1.5°$ off-axis beam is also shown for comparison.

3.1.1. Bi-probability plots

While it is relatively straightforward for the eye to interpret the way the oscillation probabilities depend on δ_{CP} and the mass ordering near the first oscillation maximum, e.g. above 1.2 GeV in Fig. 8, these plots become complicated around the second maximum, and it becomes difficult to understand the overall pattern. A popular alternative is the "bi-probability" plot, in which the $\nu_\mu \to \nu_e$ appearance probability is plotted along the horizontal axis, and the $\overline{\nu}_\mu \to \overline{\nu}_e$ probability along the vertical. Such plots in principle show CP violation in a very direct way—the diagonal is CP conserving, and everywhere in the space is CP violating, although that includes induced CP violation due to matter effects.

Assuming a specific baseline and energy, the probabilities approximated by Eq. (2) can be calculated for various values of the oscillation parameters. In particular, by allowing δ to vary with other parameters held constant, a closed ellipse is traced out on the bi-probability plot. The binary choice of mass orderings can then also be displayed as a second ellipse. The center point of the ellipse will depend on the first and fourth lines of the probability, and the binary choice of mass orderings will
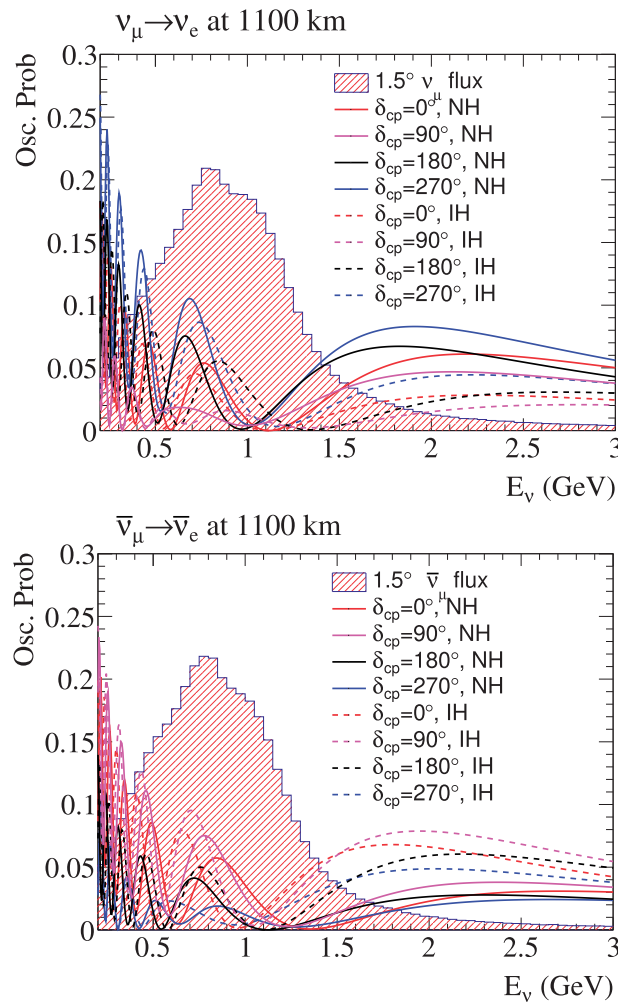
Fig. 8. The oscillation probabilities for $\delta = 0, \pi/2, \pi, 3\pi/2$ and normal and inverted mass ordering are shown for neutrinos (top) and antineutrinos (bottom). Expected muon (anti)neutrino spectra at 1.5° off-axis with arbitrary normalization are shown for comparison.

(if the matter density is non-zero) appear as a separation into two separated ellipses, one for each ordering.

Such plots have one particular weakness when considering long-baseline experiments: the ellipses are plotted for a fixed energy. An experiment that measures oscillations over a range of energies is summarized by a single value. This single-energy simplification is reasonable when comparing two experiments at the first oscillation maximum, where the oscillation is typically rather broad in comparison to the flux, but it does not represent the situation in T2HKK well, as this configuration samples a much wider range of L/E.

In order to use these plots for showing the more complex oscillation patterns at T2HKK it is necessary to show multiple neutrino energies. It is not sufficient to average the probability over the interaction spectrum; this is equivalent to doing a rate-only measurement, and suppresses all the shape information that a real analysis would use. Instead, in the following plots three curves are shown: one (in blue) for the peak interaction rate, as normal, and two more from the upper (red) and lower (green) tails of the spectrum, chosen so that 50% of the (potentially) interacting neutrinos lie between these two ellipses. (The exact method by which these points are calculated is described in Appendix A.) This results in a set of six representative ellipses instead of two.
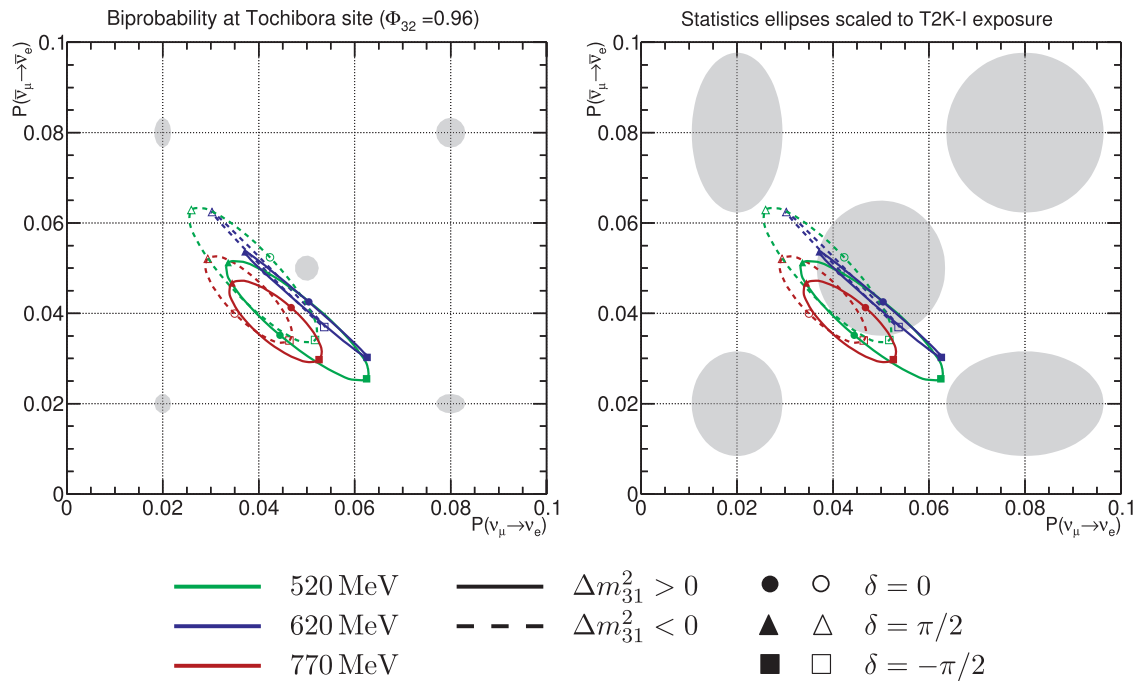
Fig. 9. Appearance bi-probabilities at the Hyper-K site in Kamioka. The gray ellipses show the relative sensitivity (left) for a ten-year exposure of one Hyper-K tank and (right) for the original T2K design goal. Full explanation is given in the text.

Figure 9 shows the resulting ellipses for the Kamioka site. The three ellipses differ in size and eccentricity, but the separation between the two mass orderings, and the dependence of the appearance probabilities on the value of $sin(\delta)$, is similar for all three energies. The similarity of the three pairs of ellipses explains why the narrow-band, first-maximum configuration can be reasonably approximated as a single ("rate-only") measurement.

Two more details are added to the plots. The first is a summary of the L/E value probed (at the peak energy) at the given site. The quantity

$$\Phi_{32} = \frac{2}{\pi} \frac{\left| \Delta m_{32}^2 \right| L}{4E} \tag{4}$$

is defined, which has (near) odd-integer values for oscillation maxima, and (near) even-integer values for oscillation minima. For calculation of Φ_{32} and drawing all bi-probability plots, a value of $2.5 \times 10^{-3} \, \mathrm{eV^2}$ is assumed for $\left| \Delta m_{32}^2 \right|$.

The second detail is the gray ellipses, which provide a comparative scale for the statistical power of the measurement: this depends on the number of events seen with energy similar to each colored ellipse. Since this will depend on the ν_e appearance probabilities and the relative size of the background contamination, this varies across the measurement space. Since this is essentially unrelated to how the analysis is actually performed, it is not possible to accurately indicate the absolute sensitivity, but does give an indication of the relative sensitivity at different sites. Full details are given in Appendix A.

Since the flux at the Hyper-K site near Kamioka should be the same as the existing T2K experiment, the benefit of a larger detector and upgraded beam is entirely due to the higher statistics. In terms of the bi-probability plots, the probability ellipses remain the same, but the statistical error ellipses shrink. This is illustrated by a comparison of the left and right panels of Fig. 9, showing that Hyper-K
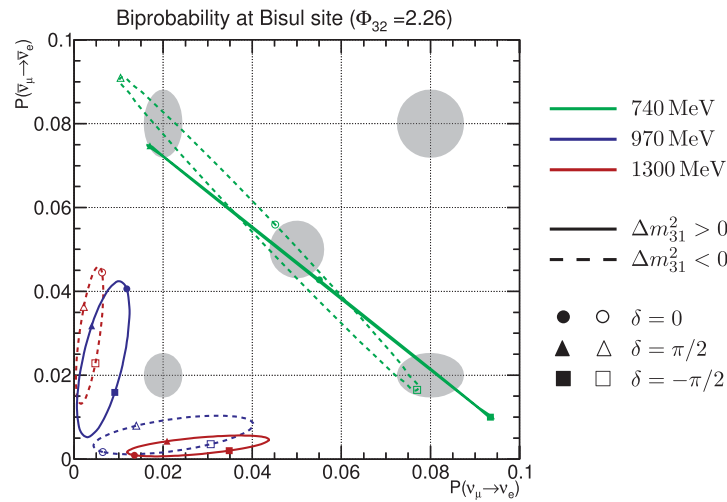
Fig. 10. Appearance bi-probabilities at the Mt. Bisul site at 1088 km.

will be much more sensitive than the design goal of T2K-I (7.8×10^{21} POT) by virtue of much smaller statistical errors. In contrast, at the Korean sites the statistical uncertainties are about three times larger than the default Hyper-K configuration, but they gain sensitivity due to the fact the probability ellipses change drastically.

The first example shown is for the most on-axis site under consideration—Mt. Bisul—in Fig. 10. A detector at Bisul would see completely separated ellipses depending on the mass ordering, i.e. the measurement is completely non-degenerate with CP violation for events at the peak, and in the high-energy tail. This reflects the benefit of high-energy neutrinos for resolving the mass ordering. At the peak energy, however, the normal ordering enhances the *antineutrino* probabilities relative to neutrinos, which is opposite to the amplitude-dominated effect seen at the first maximum. This is due to the matter effect also changing the effective oscillation length for neutrinos and antineutrinos, so that the neutrinos are closer to an appearance minimum than are antineutrinos of the same energy. Unlike a first-maximum experiment, the experimental signature determining the mass ordering uses shape as well as rate information, and the impact of systematic uncertainties (most obviously on neutrino versus antineutrino cross sections and detection efficiencies) is correspondingly different. Although most pronounced at the higher beam energies of the Bisul site, this characteristic is seen for some energies at any Korean site.

The low-energy tail of the Bisul site corresponds to an (L, E) regime more similar to the other Korean sites. Figure 11 shows the Bohyun site, which has the shortest baseline of the sites under consideration, and a flux more similar to that at Kamioka. It is immediately apparent (as it was for the lower-energy ellipse at Bisul) that the ellipses are much larger, demonstrating a greatly enhanced CP-violation signal. For the energy peak at Bohyun (which is close to the oscillation maximum), the overlap between the normal and inverted ordering ellipses is still large, but the effect for the higher and lower energy ellipses is quite different, so information provided by the spectrum of observed events is less degenerate, and correspondingly more interesting, than it is for first-maxima experiments. The larger effect size almost entirely compensates for the lower statistics compared to T2HK at Kamioka, but the absolute scale of detector systematic errors does *not* grow for a more distant site, so systematic errors are expected to be much less important.
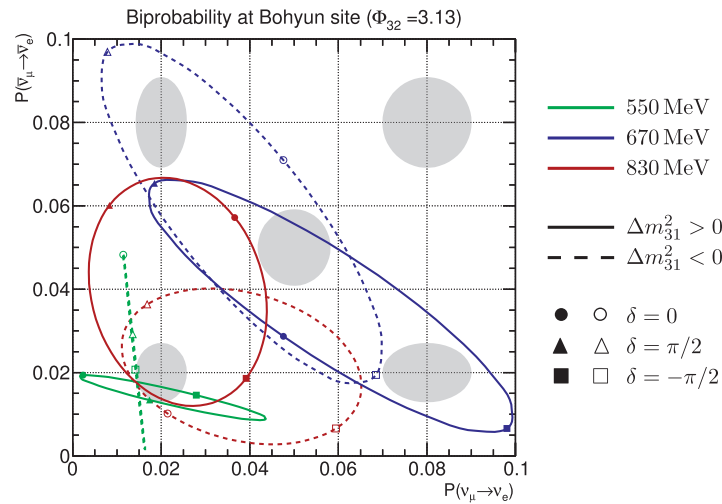
Fig. 11. Appearance bi-probabilities at the Mt. Bohyun site at 1043 km.
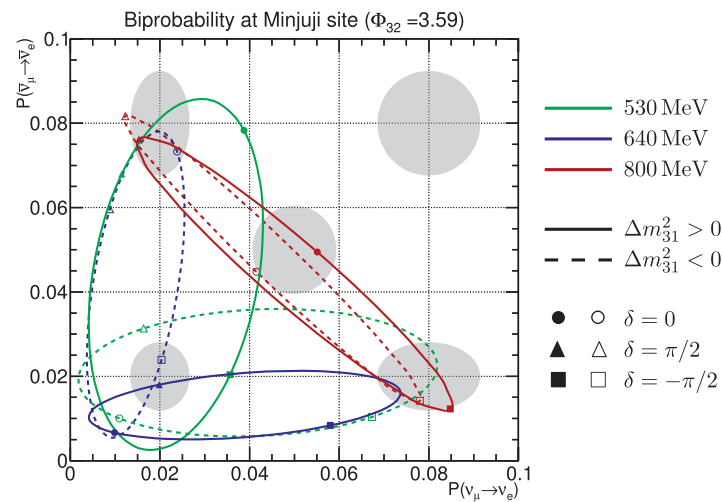

Fig. 12. Appearance bi-probabilities at the Mt. Minjuji site at 1145 km.

Finally, Fig. 12 shows the Minjuji site, which probes the largest values of L/E. For Minjuji, the low-energy tail is actually probing the region near the third oscillation maximum. The independence of information available at different energies is again clearly apparent—for the peak energy and below the ellipses are noticeably "fatter." More precisely, we can say that $dP/d\delta$ is larger in the vicinity of $\delta = \pm\pi/2$. Narrow ellipses are characteristic of an energy band near the oscillation maximum, where the dependence on δ is dominated by a $\sin\delta$ dependence. This is optimal for making a measurement of δ near $0, \pi$, and therefore for establishing (or not) CP violation. However, if the true value of δ is in the vicinity of $\pm\pi/2$, this provides the least precision on the value. The wider L/E band of a Korean detector improves the sensitivity to $\cos\delta$ and the measurement precision on the CP phase in large CP-violation scenarios.

However, we reiterate that although these kinds of plots are useful for understanding the merits of a Korean detector, they are largely unrelated to how the actual analysis is done: using binned energy spectra, multiple backgrounds, and finite energy resolution. To determine real sensitivities, more detailed studies must be done with full simulations. Such studies are presented in the following sections.

Table 2. The default oscillation parameter values and prior uncertainties used in the studies presented in this section.

Parameter	Value	Prior error
δ_{CP}	0	No prior constraint
Δm^2_{32}	$2.5 \times 10^{-3}\,\text{eV}^2$	No prior constraint
$\sin^2 \theta_{23}$	0.5	No prior constraint
Δm^2_{21}	$7.53 \times 10^{-5}\,\text{eV}^2$	$0.18 \times 10^{-5}\,\text{eV}^2$
$\sin^2 \theta_{12}$	0.304	0.041
$\sin^2 \theta_{13}$	0.0219	0.0012

4. Improved neutrino mass ordering and CP sensitivities

This section describes the sensitivity in measuring the neutrino mass ordering and discovering CP violation using a configuration of Hyper-K with one tank in Japan and the second tank in Korea. Expected reconstructed event spectra for the Korean detector are presented and the effect of the oscillation parameters on these spectra are considered. A model of systematic uncertainties is added, and studies of the resulting sensitivity for mass ordering measurement, CP violation discovery, and the precision of CP phase measurement are presented.

4.1. Event rates at Korean detectors

For the purpose of the sensitivity studies presented here, we consider generic detector locations in South Korea at a baseline of 1100 km and off-axis angles of 1.5°, 2.0°, or 2.5°. The expected event rates are estimated by using the NEUT [35] 5.3.2 neutrino interaction generator and a GEANT3-based simulation of the Super-K detector, where the fiducial mass has been scaled from 22.5 kt to 187 kt. The simulated events are scaled to give good agreement with NEUT 5.1.4.2, which has been tuned against T2K near-detector data. Following the running plan of Hyper-K, an exposure of $(1.3\,\text{MW}) \times (10 \times 10^7\,\text{s})$ is assumed with a 3 : 1 ratio of antineutrino-mode to neutrino-mode operation. This corresponds to ten years of Hyper-K operation, or 27×10^{21} protons on target. Oscillation probabilities are calculated using Prob3++ [36], and a constant matter density of $3.0\,\text{g}\,\text{cm}^{-3}$ is assumed for the 1100 km baseline [37]. Unless otherwise specified, simulated event rates are calculated with the oscillation parameters shown in Table 2. When fitting, the parameters $\sin^2 \theta_{13}$, $\sin^2 \theta_{12}$, and Δm^2_{21} are constrained by Gaussian constraint terms with the 1σ uncertainties shown in Table 2, which are extracted from the Particle Data Group (PDG) 2016 Review of Particle Physics [38]. For each detector configuration, reconstructed events are classified in four categories:

- ○ Neutrino mode, 1Re: single electron-like ring candidates collected in neutrino-mode operation of the beam.
- ○ Antineutrino mode, 1Re: single electron-like ring candidates collected in antineutrino-mode operation of the beam.
- ○ Neutrino mode, 1Rμ: single muon-like ring candidates collected in neutrino-mode operation of the beam.
- ○ Antineutrino mode, 1Rμ: single muon-like ring candidates collected in antineutrino-mode operation of the beam.

The selection cuts for these candidate samples are identical to the selection cuts used in recent T2K oscillation measurements [39], except for the reconstructed energy $E_{\text{rec}} < 1.25\,\text{GeV}$ cut on the 1Re
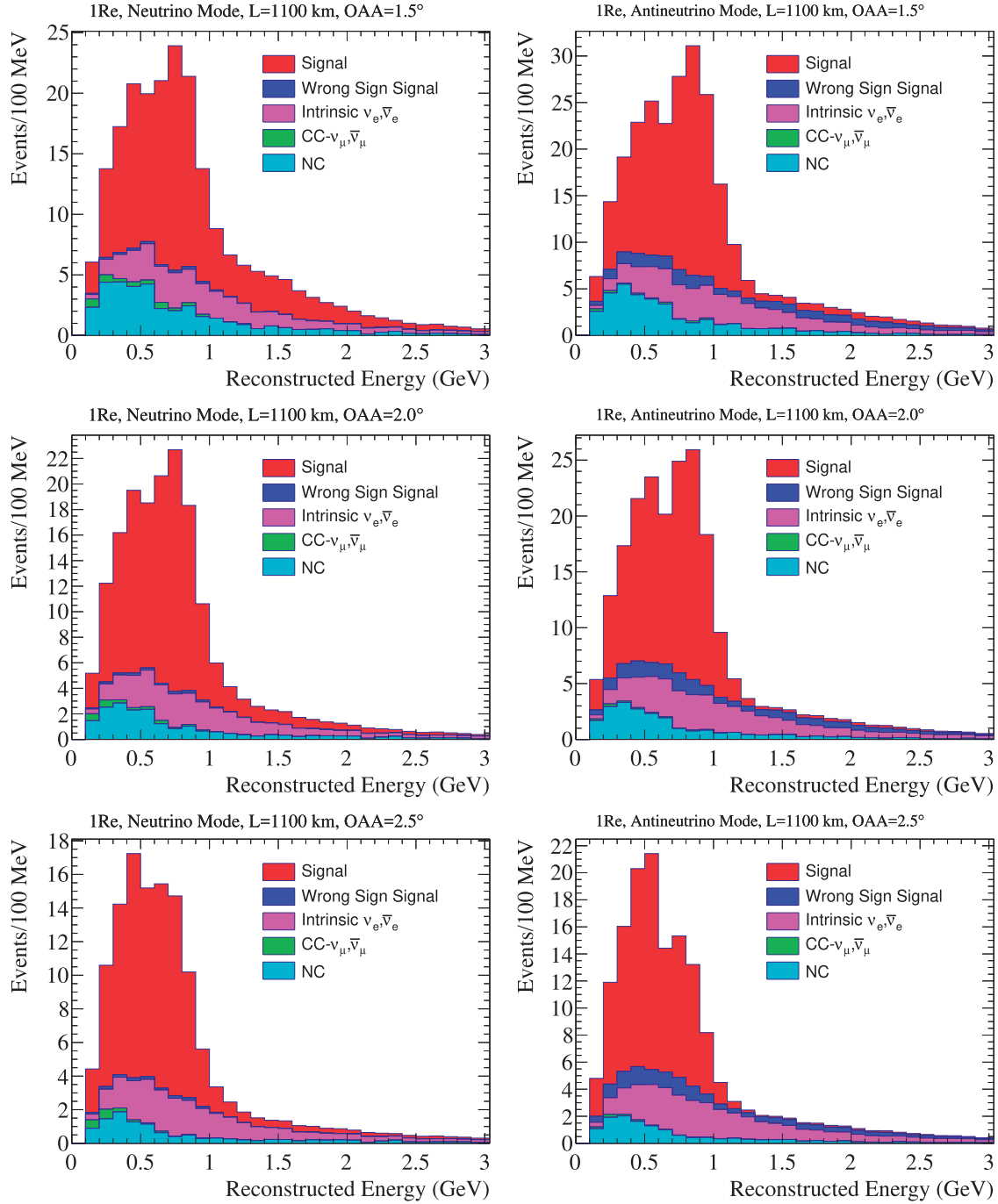
Fig. 13. Predicted 1R*e* candidate rates for neutrino mode (left) and antineutrino mode (right) with the detector at a 1.5° (top), 2.0° (middle), or 2.5° (bottom) off-axis angle. The oscillation parameters are set to $\delta_{\rm CP} = 0$, $\Delta m^2_{32} = 2.5 \times 10^{-3}$ eV² (normal mass ordering), $\sin^2 \theta_{23} = 0.5$, $\sin^2 \theta_{13} = 0.0219$.

samples. This cut has been removed, since the matter effect that constrains the mass ordering is most strongly manifested in events with reconstructed energy greater than 1.25 GeV.

Predicted event rates for normal mass ordering and $\delta_{\rm CP} = 0$ are shown for 1R*e* and 1Rμ samples in Fig. 13/Table 3 and Fig. 14/Table 4, respectively. In Tables 3 and 4, the predicted event rates for the nominal Hyper-K tank location are shown for comparison. The 1R*e* candidate rates in Korea are

Table 3. The expected number of ν_e and $\bar{\nu}_e$ 1Re candidate events. Normal mass ordering with $\sin^2\theta_{13} = 0.0219$ and $\delta_{CP} = 0$ are assumed. Background is categorized by the flavor before oscillation. "Signal" are 1Re candidates produced by ν_e in neutrino-mode operation and $\bar{\nu}_e$ in antineutrino-mode operation. "Wrong-sign signal" are 1Re candidates produce by $\bar{\nu}_e$ in neutrino mode-operation and ν_e in antineutrino-mode operation.

Detector location	Signal	Wrong-sign signal	Intrinsic $\nu_e, \bar{\nu}_e$	NC	CC-$\nu_\mu, \bar{\nu}_\mu$	Total
OAA, L			Neutrino mode			
2.5°, 295 km	1426.1	15.4	269.3	125.0	7.1	1842.9
2.5°, 1100 km	87.9	1.7	28.3	12.5	1.7	132.2
2.0°, 1100 km	122.6	2.0	33.8	21.4	2.4	182.3
1.5°, 1100 km	140.6	2.4	39.1	39.1	3.7	224.8
OAA, L			Antineutrino mode			
2.5°, 295 km	1053.1	164.3	338.3	153.5	4.2	1713.4
2.5°, 1100 km	89.8	15.5	39.4	14.3	0.8	159.8
2.0°, 1100 km	131.5	19.8	46.3	23.4	1.1	222.1
1.5°, 1100 km	159.1	23.9	54.3	39.5	1.7	278.5

$\sim$1/10 the rates at the 295 km baseline due to the $1/L^2$ dependence of the flux. In the 1Rμ samples, the first and second oscillation maxima can be observed at 2 GeV and 0.7 GeV, respectively.

The variations of the 1Re spectra in neutrino mode and antineutrino mode for different δ_{CP} values at different detector locations are shown in Fig. 15. Similarly, the asymmetries of predicted 1Re spectra between neutrino mode and antineutrino mode as a function of δ_{CP} are shown in Fig. 16. For the detectors in Korea, the magnitude of the potential neutrino/antineutrino asymmetry is larger and this effect can partially compensate for the larger statistical uncertainties at the 3.7 times longer baseline. The purely statistical separations between the maximally CP-violating and CP-conserving hypotheses are listed in Table 5, where it is assumed that the mass ordering is known. The 2.0° off-axis slice has the strongest statistical separation between CP-violating and CP-conserving hypotheses. Here, the detectors at 1100 km do not match the significance for CP violation discovery of the 295 km detectors as suggested in Sect. 3.1. The lower significance is due to a few factors. First, the 1100 km baseline means that the second oscillation maximum is at a higher energy than the first oscillation maximum at the 295 km baseline, and the neutrino flux is decreased by a factor of 14 at 1100 km compared with 295 km. The width of the second oscillation maximum is also narrower than the first oscillation maximum, so for a 2.0° off-axis beam, a larger fraction of events do not have energies very close to the second oscillation maximum. The introduction of the matter effect also decreases the CP violation significance as it introduces degeneracies between the mass ordering and δ_{CP}. Despite the lower statistical significance at the 1100 km baseline, the overall significance with a second detector in Korea is higher when systematic uncertainties are accounted for, as is shown in the sensitivity studies presented later in this section.

The impact of the matter effect and sensitivity to mass ordering is illustrated in Fig. 17. Here, a double difference is presented. First, the difference in observed neutrino-mode and antineutrino-mode 1Re candidates is calculated as a function of reconstructed energy. This difference is calculated for both the normal and inverted hierarchies, and the difference between hierarchies is taken. It can be seen that the neutrino–antineutrino difference varies differently with reconstructed energy for the normal and inverted hierarchies. For the normal mass ordering, the neutrinos are enhanced in the < 0.8 GeV and > 1.1 GeV regions and diminished in the 0.8–1.0 GeV region relative to the inverted mass ordering. This relative difference is nearly independent of the true value of δ_{CP}, as illustrated in Fig. 17. The 1.5° off-axis angle configuration allows for a significant observation of
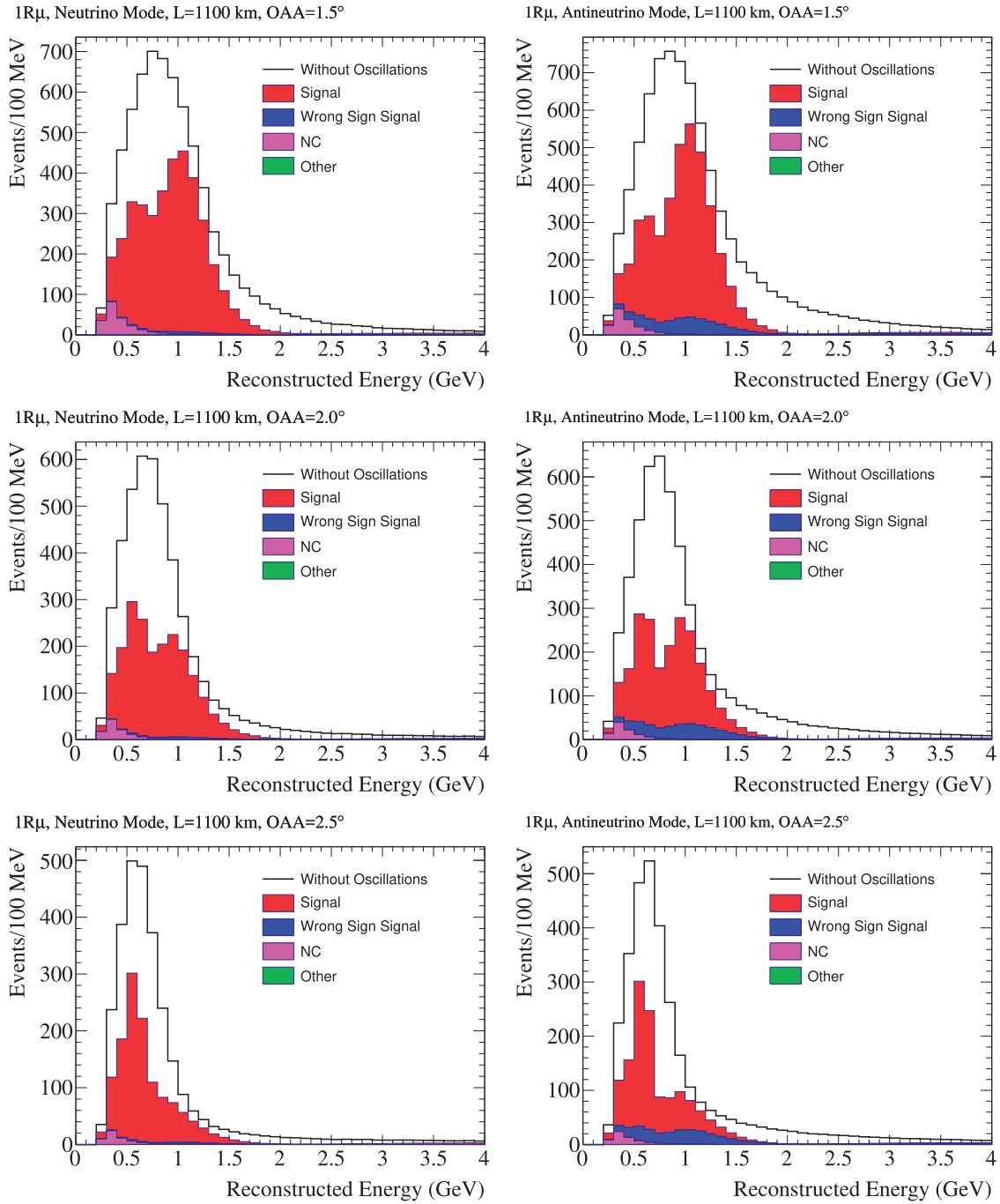
Fig. 14. Predicted 1Rμ candidate rates for neutrino mode (left) and antineutrino mode (right) with the detector at a 1.5° (top), 2.0° (middle), or 2.5° (bottom) off-axis angle. The oscillation parameters are set to $\delta_{CP} = 0$, $\Delta m^2_{32} = 2.5 \times 10^{-3}$ eV^2 (normal mass ordering), $\sin^2 \theta_{23} = 0.5$, $\sin^2 \theta_{13} = 0.0219$.

this spectral dependence of the asymmetry in the 0.8–1.0 GeV and > 1.1 GeV regions. The 2.0° off-axis angle configuration has little sensitivity to the > 1.1 GeV region, and the 2.5° off-axis configuration is only sensitive to the < 0.8 GeV region. Figure 17 illustrates the mass ordering sensitivity for the neutrino/antineutrino mode difference for fixed bins of reconstructed energy, but additional sensitivity arises from the energy-dependent enhancements and deficits observed in each mode independently.

Table 4. The expected number of ν_μ and $\bar{\nu}_\mu$ 1Rμ candidate events. Normal mass ordering with $\sin^2 \theta_{23} = 0.5$, $\Delta m^2_{32} = 2.5 \times 10^{-3}$ eV^2, and $\sin^2 \theta_{13} = 0.0219$ are assumed.

Detector location	Signal	Wrong-sign signal	NC	CC-$\nu_e, \bar{\nu}_e$	Total
OAA, L			Neutrino mode		
2.5°, 295 km	9062.5	571.2	813.6	29.5	10476.9
2.5°, 1100 km	1275.0	32.7	58.5	1.9	1368.1
2.0°, 1100 km	2047.2	42.8	107.7	2.5	2200.2
1.5°, 1100 km	3652.0	55.4	210.4	2.9	3920.7
OAA, L			Antineutrino mode		
2.5°, 295 km	8636.1	4905.9	860.8	23.6	14426.5
2.5°, 1100 km	1119.5	300.6	61.9	2.0	1484.0
2.0°, 1100 km	1888.5	390.0	102.6	2.4	2384.4
1.5°, 1100 km	3579.2	490.8	185.1	2.8	4257.9

While the CP-even and CP-odd interference terms in the electron (anti)neutrino appearance probability are enhanced at the 1100 km baseline due to the Δ_{21} dependence, no such enhancement is present in the muon (anti)neutrino survival probability. Hence, the statistical constraint from the 1Rμ samples on Δm^2_{32} and $\sin^2 2\theta_{23}$ will be stronger for the detector at $L = 295$ km due to the larger statistics. The Korean detector, however, has the unique feature of measuring the oscillation pattern over two periods, confirming the oscillatory behavior of the neutrino transitions. Figure 18 shows the ratio of the expected spectrum after oscillations to the expected spectrum without oscillations. For all three Korean detector locations, the oscillation pattern over two periods may be observed. While the measurement in Hyper-K provides higher statistics, only one period of oscillations can be observed.

4.2. Systematic errors

Due to the statistically large samples available in the Hyper-K experiment, systematic errors are likely to represent the ultimate limit on oscillation parameter measurement precision. An advantage of a Korean detector is to enhance the contribution of the δ_{CP}-dependent interference terms at the cost of fewer statistics, achieving similar sensitivity in a statistics-limited measurement. To evaluate the impact of the Korean detector on the Hyper-K sensitivities, it is necessary to implement a systematic error model that takes into account what are expected to be the dominant systematic errors for Hyper-K. The systematic error model should also account for any new systematic errors introduced by having a detector in Korea. The systematic errors considered for the sensitivity studies presented in this paper are:

○ $\sigma_{\nu_e}/\sigma_{\nu_\mu}$ **and** $\sigma_{\bar{\nu}_e}/\sigma_{\bar{\nu}_\mu}$**:** The interaction cross sections for ν_e and $\bar{\nu}_e$ are not currently precisely measured with near-detector data, although they may be more precisely measured in the Hyper-K era. When extrapolating the measured ν_μ and $\bar{\nu}_\mu$ rates from the near detectors to predict the ν_e and $\bar{\nu}_e$ appearance rates at the far detector, it is necessary to assign an uncertainty on the interaction cross section ratios $\sigma_{\nu_e}/\sigma_{\nu_\mu}$ and $\sigma_{\bar{\nu}_e}/\sigma_{\bar{\nu}_\mu}$. Here, the T2K approach based on the work of Day and McFarland [43] is taken. Separate normalization parameters are assigned to vary σ_{ν_e} and $\sigma_{\bar{\nu}_e}$. The correlation between these parameters is assigned assuming there is a 2% systematic effect that is uncorrelated between neutrinos and antineutrinos and an additional 2% systematic effect with anticorrelation between neutrinos and antineutrinos.
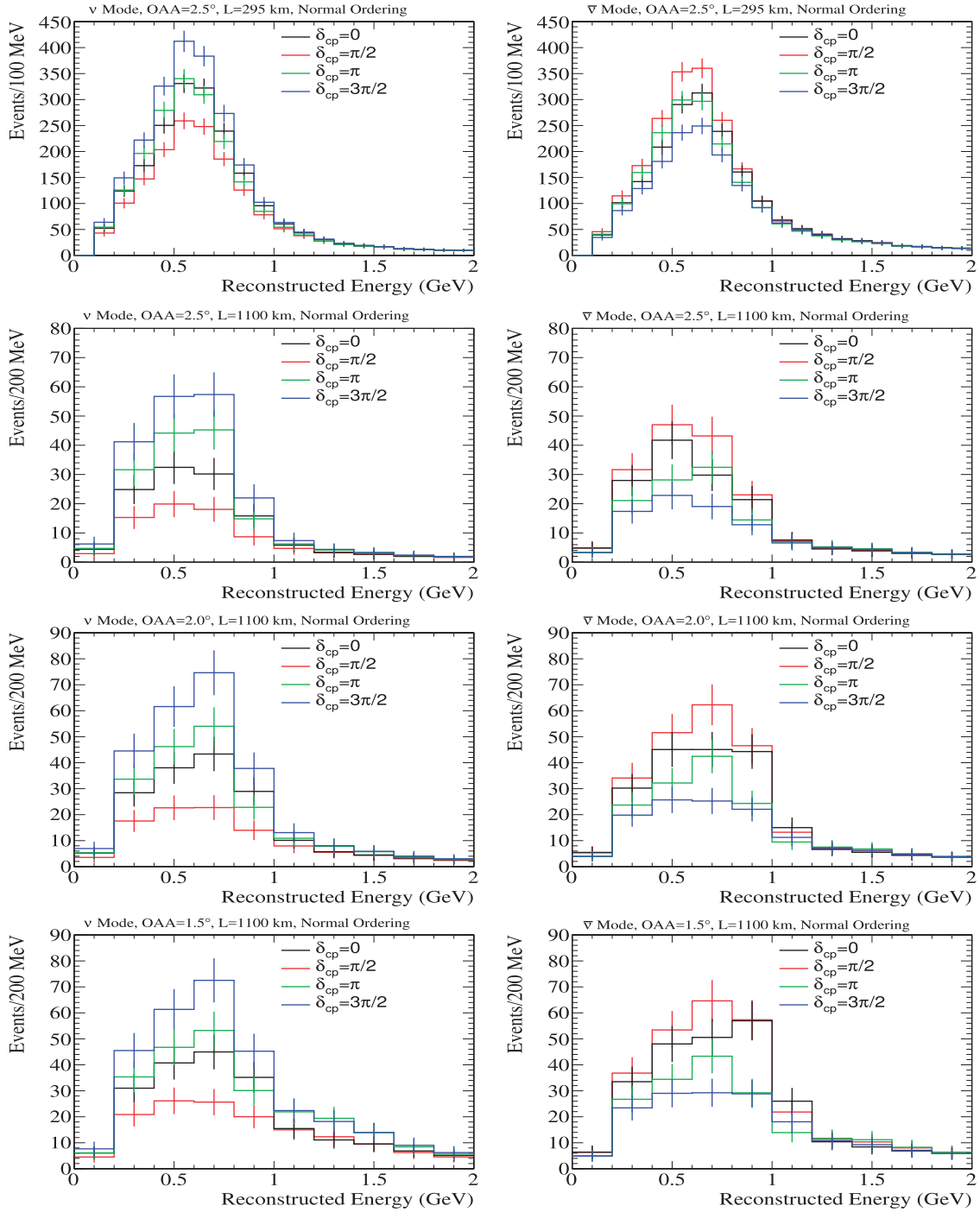
Fig. 15. The predicted 1Re spectra in neutrino mode (left) and antineutrino mode (right) for different values of δ_{CP}. The error bars represent statistical errors only.

○ **Energy scale at the far detectors:** The energy scale at Super-K is calibrated using samples of Michel electrons, π^0s, and stopping cosmic muons. In T2K oscillation analyses, the energy scale error is found to be 2.4% [39]. Here, a 2.4% energy scale uncertainty is applied to the reconstructed energy for events in Hyper-K and the Korean detector. Independent parameters with no correlation are used for Hyper-K and the Korean detector. It is assumed that there is 100% correlation between the 1Rμ and 1Re samples.
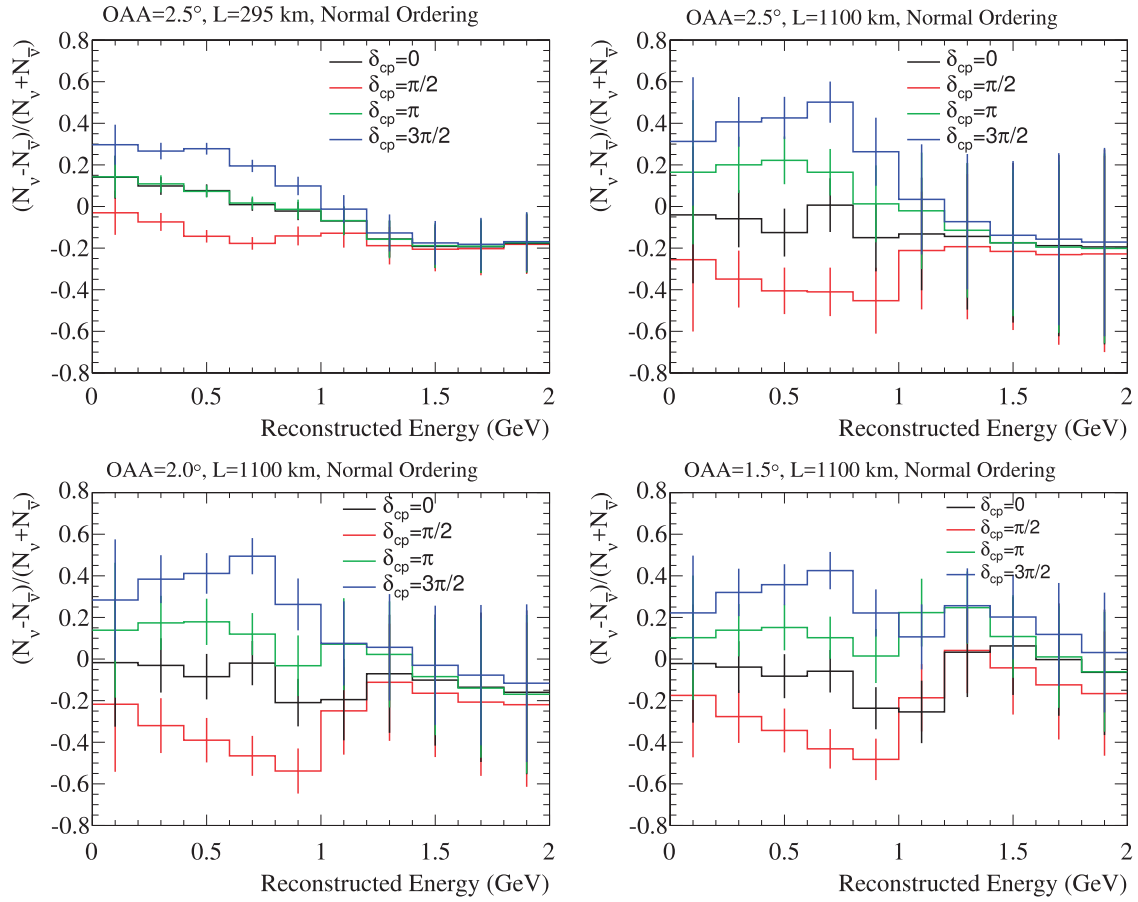
Fig. 16. The event rate asymmetry between neutrino mode and antineutrino mode for variations of δ_{CP} at different detector site locations. The error bars represent statistical errors only.

Table 5. The statistical separation of the predicted maximally CP-violating spectra from the predicted CP-conserving spectrum. Here the significance is calculated for both CP-conserving hypotheses, and the smallest significance is shown. The mass ordering is assumed to be known.

Detector location	Significance (σ)			
	NH		IH	
OAA, L	$\delta_{CP} = \pi/2$	$\delta_{CP} = 3\pi/2$	$\delta_{CP} = \pi/2$	$\delta_{CP} = 3\pi/2$
2.5°, 295 km	11.6	11.0	11.8	10.9
2.5°, 1100 km	6.1	4.9	6.5	4.9
2.0°, 1100 km	7.9	5.9	7.1	6.3
1.5°, 1100 km	6.9	5.3	5.9	5.7

○ **Matter density:** For the results presented here, a constant matter density of $3.0\,\mathrm{g\,cm^{-3}}$ is assumed for the path to the Korean detector. An uncertainty of 6% is assigned based on previous estimates [37].

○ **The NCπ^+ background:** NCπ^+ interactions are a significant background in the 1Rμ samples. Based on the approach taken by T2K [39], a 30% error is applied here.

○ **The intrinsic $\nu_e(\bar{\nu}_e)$ and NCπ^0 backgrounds:** The backgrounds for the 1Re samples are the intrinsic $\nu_e(\bar{\nu}_e)$ in the beam and NCπ^0 interactions mistaken for an electron. It is expected that

OAA=1.5°, L=1100 km

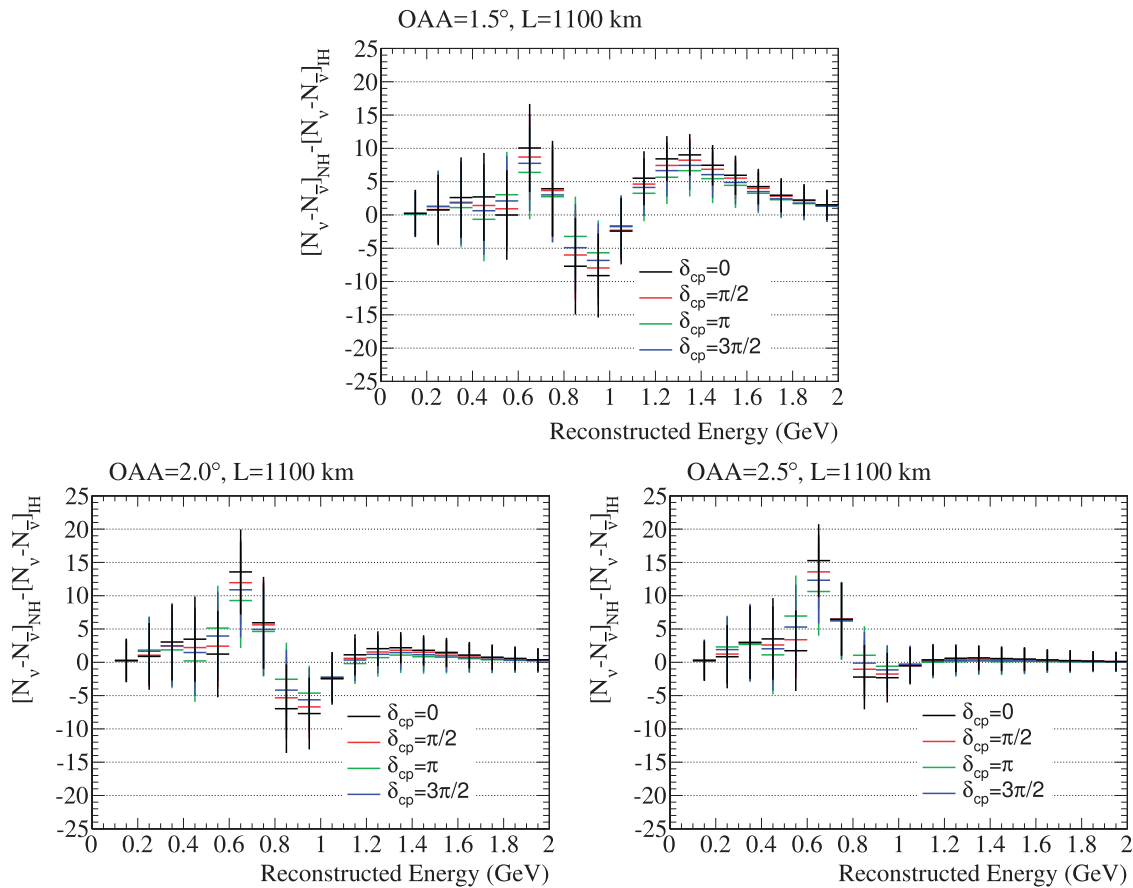
OAA=2.0°, L=1100 km

OAA=2.5°, L=1100 km

Fig. 17. The difference of the observed neutrino–antineutrino difference in the 1Re samples for normal mass ordering relative to the expected differences for inverted mass ordering. The error bars are the propagated statistical errors for the neutrino-mode and antineutrino-mode 1Re samples.

these backgrounds will be measured by an intermediate water-Cherenkov detector with similar $\nu_e(\bar{\nu}_e)$ and total fluxes to the far detector fluxes. The fluxes are similar since the oscillation effect on $\nu_e(\bar{\nu}_e)$ is ~5%, and oscillations do not affect the neutral current event rate. Studies of this measurement with the NuPRISM detector show an expected statistical error of 3%. A total error of 5% is considered to account for uncertainties in the different efficiency and fluxes between the near and far detectors. It is assumed that there is 100% correlation between Hyper-K and the Korean detector, but no correlation is assumed between the neutrino and antineutrino beam modes.

○ **The CC non-quasielastic fraction:** The fraction of non-quasielastic interactions in the candidates' samples affects the predicted normalization and reconstructed energy distribution. In T2K near-detector fits, the normalization of the non-quasielastic 2p–2h component of the cross section is fitted with a 20% error [40]. The 2p–2h interactions are sometimes called multi-nucleon interactions, and they consist of interactions on correlated pairs of nucleons rather than a single nucleon. T2K models these interactions based on the work of Nieves et al. [41,42]. Here, a 20% error is applied to the normalization of the non-quasielastic interactions, which includes 2p–2h events, as well as events where a pion is produced but is absorbed before exiting the nucleus. An anticorrelated parameter is applied to the quasielastic interactions, and its error is chosen such that the normalization of the unoscillated event rate is
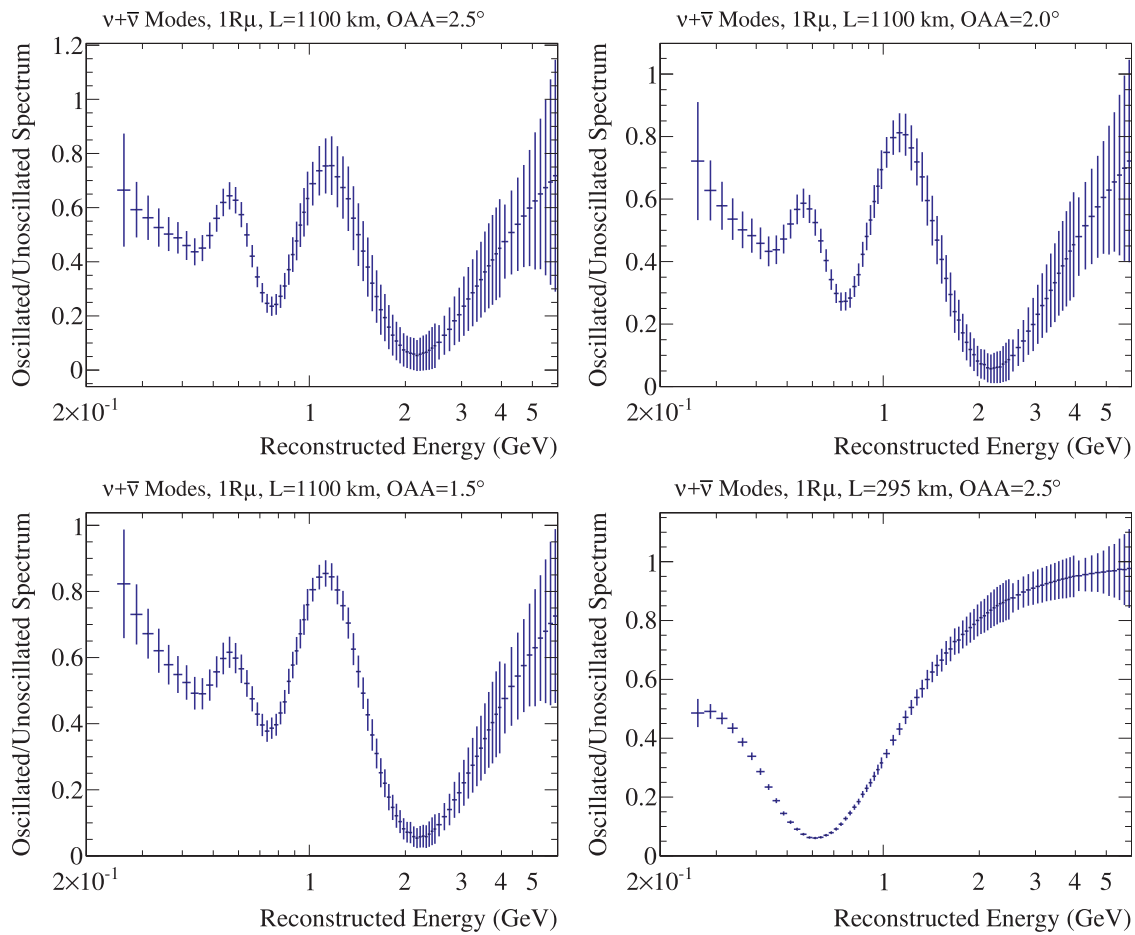
Fig. 18. The ratio of the predicted 1Rμ spectrum with oscillations to the predicted 1Rμ spectrum without oscillations. Here, the neutrino-mode and antineutrino-mode data have been summed. The bin width varies from 25 MeV at low energy to 100 MeV at high energy, and the errors on each bin represent the statistical error for that bin.

conserved for variations of these parameters. This approach models the effect of the near-detector constraint.

○ **Near to far extrapolation:** The T2K oscillation analysis [39] accounts for an uncertainty from the flux and cross section model parameters that are constrained by the near-detector data. This error includes the near-detector measurement error and extrapolation uncertainties in the flux and cross section models that arise due to different neutrino fluxes and detector acceptances at the near and far detectors. To model this uncertainty, the T2K errors are applied as an overall uncertainty on the charged current event rate. In principle, the extrapolation error includes the effect of the previously described uncertainty on the non-quasielastic fraction. To avoid double counting the error on the non-quasielastic fraction, the T2K errors are corrected by subtracting in quadrature the normalization uncertainty that is explicitly calculated from the non-quasielastic uncertainty.

○ **Far detector modeling:** In addition to the energy scale uncertainty, there are uncertainties related to the modeling of efficiencies in the far detector. This uncertainty is estimated based on the uncertainty evaluated for T2K. Since the far detector efficiency model is tuned using atmospheric neutrino control samples, it is assumed that the uncertainty will be reduced with

the larger sample of atmospheric neutrinos available in Hyper-K. For the studies presented here, the assumption is that 50% of the error is reduced by a factor of $1/\sqrt{8.3}$, where 8.3 is the fiducial mass ratio between Hyper-K and Super-K. The remaining 50% of the error remains unchanged under the assumption that perfect agreement between the detector model and control samples may not be achieved and systematic errors may be applied to cover any disagreement. For this error source, there are no correlations between Hyper-K and the Korean detector.

For the purpose of this document, the above systematic error model is used in place of the model adopted for the Hyper-K design report. This is done because the systematic errors used in the Hyper-K design report are based on the T2K systematic error estimate for a 2.5° off-axis angle flux and a 1Re sample with a $E_{\rm rec} < 1.25\,{\rm GeV}$ cut applied. The T2K systematic error model has not yet been applied to the other off-axis angle positions and 1Re samples with the reconstructed energy cut removed.

The effects of systematic errors propagated to the normalization uncertainties on the 1Rμ and 1Re samples are summarized in Table 6. The normalization uncertainties for individual samples are in the 4%–5% range. These uncertainties are slightly more conservative than those presented in the Hyper-K design report, which included a total systematic error between 3% and 4% depending on the sample. The uncertainties for the more on-axis detector locations appear marginally smaller because the broader spectrum tends to average over shape uncertainties more. The uncertainties as a fraction of the total predicted event rate and as a function of reconstructed energy are shown in Fig. 19. Here, the most prominent feature is the large uncertainty in the 1–3 GeV region of the 1Rμ samples for the detector at $L = 1100\,{\rm km}$. This energy range is the location of the first oscillation maximum and the large uncertainty arises from energy scale and non-quasielastic fraction uncertainties that can cause feed-down or feed-up (in the case of energy scale) into the region of the oscillation maximum.

The relationship between systematic uncertainties and the physics sensitivity with a Korean detector can be better understood by investigating a specific measurement, the precision measurement of $\delta_{\rm CP}$ when $\delta_{\rm CP}$ is near a maximally CP-violating value of $\pi/2$ or $3\pi/2$. Near these values, the derivative of $\sin(\delta_{\rm CP})$ approaches zero, degrading the sensitivity to the CP-odd term in the oscillation probability. Here, the CP-even term, which depends on $\cos(\delta_{\rm CP})$, may contribute to the precision measurement of the phase. Figure 20 shows the changes to the spectra for a change in a $\delta_{\rm CP}$ by $+13°$ from an initial value of $\pi/2$ for the Hyper-K detector. Here, 13° is chosen since it is expected to be the ultimate precision of Hyper-K after a $10\,{\rm yr} \times 1.3\,{\rm MW}$ exposure with two tanks. It can be seen that the change to $\delta_{\rm CP}$ by 13° largely affects the spectrum through the $\cos(\delta_{\rm CP})$ term, causing a downward shift in energy with little change to the overall normalization. Figure 20 also shows the effect of an energy scale shift by -0.5% for comparison. The energy scale shift has a similar effect on the spectrum, indicating that even a 0.5% uncertainty on the energy scale can degrade the $\delta_{\rm CP}$ precision near maximally CP-violating values.

The Korean detector is constraining $\delta_{\rm CP}$ with a significant number of events at the second and third oscillation maxima. Near the second oscillation maximum, the effect of the CP-odd interference term in the oscillation probability is three times larger, and for the same shift in $\delta_{\rm CP}$, the CP-odd effect may be observable. Figure 21 shows the spectrum ratios for the Korean detector at 1100 km baseline and 1.5° off-axis. Here, the effect of both the CP-even terms can be seen in the increased rate from 1.3 GeV and above for both neutrino and antineutrino modes. The CP-odd term causes an

Table 6. Percentage error on the normalization of the predicted 1Rμ and 1Re samples in neutrino and antineutrino mode for each systematic error source. The error on the ratio of neutrino mode to antineutrino mode is also shown for 1Re since this uncertainty is relevant for the detection of a CP asymmetry.

	Percent error (%)				
Error source	ν 1Rμ	$\bar{\nu}$ 1Rμ	ν 1Re	$\bar{\nu}$ 1Re	(ν 1Re)/($\bar{\nu}$ 1Re)
OAA=2.5°, $L = 1100$ km					
$\sigma_{\nu_e}/\sigma_{\nu_\mu}$, $\sigma_{\bar{\nu}_e}/\sigma_{\bar{\nu}_\mu}$	0.00	0.00	2.10	1.68	3.12
Energy scale	0.02	0.02	0.01	0.01	0.01
Matter density	0.04	0.08	0.43	0.09	0.53
NCπ^+ background	1.28	1.25	0.00	0.00	0.00
ν_e & NCπ^0 background	0.00	0.00	1.32	1.41	1.88
CC non-QE fraction	2.76	1.88	1.98	1.29	2.35
Extrapolation	2.70	2.60	2.44	3.06	1.95
Far detector model	2.64	2.64	2.08	2.08	0.00
Total	4.69	4.16	4.54	4.47	4.86
OAA=2.0°, $L = 1100$ km					
$\sigma_{\nu_e}/\sigma_{\nu_\mu}$, $\sigma_{\bar{\nu}_e}/\sigma_{\bar{\nu}_\mu}$	0.00	0.00	2.01	1.67	3.07
Energy scale	0.02	0.01	0.01	0.01	0.01
Matter density	0.02	0.06	0.55	0.12	0.67
NCπ^+ background	1.47	1.29	0.00	0.00	0.00
ν_e & NCπ^0 background	0.00	0.00	1.26	1.29	1.76
CC non-QE fraction	0.87	0.82	1.24	0.76	1.51
Extrapolation	2.68	2.68	2.38	3.00	1.92
Far detector model	2.64	2.64	2.08	2.08	0.00
Total	3.89	3.83	4.18	4.27	4.39
OAA=1.5°, $L = 1100$ km					
$\sigma_{\nu_e}/\sigma_{\nu_\mu}$, $\sigma_{\bar{\nu}_e}/\sigma_{\bar{\nu}_\mu}$	0.00	0.00	1.72	1.41	2.67
Energy scale	0.01	0.01	0.01	0.01	0.01
Matter density	0.01	0.06	0.24	0.28	0.53
NCπ^+ background	1.61	1.30	0.00	0.00	0.00
ν_e & NCπ^0 background	0.00	0.00	1.42	1.37	1.93
CC non-QE fraction	0.44	0.30	0.52	0.37	0.75
Extrapolation	2.67	2.60	2.23	2.88	1.84
Far detector model	2.64	2.64	2.08	2.08	0.00
Total	3.83	3.81	3.84	4.11	3.91
OAA=2.5°, $L = 295$ km					
$\sigma_{\nu_e}/\sigma_{\nu_\mu}$, $\sigma_{\bar{\nu}_e}/\sigma_{\bar{\nu}_\mu}$	0.01	0.00	2.44	1.82	3.53
Energy scale	0.04	0.03	0.42	0.63	0.21
Matter density	—	—	—	—	—
NCπ^+ background	2.33	1.79	0.00	0.00	0.00
ν_e & NCπ^0 background	0.00	0.00	0.94	1.22	1.51
CC non-QE fraction	1.68	1.72	2.07	1.00	2.25
Extrapolation	2.60	2.56	2.51	3.05	1.96
Far detector model	2.64	2.64	2.08	2.08	0.00
Total	4.13	4.15	4.71	4.47	4.90
OAA=2.5°, $L = 295$ km (Hyper-K design report)					
Total	3.6	3.6	3.2	3.9	—

asymmetry in the normalization of the neutrino-mode and antineutrino-mode samples below 1 GeV. These effects cannot be reproduced with a small variation of the energy scale parameter, as is the case for Hyper-K. This study shows that the constraint on δ_{CP} near $\delta_{CP} = \pi/2, 3\pi/2$ is sensitive to different systematic errors for Hyper-K and the Korean detector. It also shows that the fractional
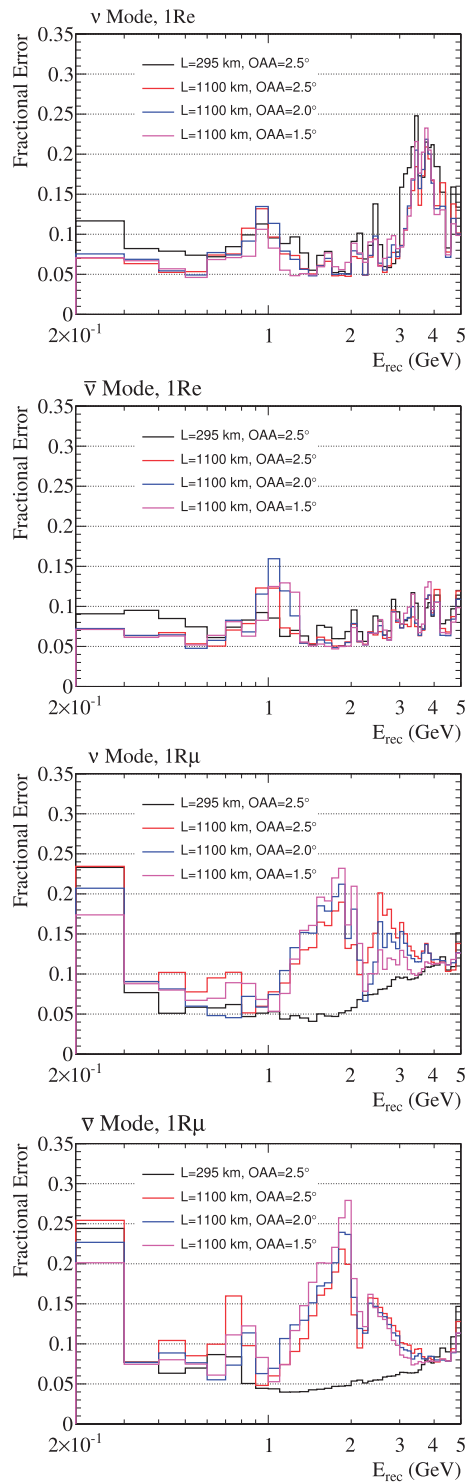
Fig. 19. The fractional systematic errors per bin on the predicted spectra binned in reconstructed energy.

change to the spectrum from the δ_{CP} variation is larger for the detector at a longer baseline, suggesting that the measurement is less likely to be systematics limited. The full impact of the Korean detector on the δ_{CP} precision will be shown in the following section, where the physics sensitivities are presented.
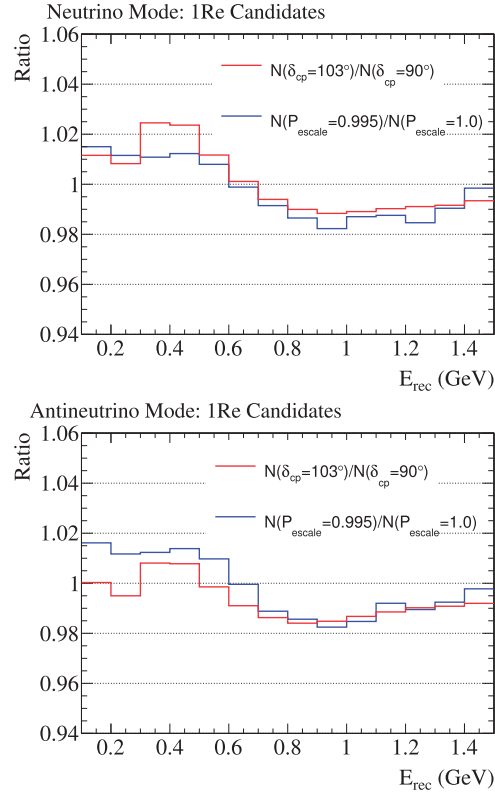
Neutrino Mode: 1Re Candidates

Antineutrino Mode: 1Re Candidates

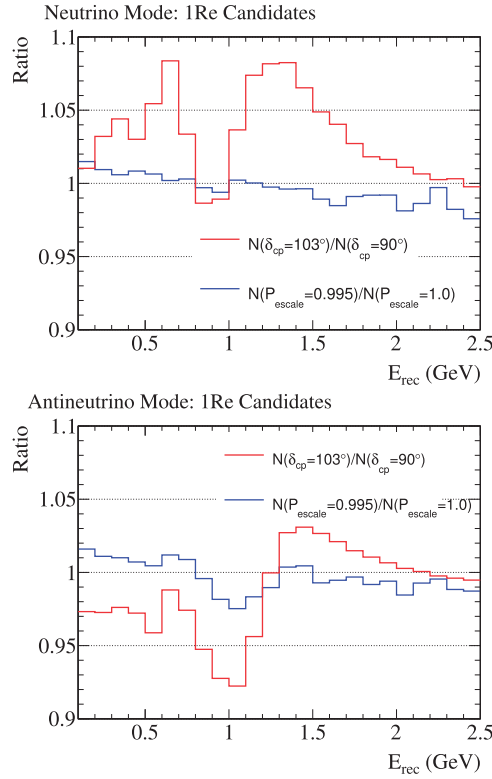**Fig. 20.** The ratios to nominal predicted spectra ($\delta_{CP} = \pi/2$) for a δ_{CP} shift of $+13°$ and an energy scale shift of -0.5%. The ratios are shown for the 1Re samples in neutrino mode (top) and antineutrino mode (bottom). The ratios are calculated for the Hyper-K detector at 295 km and 2.5° off-axis.

4.3.   Impact of the Korean detector on physics results

For the physics sensitivity studies presented here, it is assumed that one or two 187 kt detectors will be operated for ten years (10×10^7 s) at 1.3 MW beam power, corresponding to 27×10^{21} protons on target. For the initial studies, five configurations are considered:

- **JD×1:** A single detector is located in Japan at the Tochibora site with a baseline of 295 km and an off-axis angle of 2.5°.
- **JD×2:** Two detectors are located in Japan at the Tochibora site with a baseline of 295 km and an off-axis angle of 2.5°.
- **JD+KD at 2.5°:** One detector is located in Japan at a baseline of 295 km and an off-axis angle of 2.5°, while the second is located in Korea at a baseline of 1100 km and an off-axis angle of 2.5°.
- **JD+KD at 2.0°:** One detector is located in Japan at a baseline of 295 km and an off-axis angle of 2.5°, while the second is located in Korea at a baseline of 1100 km and an off-axis angle of 2.0°.
- **JD+KD at 1.5°:** One detector is located in Japan at a baseline of 295 km and an off-axis angle of 2.5°, while the second is located in Korea at a baseline of 1100 km and an off-axis angle of 1.5°.

Later in this section, the sensitivities for the Mt. Bisul site ($L = 1084$ km and OAA=1.3°) and the Mt. Bohyun site ($L = 1043$ km and OAA=2.3°) will also be presented.

Fig. 21. The ratios to nominal predicted spectra ($\delta_{CP} = \pi/2$) for a δ_{CP} shift of $+13°$ and an energy scale shift of -0.5%. The ratios are shown for the 1Re samples in neutrino mode (top) and antineutrino mode (bottom). The ratios are calculated for the Korean detector at 1100 km and 1.5° off-axis.

The initial physics sensitivity studies focus on three measurements: the determination of the mass ordering, the discovery of CP violation through the exclusion of the $\sin(\delta_{CP}) = 0$ hypothesis, and the precision measurement of δ_{CP}. In all cases, the sensitivities are evaluated on pseudo-data generated with the following true oscillation parameter values:

- $|\Delta m^2_{32}| = 2.5 \times 10^{-3} \, \text{eV}^2$
- $\sin^2 \theta_{23} = 0.5$
- $\sin^2 \theta_{13} = 0.0219$
- $\Delta m^2_{21} = 7.53 \times 10^{-5} \, \text{eV}^2$
- $\sin^2 \theta_{12} = 0.304$.

The pseudo-data are also generated for multiple values of δ_{CP} and both mass orderings, and the sensitivities are presented as a function of the true value of δ_{CP} and the mass ordering. In the fits to the pseudo-data, Δm^2_{32}, $\sin^2 \theta_{23}$, and δ_{CP} are free parameters with no prior constraints. $\sin^2 \theta_{13}$, $\sin^2 \theta_{12}$, and Δm^2_{21} also vary in the fits, but they have prior Gaussian constraints with 1 σ uncertainties of 0.0012, 0.041, and $0.18 \times 10^{-5} \, \text{eV}^2$, respectively. The prior uncertainties on these parameters are taken from the 2015 edition of the PDG Review of Particle Physics [38]. The systematic parameters described in the previous section are also allowed to vary as nuisance parameters in the fit within their prior constraints. In all cases, the sensitivities are evaluated on the fit to the so-called Asimov set, where the prediction for each sample is made for the nominal values of the oscillation parameters and systematic parameters, and no statistical variations are applied. All four samples (neutrino-mode 1Re, 1Rμ and antineutrino-mode 1Re, 1Rμ) are used to construct a binned likelihood, and the

product of the pseudo-data likelihood is taken with the Gaussian priors for constrained oscillation parameters and systematic parameters to construct the full likelihood, L. To simplify the notation, we write $-2\log(L)$ as $\Delta\chi^2$.

The test statistic used for the mass ordering determination is:

$$\sqrt{\Delta\chi^2_{\mathrm{MH}}} = \sqrt{\chi^2_{\mathrm{WH}} - \chi^2_{\mathrm{CH}}}. \tag{5}$$

Here, χ^2_{WH} and χ^2_{CH} are the best-fit $-2\log(L)$ for the wrong and correct mass hierarchies, respectively. In the Gaussian limit, the test parameter can be interpreted as the significance of the mass ordering determination. Here, sensitivities are shown for the Hyper-K accelerator neutrinos only and do not account for the additional constraint from Hyper-K atmospheric neutrinos.

The test statistic used for the CP violation discovery potential is:

$$\sqrt{\Delta\chi^2_{\mathrm{CPV}}} = \sqrt{\min[\chi^2_{\mathrm{BF}}(\delta_{\mathrm{CP}} = 0), \chi^2_{\mathrm{BF}}(\delta_{\mathrm{CP}} = \pi)] - \chi^2_{\mathrm{BF}}}. \tag{6}$$

Here, $\chi^2_{\mathrm{BF}}(\delta_{\mathrm{CP}} = 0)$ and $\chi^2_{\mathrm{BF}}(\delta_{\mathrm{CP}} = \pi)$ are the best-fit $-2\log(L)$ where δ_{CP} is fixed to one of the CP-conserving values. The minimum of these two is used for the test statistic. χ^2_{BF} is the best-fit minimum of $-2\log(L)$ where δ_{CP} is allowed to vary. Two cases are treated for the CP violation studies. In the first case, the mass ordering is assumed to be known based on external measurements and the measurement using the Hyper-K atmospheric neutrinos. In the second case, the constraints from external measurements and Hyper-K atmospheric neutrinos are not used, in order to estimate the sensitivity from the accelerator neutrinos alone. When the mass ordering is determined with Hyper-K accelerator neutrinos alone, the sign of Δm^2_{32} is allowed to vary in the minimization procedure. The test parameter can be interpreted as the significance to exclude the CP-conserving hypotheses.

For the evaluation of the δ_{CP} measurement precision the fitted value of δ_{CP} is scanned and the $-2\log(L)$ is minimized at each value of δ_{CP}, i.e. the profiling method. The δ_{CP} values that correspond to a one-unit change in $-2\log(L)$ relative to the minimum are taken as the bounds for the 68% confidence interval. The plotted 1σ error is the width of the 68% confidence interval divided by two.

The significances to reject the wrong mass ordering are shown in Fig. 22, and the fraction of δ_{CP} values for which a given significance is achieved is shown in Fig. 23. As is expected based on Fig. 17, the significance is largest for the configuration with the Korean detector at 1.5° off-axis since the more on-axis position gives more events in the 1–2 GeV range where the matter effect is large. For this configuration, the significance to reject the wrong mass ordering is greater than 6σ for most values of δ_{CP}, and greater than 5σ for all values of δ_{CP}. The significance of the wrong mass ordering rejection degrades as the Korean detector is moved to more off-axis locations. However, even the configuration with the 2.5° off-axis Korean detector has 3σ rejection sensitivity for most values of δ_{CP}, and improved sensitivity over the configuration with one (both) detector(s) in Japan for all (most) values of δ_{CP}. Based on this study, it is clear that the sensitivity may be improved further by adding events above 1 GeV in reconstructed energy. This may be achieved by moving to a more on-axis position (see Mt. Bisul) or by including multi-ring event reconstruction that allows the inclusion of higher-energy events with one or more detected pions. Multi-ring event reconstruction will be the topic of a future study. Based on this study of the configurations with a detector in Korea, the accelerator neutrinos can provide an alternative measurement of the mass ordering that is complementary to the measurement using atmospheric neutrinos. By combining the two measurements, an even stronger constraint can be obtained, and better sensitivity can be achieved earlier in the lifetime of Hyper-K.
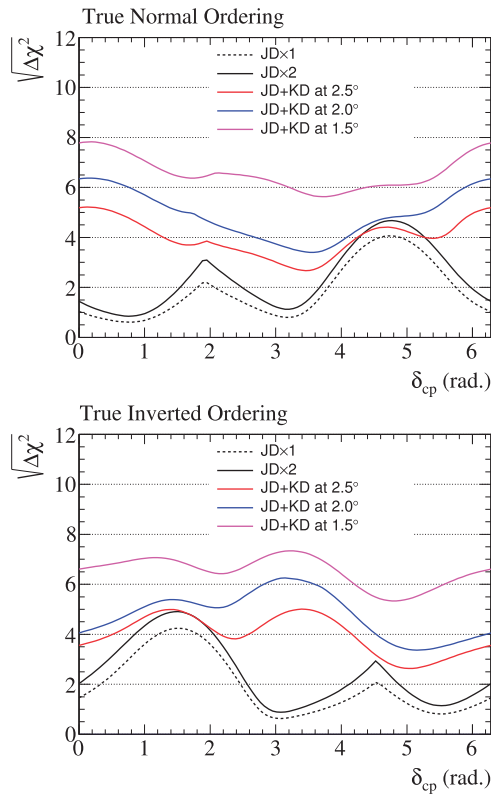
Fig. 22. The significance for the wrong mass ordering rejection as a function of the true value of δ_{CP} and the true mass ordering (top=normal, bottom=inverted).
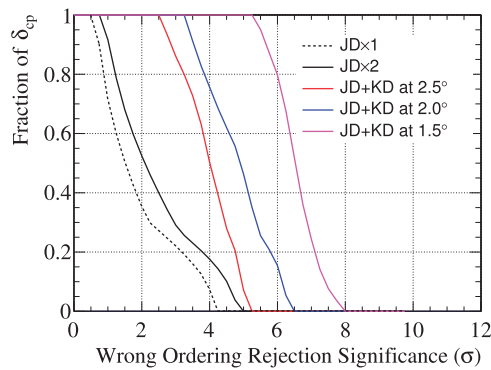

Fig. 23. The fraction of δ_{CP} values (averaging over the true mass ordering) for which the wrong hierarchy can be rejected with a given significance or greater.

The plots showing the significance to reject the CP-conserving hypotheses are in Fig. 24, and Fig. 25 shows the fraction of δ_{CP} values for which a given significance can be achieved. The fractions of true δ_{CP} values for which 3σ and 5σ sensitivity are achieved are listed in Table 7. When the mass ordering is already known, all four two-detector configurations have similar sensitivity, but the best sensitivity is available when the Korean detector is placed at $2.0°$ off-axis. It should be mentioned that in this study, it is assumed that the mass ordering is determined by external experiments and Hyper-K atmospheric neutrinos with a significance greater than the CP conservation rejection significance being studied. Compared to a single detector in Japan, the configuration with a second detector in
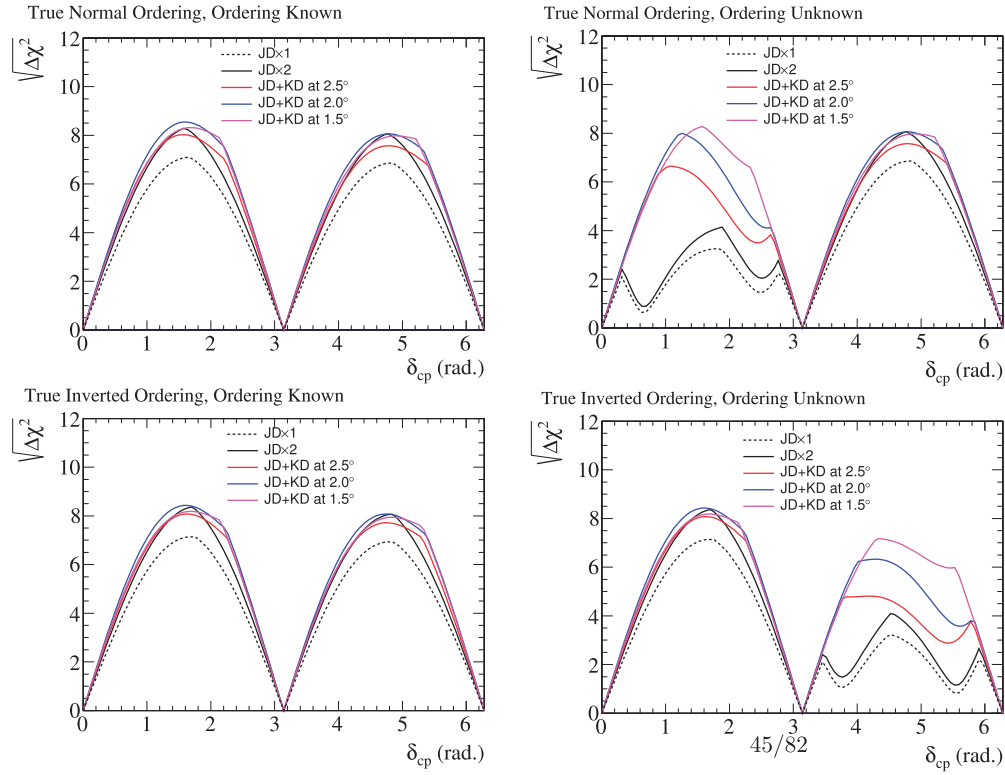
Fig. 24. The significance for CP conservation rejection as a function of the true value of δ_{CP} and the true mass ordering (left=normal, right=inverted). The top row shows the significance when the mass ordering is determined independently from the accelerator neutrinos, while the bottom row shows the significance when the mass ordering is determined only by accelerator neutrinos observed in the Hyper-K detectors.

Korea at 2.0° off-axis has 3σ (5σ) sensitivity for an additional 7%–8% (13%–14%) of δ_{CP} values depending on the mass ordering. When the mass ordering is only determined by the accelerator neutrinos, the configuration with the Korean detector at 1.5° off-axis gives the largest fraction of true δ_{CP} values for which a 5σ discovery is possible. This is true because this configuration has the best sensitivity to determine the mass ordering, breaking the mass ordering–δ_{CP} degeneracy. For the case with the 1.5° off-axis configuration, the dependence of the CP violation discovery sensitivity on the relative fraction of antineutrino-mode to neutrino-mode operation has been evaluate for ratios ranging from 3 : 1 (default) to 1 : 3. The fraction of δ_{CP} values with a 5σ discovery changes by only 0.01 depending on the relative fraction of antineutrino-mode and neutrino-mode operation.

The evolution of the CP violation discovery potential with exposure is summarized in Fig. 26. At a 20 yr×1.3 MW exposure, the presence of the Korean detector can increase the fraction of δ_{CP} values for which a 5σ discovery is possible by up to 8%. This is a 27% reduction in the number of δ_{CP} values for which a 5σ discovery of CP violation would not be possible.

The δ_{CP} measurement precision is shown in Fig. 27, and Fig. 28 shows the fraction of δ_{CP} values for which a given level of precision can be achieved. The configurations with the Korean detector give the best δ_{CP} precision on average. Near the CP-conserving values, the configurations with the 2.0° and 1.5° off-axis Korean detectors have similar precision. However, near the maximally CP-violating values of δ_{CP} the 1.5° off-axis configuration has 1.5° better precision for δ_{CP} than the 2.0° off-axis configuration. The configuration with the 1.5° off-axis Korean detector also improves on
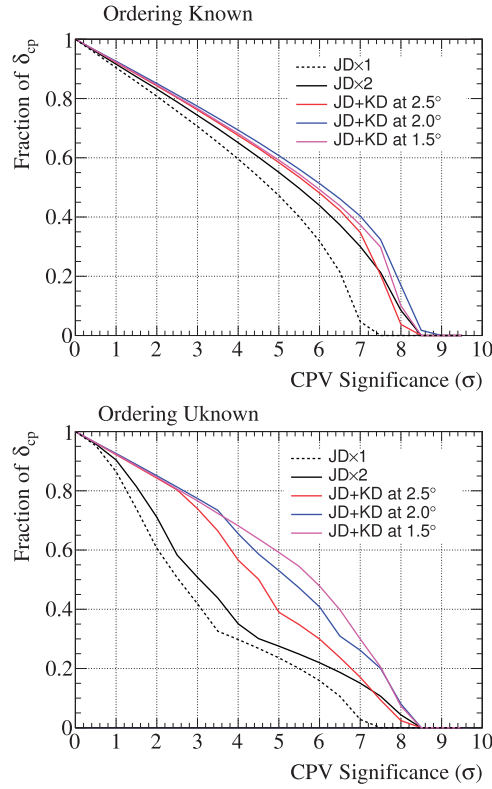
Fig. 25. The fraction of δ_{CP} values (averaging over the true mass ordering) for which the CP-conserving values can be rejected with a given significance or greater. The top figure shows the significance when the mass ordering is determined independently from the accelerator neutrinos, while the bottom figure shows the significance when the mass ordering is determined only by accelerator neutrinos observed in the Hyper-K detectors.

Table 7. The fraction of true δ_{CP} values for which CP violation can be discovered at 3σ or 5σ.

	True NH, known		True IH, known		True NH, unknown		True IH, unknown	
	3σ	5σ	3σ	5σ	3σ	5σ	3σ	5σ
JD×1	0.70	0.47	0.71	0.48	0.43	0.23	0.41	0.24
JD×2	0.74	0.55	0.74	0.55	0.52	0.27	0.50	0.28
JD+KD at 2.5°	0.76	0.58	0.76	0.59	0.76	0.48	0.72	0.30
JD+KD at 2.0°	0.78	0.61	0.78	0.61	0.77	0.55	0.79	0.51
JD+KD at 1.5°	0.77	0.59	0.77	0.59	0.77	0.59	0.77	0.59

the precision of the configuration with two detectors in Japan by 3° near the maximally CP-violating values of δ_{CP}. The precision for the configuration with two detectors in Japan is 3° better than what is presented in the Hyper-K design report. An improved sensitivity is expected since the Hyper-K design report assumes a staged approach with the second detector starting operation after six years, while these studies assume that both detectors start operation simultaneously.

The evolution of the δ_{CP} precision with exposure is summarized in Fig. 29. For the worst-case uncertainty, when δ_{CP} is near the maximally CP-violating values, the relative advantage of the detector in Korea remains constant with exposure. It should be noted that these conclusions depend on the systematic errors that are assumed, and may change if different levels of systematic uncertainty can be achieved.
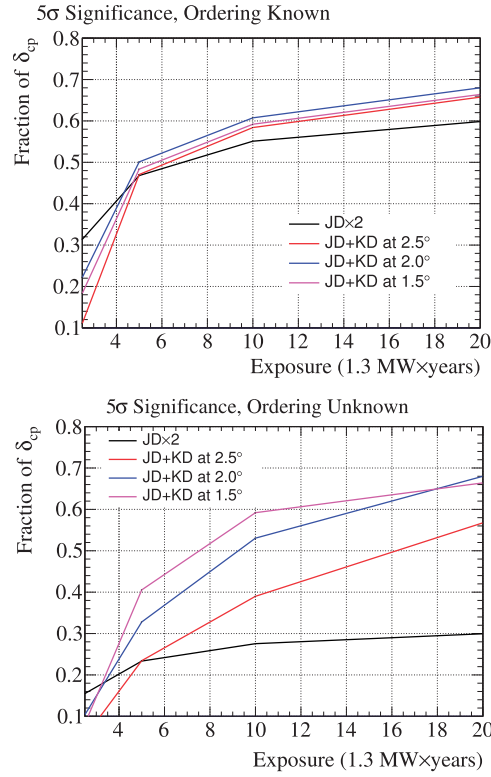
Fig. 26. The fraction of δ_{CP} values (averaging over the true mass ordering) with at least a $5\,\sigma$ significance to reject the CP-conserving values of δ_{CP}. The top figure shows the significance when the mass ordering is determined independently from the accelerator neutrinos, while the bottom figure shows the significance when the mass ordering is determined only by accelerator neutrinos observed in the Hyper-K detectors.

4.3.1.   Sensitivity studies for the Mt. Bisul and Mt. Bohyun sites

The potential Mt. Bisul site is located at a baseline of 1084 km and an off-axis angle of 1.3°. The primary effect of the off-axis angle change from 1.5° to 1.3° is to decrease the (anti)neutrino flux at 700 MeV by ∼10% while increasing the flux above 1.2 GeV by ∼50%. With these flux changes, it is expected that the Mt. Bisul location should provide better sensitivity to determine the mass ordering, while the CP violation discovery potential may be slightly degraded. The Mt. Bohyun site is located at a baseline of 1043 km and an off-axis angle of 2.3°. With a lower energy flux that more directly probes the second oscillation maximum, it is expected that Mt. Bohyun should have a slightly improved CP violation discovery sensitivity compared to the Mt. Bisul site, but will have less sensitivity to the mass ordering.

For the sensitivities presented here, the combinations of the detector in Japan with a detector at Mt. Bisul or Mt. Bohyun are shown. For comparison, the sensitivity with two detectors in Japan is shown. Here, the sensitivities are shown as a function of true δ_{CP} and the band of sensitivities shows the variation of the sensitivity for the range of true $\sin^2\theta_{23}$ values between 0.4 and 0.6.

The wrong mass ordering rejection significances including the Mt. Bisul and Mt. Bohyun configurations are shown in Fig. 30. The wrong mass ordering rejection significance is largest for the Mt. Bisul configuration for all true values of the mass ordering and δ_{CP}, and is above $6\,\sigma$ for almost all true values of the oscillation parameters. The mass ordering rejection sensitivity with the Mt. Bohyun site is above $3\,\sigma$ for almost all true values of the oscillation parameters and higher than the configuration with two detectors in Japan for most values.

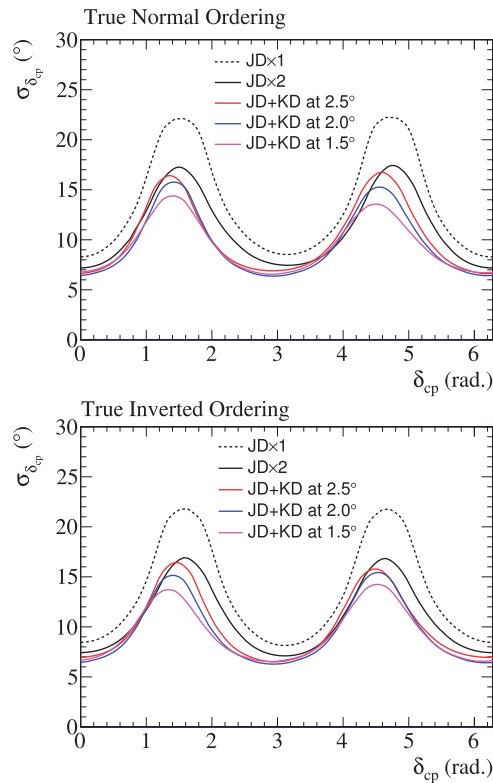**Fig. 27.** The 1σ precision of the δ_{CP} measurement as a function of the true δ_{CP} value. Here, it is assumed that there is no prior knowledge of the mass ordering.
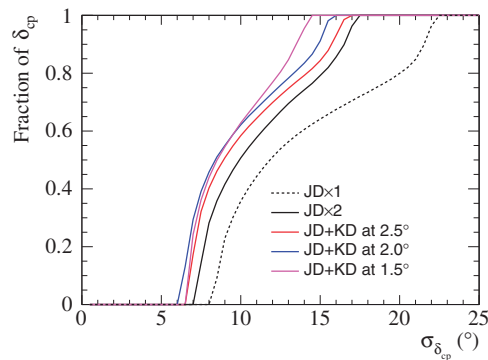
Fig. 28. The fraction of δ_{CP} values (averaging over the true mass ordering) for which a given precision or better on δ_{CP} can be achieved.

The CP conservation rejection significances including the Mt. Bisul and Mt. Bohyun configurations are shown in Fig. 31. There is little change to the fraction of δ_{CP} values with 3σ or 5σ rejection compared to the configuration with the Korean detector at 1.5° and 2.5° off-axis. For the scenarios where the mass ordering is determined by the accelerator neutrinos only, better CP conservation rejection with Mt. Bisul is achieved for some values of δ_{CP} where the improved wrong mass ordering rejection impacts the CP violation measurement.

The δ_{CP} precision is shown in Fig. 32. Near the maximally CP-violating values, the Mt. Bisul site has the best precision, indicating that the measurement is in part due to the spectrum distortion in the > 1 GeV region arising from the $\cos(\delta_{CP})$-dependent term. Near the CP-conserving values,
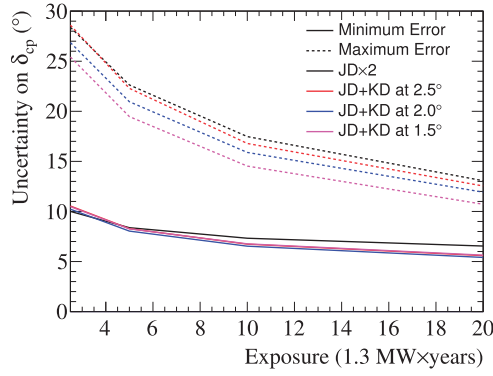
Fig. 29. The evolution of the δ_{CP} measurement precision with exposure. The "Minimum" and "Maximum" errors are the uncertainties at the true δ_{CP} and mass ordering values with the best and worst measurement resolution, respectively.
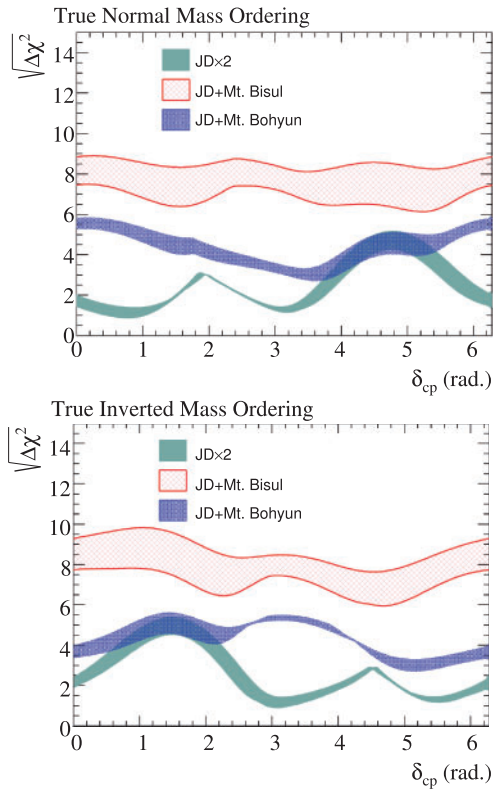
Fig. 30. The significance for the wrong mass ordering rejection as a function of the true value of δ_{CP} and the true mass ordering (top=normal, bottom=inverted). Results are shown for the Mt. Bisul and Mt. Bohyun sites. The bands represent the dependence of the sensitivity on the true value of $\sin^2 \theta_{23}$ in the range $0.4 < \sin^2 \theta_{23} < 0.6$.

the configurations with the Mt. Bisul and Mt. Bohyun sites give nearly identical precision. Both configurations with a detector in Korea show improved precision compared to the configuration with two detectors in Japan for almost all true values of the oscillation parameters.

4.3.2. *Atmospheric parameters and octant sensitivity*

The Korean detector has enhanced sensitivity for the CP violation and CP phase measurements due to the L/E dependence in the δ_{CP}-dependent interference terms of the electron (anti)neutrino appearance probability. No such enhancement is present in the leading terms of the muon (anti)neutrino
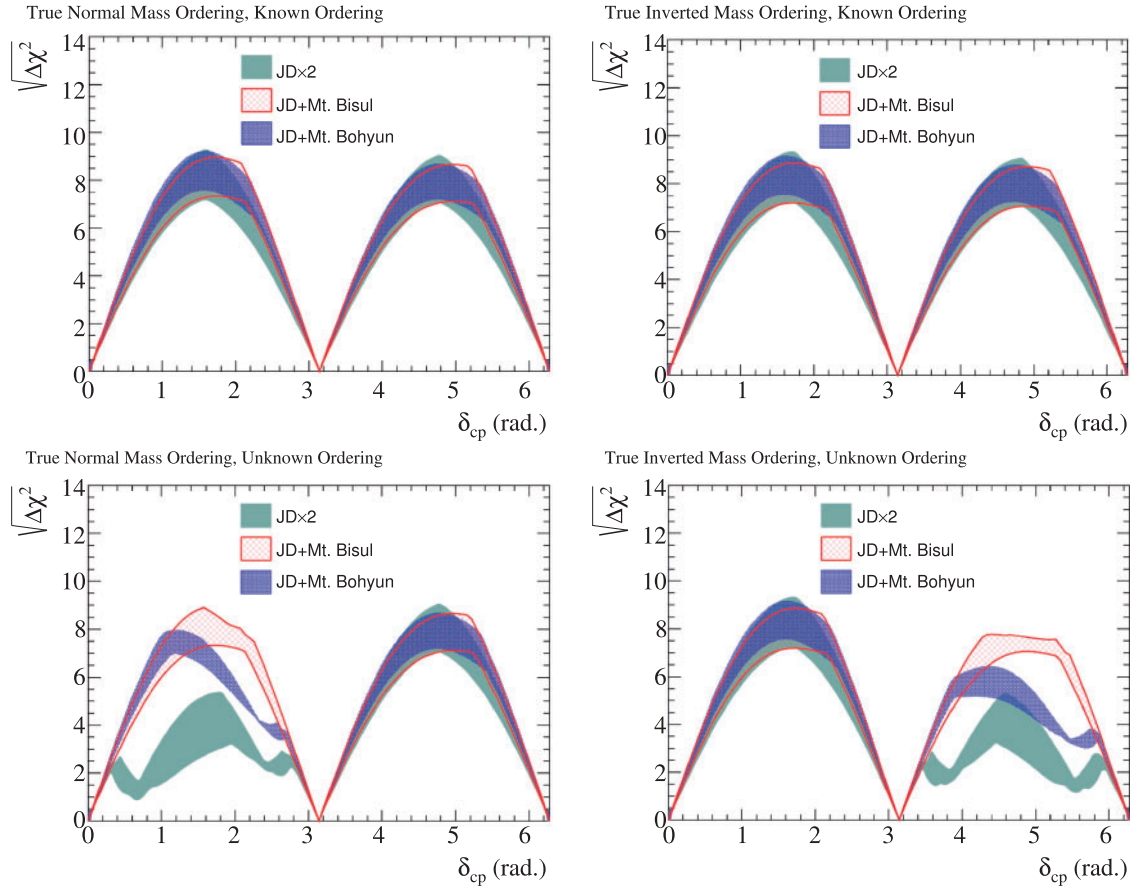
Fig. 31. The significance for CP conservation rejection as a function of the true value of δ_{CP} and the true mass ordering (left=normal, right=inverted). The top row shows the significance when the mass ordering is determined using external data and Hyper-K atmospheric neutrinos, while the bottom row shows the significance when the mass ordering is determined only by accelerator neutrinos observed in the Hyper-K detectors. Results are shown for the Mt. Bisul and Mt. Bohyun sites. The bands represent the dependence of the sensitivity on the true value of $\sin^2 \theta_{23}$ in the range $0.4 < \sin^2 \theta_{23} < 0.6$.

survival probability or the electron (anti)neutrino appearance probability. Since the leading terms in these probabilities provide the constraints on Δm_{32}^2 and $\sin^2 \theta_{23}$ we may expect no advantage for a configuration with one detector in Japan and one in Korea over a configuration with two detectors in Japan. In fact, there may be a reduced sensitivity with one detector in Korea due to the lower statistics at the longer baseline. We have studied the sensitivity to Δm_{32}^2 and $\sin^2 \theta_{23}$ as well as the θ_{23} octant determination in configurations that include detectors in Japan and Korea or detectors only in Japan.

Figure 33 shows the 2σ sensitivities for the Δm_{32}^2 and $\sin^2 \theta_{23}$ parameter determination for different true values of these parameters. There is a reduction in the sensitivity when a configuration with a Japanese and Korean detector is used relative to a configuration with two Japanese detectors, but the reduction in sensitivity is not large. Figure 34 shows the significance of the octant determination as a function of the true value of $\sin^2 \theta_{23}$ for different detector configurations. The addition of a second detector in Japan or Korea does little to improve the octant sensitivity.

From the sensitivity studies presented here, we conclude that a configuration with one detector in Japan and the second in Korea has similar but slightly worse sensitivity for atmospheric parameter determination than a configuration with two detectors in Japan. The measurement program for these
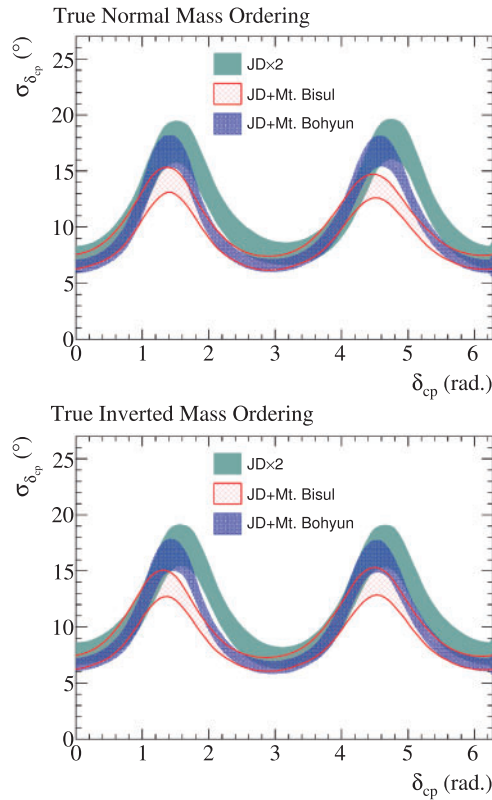
True Normal Mass Ordering

True Inverted Mass Ordering

Fig. 32. The 1σ precision of the δ_{CP} measurement as a function of the true δ_{CP} value. Results are shown for the Mt. Bisul and Mt. Bohyun sites. The bands represent the dependence of the sensitivity on the true value of $\sin^2\theta_{23}$ in the range $0.4 < \sin^2\theta_{23} < 0.6$.

parameters will not be significantly degraded in a configuration where the second detector is in Korea.

5.   Sensitivities with long-baseline and atmospheric neutrinos

In addition to neutrino data from the J-PARC beam, Hyper-K will collect atmospheric neutrino data, which will add sensitivity to its oscillation measurements. These neutrinos are produced in decays of particles emerging from the interaction of primary cosmic rays with nuclei in the atmosphere. Indeed, the production mechanism is identical to that of beam neutrinos, with the notable exception that the lack of an absorber results in a significant fraction of ν_e and $\bar{\nu}_e$ in the flux. Up to $\sim 10\,\text{GeV}$, the ratio of muon- to electron-type neutrinos is roughly $2:1$, with the fraction of muon neutrinos increasing at higher energies. Since the primary cosmic ray flux spans several orders of magnitude and is roughly isotropic about the Earth, the resulting atmospheric neutrino spectrum covers an equally wide range of energies and a given detector can expect to observe neutrinos with a variety of pathlengths from $O(10)\,\text{km}$, for neutrinos produced overhead, to $\sim 10{,}000\,\text{km}$, for those produced on the opposite side of the planet. Importantly, these events will be accumulated at both detectors in Japan and Korea in similar proportion, modulo differences in the atmospheric densities and the local geomagnetic fields.

   Though atmospheric neutrinos lack the precise timing and directional information afforded by the beam, they offer a high-statistics sample, roughly 150×10^3 events/Mton-year, with large matter effects. These matter effects provide mass hierarchy sensitivity in a manner analogous to the beam
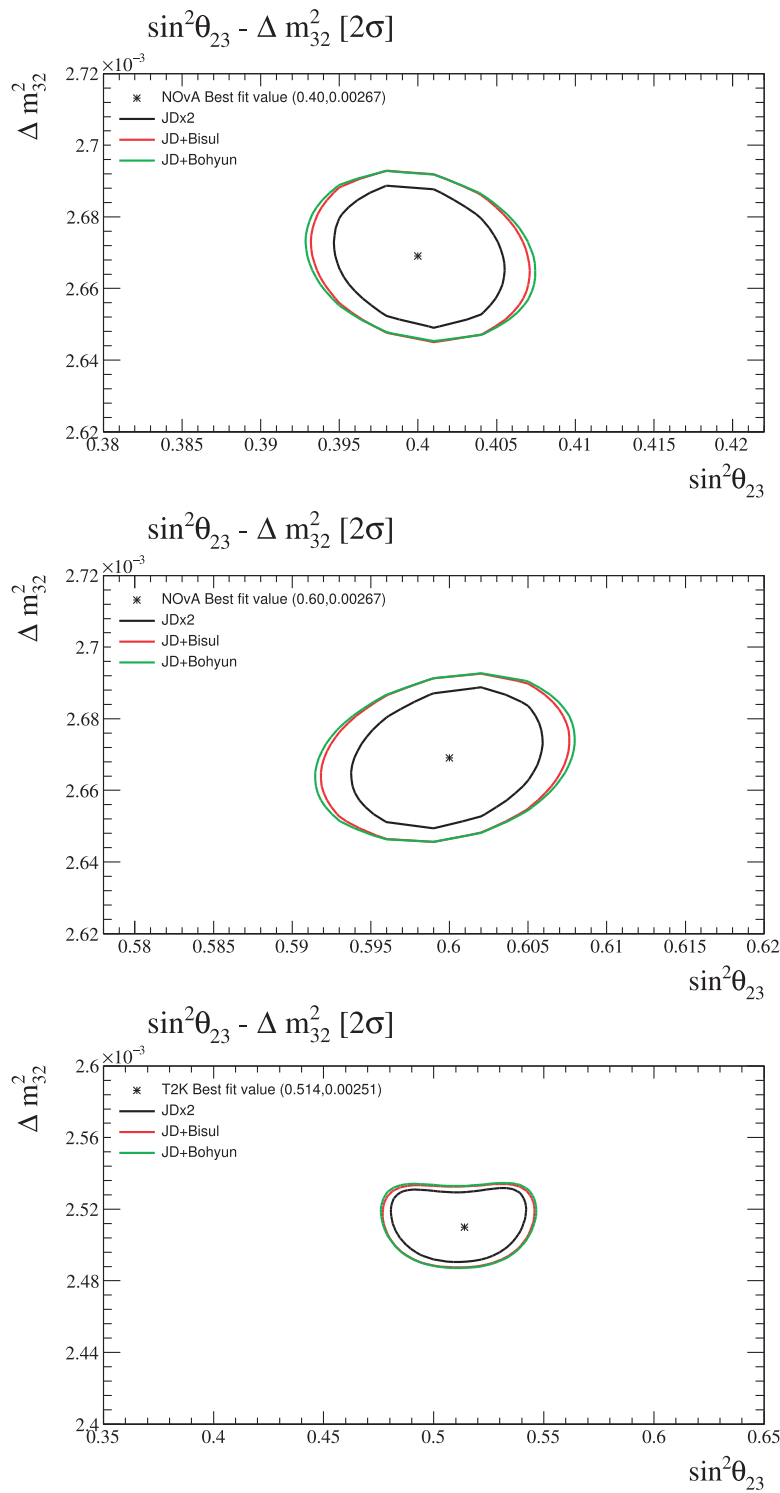
Fig. 33. Two-σ sensitivity curves for the atmospheric parameter determination at true values of $\Delta m^2_{32} = 2.67 \times 10^{-3}$ eV^2 and $\sin^2 \theta_{23} = 0.4$ (top), $\Delta m^2_{32} = 2.67 \times 10^{-3}$ eV^2 and $\sin^2 \theta_{23} = 0.6$ (middle), $\Delta m^2_{32} = 2.51 \times 10^{-3}$ eV^2 and $\sin^2 \theta_{23} = 0.514$ (bottom).

neutrinos, but more enhanced oscillations. Neutrinos traversing the core of the Earth pass through a matter profile whose density varies from 1 to 13 g cm^{-3}, which induces a parametric oscillation resonance for energies between 2 and 10 GeV. For neutrinos experiencing this effect the $\nu_\mu \rightarrow \nu_e$ (appearance channel) oscillation probability can be as large as 50% (Fig. 35). This effect depends on
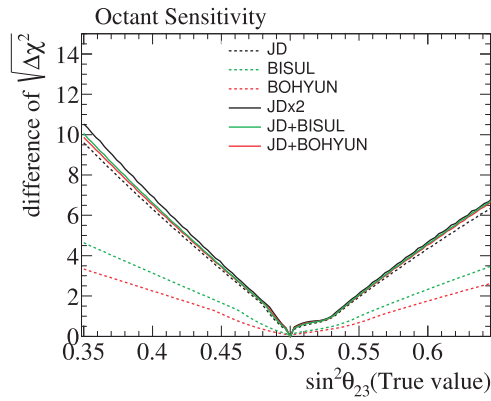
Fig. 34. The significance of the octant determination as a function of the true value of $\sin^2 \theta_{23}$ for different detector configurations.
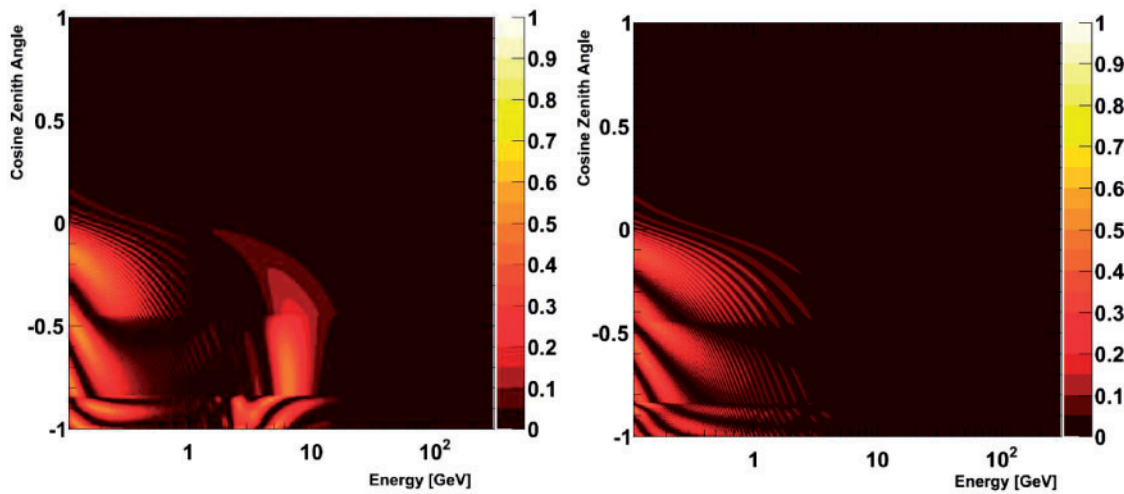
Fig. 35. Atmospheric neutrino oscillation probabilities as a function of energy and cosine of the neutrino zenith angle (-1 corresponds to upward-going). The left (right) plot shows the $\nu_\mu \rightarrow \nu_e$ ($\bar{\nu}_\mu \rightarrow \bar{\nu}_e$) probability. In this plot the normal mass hierarchy is assumed. For an inverted hierarchy the features in the neutrino plot move to the antineutrino plot and vice versa.

both the sign of the mass hierarchy and whether the neutrino is a particle or antiparticle; for a normal (inverted) mass hierarchy only neutrinos (antineutrinos) undergo these oscillations. Sensitivity to the mass hierarchy is obtained by studying the upward-going electron neutrino event rate in this energy region. It should be noted that this sample will provide a test of the mass hierarchy largely independent of the beam measurement.

Resonant oscillations in the Earth also depend on the value of $\sin^2 \theta_{23}$. Not only does it affect the appearance of electron neutrinos described above, but it also impacts the upward-going muon rate. Atmospheric neutrino sensitivity to the mixing parameters Δm^2_{32} and θ_{23} is driven primarily by the oscillation of $\nu_\mu \rightarrow \nu_{\tau,e}$ seen in this sample, and these matter effects provide additional power to discriminate the octant of θ_{23}.

At energies below a few GeV atmospheric neutrinos carry additional sensitivity to δ_{CP}, again through an appearance channel. However, with no precise knowledge of the incoming neutrino direction and poor correlation between the outgoing lepton from an interaction and its parent neutrino direction at these energies, the atmospheric neutrino sensitivity is weaker than that from the beam sample.
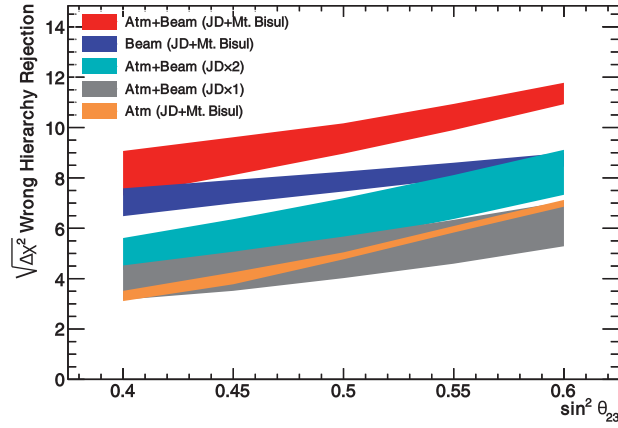
Fig. 36. Sensitivity to the normal mass hierarchy for components of a combined measurement of beam and atmospheric neutrinos for a ten-year exposure. Here, JD refers to a single Hyper-K detector in Kamioka, Japan, and JD×2 refers to two such detectors operating simultaneously. The horizontal axis shows the assumed value of $\sin^2 \theta_{23}$, and the width of the bands shows the variation in sensitivity with δ_{CP}.

5.1. *Combination of beam and atmospheric neutrino data*

As described above, atmospheric neutrinos provide complementary sensitivity to the same oscillation physics as the beam neutrino samples. Though there are common systematic error effects between the two samples from the cross section and detector modeling, the disparate energy regimes and flux systematics allow for a nearly independent study of oscillations. More importantly, the atmospheric neutrino data are accumulated continuously and independently of the beam, such that the combination of the two samples provides improved sensitivity on shorter time scales. In this section we present a combined analysis of beam and atmospheric neutrino data assuming a Hyper-K detector in Japan (JD) and at the Mt. Bisul site (off-axis angle 1.3°) and compare with sensitivities assuming two detectors in Japan (JD×2). The treatment of the atmospheric neutrino samples and their systematic errors follows that of Super-Kamiokande, with no assumed improvements (cf. the discussion in Ref. [44]).

Figure 36 shows the sensitivity to the mass hierarchy for the combined analysis using the same test statistic as Eq. 5. After ten years of running, the expected ability to reject the wrong mass hierarchy is better than $\sqrt{\Delta\chi^2} = 7$. Atmospheric neutrinos by themselves provide sensitivity better than $\sqrt{\Delta\chi^2} > 3$ for all currently allowed values of $\sin^2 \theta_{23}$ and have comparable sensitivity to the beam measurement at the Korean detector for the largest values of this parameter. Though the combined JD and Mt. Bisul beam measurement has better sensitivity than the atmospheric neutrino measurement alone, when all of the samples are combined the sensitivity improves further. The power of this improvement manifests as an earlier realization of the hierarchy, as shown in the left panel of Fig. 37. Within two years of operation the sensitivity will exceed $\sqrt{\Delta\chi^2} > 4$.

Sensitivity to $\sin^2 \theta_{23}$ for the combined analysis and its components appears in Fig. 38. Here, the test statistic reflects the ability to reject the incorrect octant as

$$T_{\text{octant}} = \sqrt{\Delta\chi^2_{\text{WO}} - \Delta\chi^2_{\text{CO}}}, \tag{7}$$

where $\Delta\chi^2_{\text{WO}}$ and $\Delta\chi^2_{\text{CO}}$ represent the minimum likelihood value taken over the wrong and correct octants, respectively. The minimum for the first (second) octant is taken over values of the likelihood in the range of parameters $\sin^2 \theta_{23} < 0.5$ (> 0.5). If θ_{23} differs from maximal mixing by 2° or more,
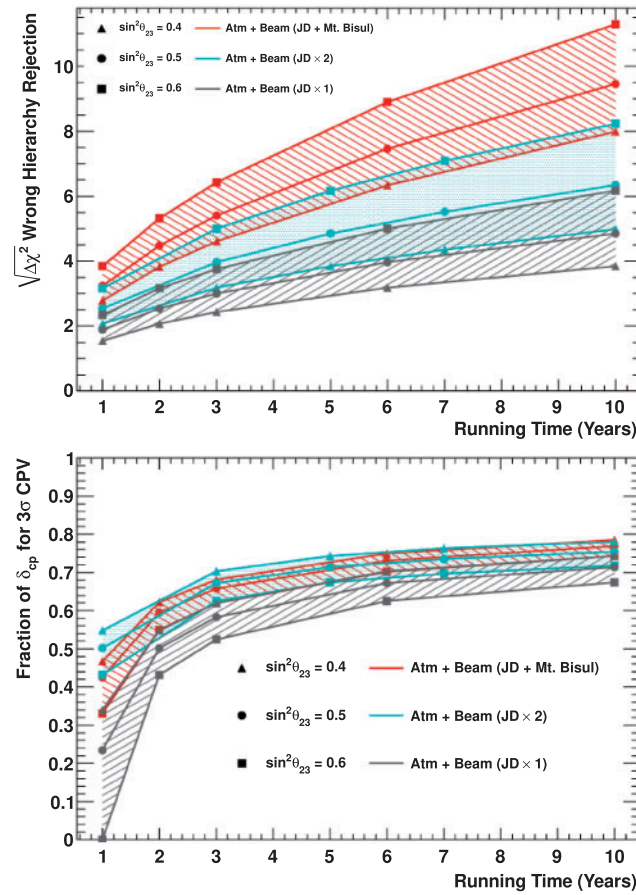
Fig. 37. Sensitivity as a function of year to the mass hierarchy (left) and the fraction of δ_{CP} phase space for which CP violation ($\sin\delta_{CP} \neq 0$) can be determined at $3\,\sigma$ or better. Red lines show a combined beam and atmospheric neutrino measurement with one Hyper-K detector in Kamioka, Japan (JD) and one at the Mt. Bisul site in Korea. Cyan lines show the same analysis assuming two detectors in Kamioka (JD×2), and gray lines assume only one detector in Kamioka (JD×1). Different symbols show the assumed value of $\sin^2\theta_{23}$.

the octant will be resolved at better that three units of the test statistic. As shown in the figure, this marks a considerable improvement over the beam-only measurement.

While atmospheric neutrinos themselves have less sensitivity to δ_{CP} than the beam measurement, they provide additional constraints on extreme values of the parameter as shown in Fig. 39. Typically, the atmospheric neutrino constraint covers about 50% of the parameter space, such that one of the CP-conserving points $\sin\delta_{CP} = 0$ is weakly allowed regardless of the parameter's true value. For this reason, the constraint on CP violation shown in Fig. 40 is weaker than that from the beam and provides only a slight improvement in sensitivity. The test statistic used in this figure is the same as in Eq. 6. However, as with the other oscillation measurements the power of the combined beam and atmospheric measurement comes in the early realization of this sensitivity (cf. the right panel of Fig. 37).

6. Additional benefits

In addition to the long-baseline program with multiple baselines, there are potential benefits to the Hyper-K physics program by placing a second detector in Korea. There are two main benefits that arise from the second Hyper-K detector in Korea. First, the candidate sites for a Korean detector are
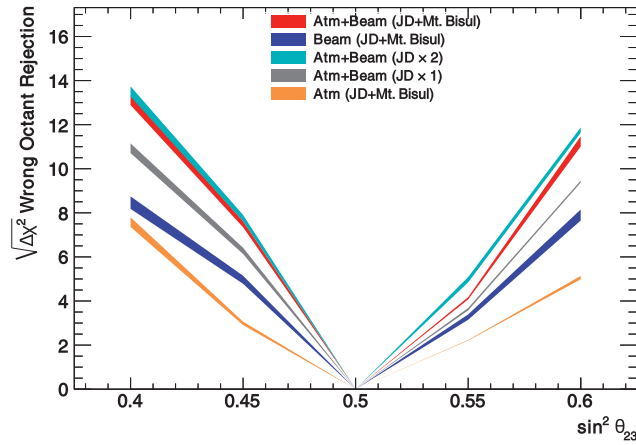
Fig. 38. Sensitivity to the θ_{23} octant (right) assuming the normal mass hierarchy for components of a combined measurement of beam and atmospheric neutrinos for a ten-year exposure. The plot has been produced in the same manner as Fig. 36.
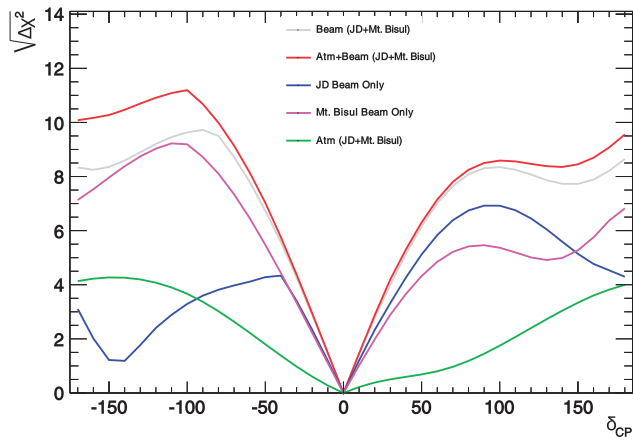

Fig. 39. Sensitivity to $\delta_{CP} = 0$ for components of a combined measurement of beam and atmospheric neutrinos for a ten-year exposure. Here, JD refers to a single Hyper-K detector in Kamioka, Japan.
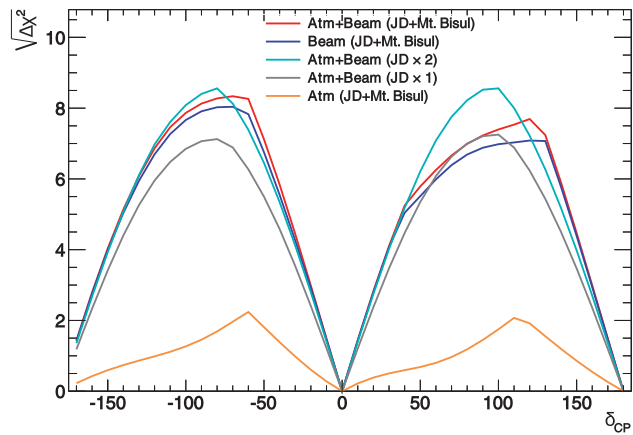

Fig. 40. Sensitivity to CP violation ($\sin \delta_{CP} \neq 0$) for components of a combined measurement of beam and atmospheric neutrinos for a ten-year exposure. Here, JD refers to a single Hyper-K detector in Kamioka, Japan, and JD×2 refers to two such detectors operating simultaneously. The horizontal axis shows the assumed true value of δ_{CP}.

Table 8. Position and altitude for simulated locations.

	Mt. Bisul	Mt. Bohyun
Latitude	35°43′00″ N	36°09′47″ N
Longitude	128°31′28″ E	128°58′26″ E
Altitude (820 m overburden)	264 m	304 m
Altitude (1000 m overburden)	84 m	124 m

deeper than their Japanese counterparts, providing a greater overburden to reduce the flux of cosmic ray muons. This translates into a reduced rate of spallation-induced isotopes that are backgrounds to lower-energy physics, such as solar and supernova neutrino studies. Second, the large geographical separation between the Japanese and Korean detectors provides two horizons for studying supernova neutrinos. For a supernova burst, the likelihood of observing neutrinos below at least one of the horizons is increased, allowing broader study of the Earth-matter effect on these events. This section explores the potential benefits to the Hyper-K physics program beyond studies of PMNS mixing provided by a Korean detector.

6.1. Solar and supernova neutrino physics

Observations of low-energy neutrinos, such as those from the Sun ($E < 10$ MeV) or the diffuse supernovae flux ($E < 30$ MeV), are complicated by backgrounds from natural sources. Among these cosmic-ray-muon-induced spallation products, which decay to produce photons or electrons of similar energies, are a background that can be readily mitigated with the larger overburden afforded by a detector in Korea. The rate of such spallation backgrounds at each of the candidate sites has been estimated with simulations based on their local tomographies.

6.1.1. Estimate of muon spallation background

The muon flux and average energy at each site are estimated using the muon simulation code `MUSIC` [47,48], a three-dimensional Monte Carlo (MC) tool dedicated to muon transportation in matter. Elevation data for the areas around Mt. Bisul and Mt. Bohyun have been extracted from the "ALOS World 3D-30m" database published by JAXA [50] for input to the simulation. The latitude, longitude, and altitude of each of the simulated locations are summarized in Table 8. For both Mt. Bisul and Mt. Bohyun, simulations assuming 820 m and 1000 m overburdens have been performed using muons that are generated at the surface following the parameterization in Ref. [49]. The rock type is assumed to be the same as the Super-K site (Inishi rock) with a density of 2.70 g cm^{-3}. Table 9 summarizes the calculated muon flux (Φ) and average energy ($\overline{E}_\mu$) at the Mt. Bisul, Mt. Bohyun, Hyper-K (Tochibora), and Super-K sites. Based on the uncertainty of the exact rock composition, the uncertainty of the muon flux is assumed to be $\pm 20\%$.

Figure 41 shows the calculated muon energy spectra for Hyper-K (Tochibora, 650 m overburden), Mt. Bisul (1000 m overburden), Mt. Bisul (1000 m overburden), and Super-K. The corresponding fluxes as a function of zenith and azimuthal angles are shown in Fig. 42. Note that the absolute flux and shape of the Super-K data are reproduced well by the simulation. Further, with 1000 m overburdens, the Korean sites are expected to have similar muon fluxes and energies as those observed at Super-K. For the shallower 820 m overburden the flux is expected to increase by more than a factor of two according to Table 9). Using this information the muon flux ratio at Mt. Bisul relative to Super-K,

Table 9. Calculated muon flux (Φ) and average energy ($\overline{E}_\mu$) at Mt. Bisul, Mt. Bohyun, Hyper-K, and Super-K.

Detector site (overburden)	Φ (10^{-7} cm^{-2} s^{-1})	$\overline{E}_\mu$ (GeV)
Mt. Bisul (820 m)	3.81	233
Mt. Bohyun (820 m)	3.57	234
Mt. Bisul (1000 m)	1.59	256
Mt. Bohyun (1000 m)	1.50	257
Hyper-K (Tochibora, 650 m)	7.55	203
Super-K	1.54	258
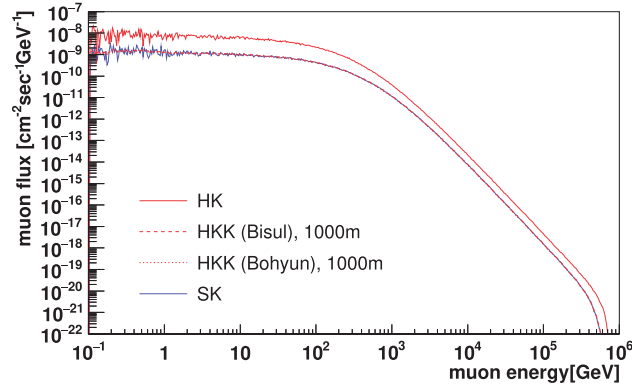
Fig. 41. Calculated muon energy spectra for Hyper-K (Tochibora), Mt. Bisul (1000 m overburden), Mt. Bohyun (1000 m overburden), and Super-K, based on the MUSIC simulation.

$\Phi(\text{HKK}_{\text{Bisul}})/\Phi(\text{Super-K})$, is estimated to be 1.03 ± 0.21 (2.47 ± 0.49) assuming a 1000 m (820 m) overburden.

Based on these calculated muon fluxes, isotope production rates due to muon spallation have been calculated using FLUKA [45,46] version 2011.2b. The isotope yield per muon track length, Y, depends on the muon energy, which increases with larger overburdens. As a result, the isotope yield per muon becomes larger for deeper experimental sites. For the 1000 m overburden case the average muon energy is similar to that of Super-K, and thus the ratio of their isotope yields per muon are similar: 1.03 ± 0.21. The same ratio calculated for the Hyper-K (Tochibora) site is about 0.8 [25]. Interpolating from these two, the isotope yield per muon for the 820 m overburden is estimated to be 0.9, and similarly the isotope production rate for 820 m overburdens becomes about 2.22 ± 0.44 larger than that at Super-K. In contrast, the Tochibora site is estimated to be about 4 ± 1 times larger. For similar overburdens the isotope yield is not expected to differ largely between the two Korean sites. Accordingly, the yield is expected to be between two to four times smaller than at the Tochibora site in Japan.

6.1.2. Potential benefits

Lower spallation backgrounds at a Korean detector will result in improved sensitivity to solar neutrinos. The day–night asymmetry in the rate of solar neutrinos due to Mikheyev–Smirnov–Wolfenstein (MSW) matter effects in the Earth [51–53] is expected to be larger for the higher-energy region of the ^{8}B neutrino spectrum, where spallation is the dominant background source. Neutrinos from the Hep reaction chain fall in a similar energy region, and as they are produced in a different region of the
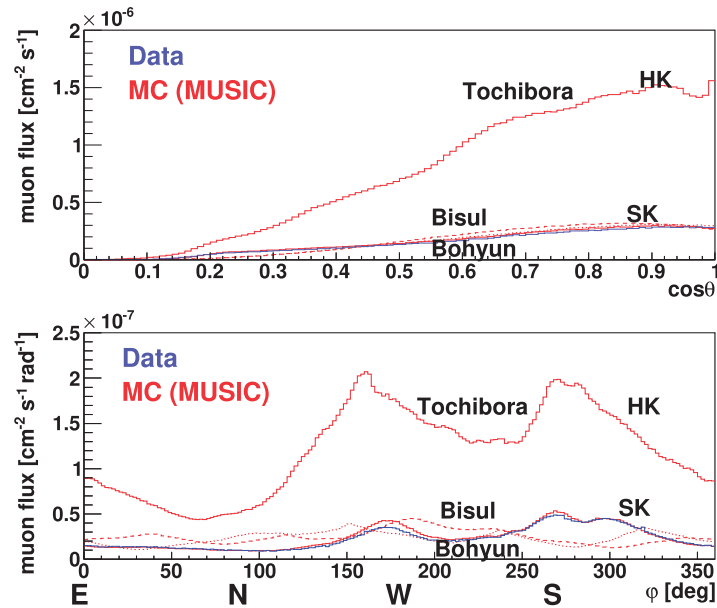
Fig. 42. Muon flux as a function of the cosine of the zenith angle, $\cos\theta$, (upper) and azimuth angle ϕ (lower) for Hyper-K (Tochibora), Mt. Bisul (1000 m overburden), Mt. Bohyun (1000 m overburden), and Super-K. Here, zero degrees represents the eastern direction. The blue lines show the data from Super-K, while the red lines show the MC prediction from the MUSIC simulation of the Tochibora (solid), Mt. Bisul (dashed), and Mt. Bohyun (dotted) sites.

solar interior they can potentially provide new information on solar physics. With lower spallation backgrounds, the short-time variability of the temperature in the solar core could be monitored more precisely with these neutrinos. Further, lower backgrounds in the higher-energy sample can improve resolution of the solar neutrino spectrum shape, whose lower-energy region is a sensitive probe of matter effects, both standard and otherwise, in the Sun.

Spallation backgrounds can be rejected based on their correlation with preceding muons. For solar neutrino analysis, the effect of spallation reduction is estimated, keeping the signal efficiency to 80%. The remaining spallation fraction is estimated, based on a study using Super-K data, to be 1.2% (2.3%) for the 1000 m (820 m) overburden. This can be compared to 3.9% estimated for the Hyper-K Tochibora site.

The search for the diffuse flux of neutrinos produced by all supernova explosions since the beginning of the universe, the supernova relic neutrino (SRN) flux, similarly benefits from larger overburdens. For the SRN analysis, because the signal flux is expected to be only a few tens/cm^2/the small signal flux, a more stringent event selection requiring a negligible spallation background contribution is used. In this case, the signal efficiency is 79% (56%) for neutrinos reconstructed with energies between 17.5 and 20 MeV and 90% (75%) between 20 and 26 MeV for the 1000 m (820 m) overburden site. These can be compared to 29% and 54%, respectively, for Hyper-K at Tochibora. Above 26 MeV the spallation background decreases exponentially, but the signal is overwhelmed by backgrounds from atmospheric neutrinos. In this way, reduced spallation backgrounds will enhance the SRN detection capability, particularly below 20 MeV. After ten years of operation, the number of events and the significance of non-zero observation of SRN are 100 (90) events and $5.2\,\sigma$ ($4.8\,\sigma$), respectively, for the 1000 m (820 m) overburden site in Korea assuming the SRN flux of Ref. [55]. Hyper-K at Tochibora is expected to observe 70 events with a corresponding significance of $4.2\,\sigma$.

It is worth noting that the ability to observe neutrons via high-photon-yield photosensors or gadolinium doping will provide other physics opportunities for a Korean detector. Among these, the observation of neutrinos from nuclear reactors in Korea via their inverse beta decay reactions becomes possible. Similarly, such neutron tagging is expected to provide highly efficient suppression of atmospheric neutrino backgrounds to searches for proton decay. Detailed studies of the expected sensitivity of such measurements is planned for a future document.

6.2.   *Neutrino geophysics*

The inner Earth's chemical composition is one of the most important properties of our planet. While the matter density is well known through seismic measurements [67], the chemical composition is much less understood [54]. Neutrino oscillations depend on the electron density of the medium traversed by the neutrinos [51,52], and hence the electron density distribution of the Earth can be reconstructed from the neutrino energy spectrum. Accordingly, the chemical composition of the Earth can be constrained for a given mass density distribution [56,57]. Hyper-K is expected to be the first experiment that could experimentally confirm that the Earth's core is composed of iron, ruling out lead or water scenarios at the 3σ level [25]. The measurement relies on precisely measuring atmospheric muon neutrino disappearance and electron neutrino appearance in the energy range between 1 and 8 GeV as a function of the zenith angle. This measurement is limited by the reduced neutrino flux at these energies, such that a detector in Korea will double the statistics available.

If a supernova occurs such that the neutrinos travel through the Earth before reaching the detector, i.e. below the detector's local horizon, they will be subject to energy-dependent matter effects. This would manifest as a distortion of the energy spectrum of neutrinos or antineutrinos depending on the mass hierarchy, which can be observed under favorable conditions [58,60]. Having two geographically separated detector locations increases the likelihood of the Earth shadowing the neutrino flux reaching one of the detectors. In addition, comparing the energy spectra in two detectors that observe different shadowing scenarios (see Fig. 43) may make it easier to disentangle matter effects from supernova burst neutrino properties.

6.3.   *Dark matter searches*

Hyper-K can search for physics beyond the standard model in the form of self-annihilating dark matter captured in the Sun or the Earth, or from the Galactic dark matter halo. Super-K has demonstrated this physics potential through the world's best constraints on spin-dependent scattering of dark matter with matter [61]. Hyper-K can improve upon Super-K's results and is expected to provide the best indirect dark matter search sensitivities for masses below 100 GeV. As the background to a neutrino signal from dark matter annihilation in the Sun comes from atmospheric neutrinos, a benefit from a second site could come from reduced systematic uncertainties associated with atmospheric neutrino fluxes. A neutrino signal originating from the decays of the dark matter annihilation products in the Sun is also accompanied by a high-multiplicity stopped meson decay low-energy neutrino signal from hadronic showers of the annihilation products in the center of the Sun [62–64]. The expected signal consists of neutrinos of a few tens of MeV from muon decays at rest in the Sun, as well as neutrino line signals at 29.8 MeV and 235.5 MeV from two-body charged pion and kaon decays at rest. The possible addition of gadolinium in water [65] would reduce (invisible muon) backgrounds significantly for this signal, which can very efficiently be detected through the inverse beta decay reaction [62].
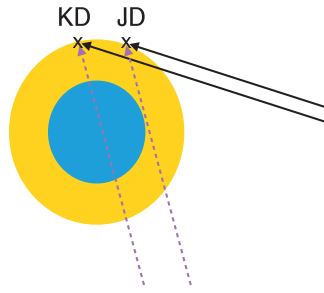
Fig. 43. Due to the distance between the Korean (KD) and Japanese (JD) detector locations, both detectors could observe a supernova neutrino burst with different Earth shadowing. In scenario 1 (solid black arrows), one detector would observe an unshadowed flux, while neutrinos detected in the other detector would travel through the Earth for up to 1800 km. In scenario 2 (dashed purple arrows), one detector would be shadowed by the Earth's mantle (yellow) only, while the other detector would be shadowed by the mantle and the outer core (blue). While the resulting difference in path length is small, up to 4400 km of the path of neutrinos reaching one detector would go through the outer core instead of the mantle. Since the matter density of the outer core is much larger than that of the mantle, the matter effect along these two paths would be markedly different. Using an online tool for calculating Earth crossing probabilities for different detector locations, we find that the combined probability of these two scenarios is 6.4% [59]. (The difference between Mt. Bohyun and Mt. Bisul is $< 0.1\%$.)

6.4.   Modifications to neutrino propagation

T2HKK can also be a powerful probe of non-standard physics affecting neutrino propagation, in particular effects observable as modifications to the standard PMNS survival or appearance probability. In Ref. [66], various types of non-standard physics scenarios for a beam experiment with detectors in both Korea and Japan were considered, including models of quantum decoherence, violations of Lorentz symmetry with and without charge, parity, and time invariance, and non-standard neutrino interactions with matter. In most cases, configurations with a large detector in both countries have significantly improved sensitivity to such types of new physics, relative to having the equivalent detector mass in just one of them. Not only do the two baselines provide a more complete measure of the neutrino spectrum, and hence distortions arising from new physics, but they also provide distance L/E ranges to constrain scenarios with non-oscillating (or with oscillating admixtures) L/E effects. See Tables I and II and Fig. 6 of Ref. [66] for more details. As one example, the expected sensitivity to an enhanced matter effect caused by non-standard interactions is presented in the next section.

6.5.   Potential for improvement with a $CC1\pi$ event selection

For Korean detector sites with a smaller off-axis angle, a harder (anti)neutrino spectrum is present. The (anti)neutrinos above 1 GeV probe the first oscillation maximum and the region between the first and second oscillation maxima. These (anti)neutrinos are important for determining the mass ordering, and measuring δ_{CP} if the phase is near $\pi/2$ and $3\pi/2$. The quasi-elastic scattering cross section is nearly constant above 1 GeV, while the rate of other processes that include pion production increases. Higher statistics in the >1 GeV region may be achieved by including candidate events with evidence of pion production in addition to the charged lepton. These additional candidate events may include events where a Michel electron from a pion decay chain is detected, or where a pion is directly detected by the reconstruction of a second visible ring in the detector. The inclusion of these pion production events will be the subject of future studies.

7.   Sensitivity of T2HKK to non-standard interactions

In this section we discuss the capability of the T2HKK experiment to put constraints on non-standard interactions (NSI) in neutrino propagation. We present our results for only the 1.5° off-axis and normal mass ordering. However, at the end we will comment on the results for other off-axis configurations of T2HKK and also for inverted ordering. The discussions in this section are based on Refs. [68,69].

7.1.   Non-standard interactions

In the presence of flavor-changing neutral currents the standard neutrino–matter interaction potential is modified, allowing for neutrino flavor change via neutral current interactions with matter [51,70–73]. The presence of such NSI effects can be studied in neutrino oscillation experiments, especially in long-baseline and atmospheric neutrino oscillation experiments where the neutrinos experience the Earth matter effect of long distances. Theoretically this kind of interaction can arise from the following four-fermion interaction:

$$\mathcal{L}_{\mathrm{eff}}^{\mathrm{NSI}} = -2\sqrt{2}\,\varepsilon_{\alpha\beta}^{ff'P} G_{\mathrm{F}} \left(\overline{\nu}_{\alpha L}\gamma_\mu \nu_{\beta L}\right) \left(\overline{f}_P \gamma^\mu f_P'\right), \tag{8}$$

where f_P and f_P' are fermions with chirality P, $\varepsilon_{\alpha\beta}^{ff'P}$ is a dimensionless constant, and G_{F} is the Fermi coupling constant. If these kinds of interactions exist in nature, then the MSW matter potential looks like:

$$\mathcal{A} \equiv \sqrt{2} G_{\mathrm{F}} N_e \begin{pmatrix} 1 + \varepsilon_{ee} & \varepsilon_{e\mu} & \varepsilon_{e\tau} \\ \varepsilon_{\mu e} & \varepsilon_{\mu\mu} & \varepsilon_{\mu\tau} \\ \varepsilon_{\tau e} & \varepsilon_{\tau\mu} & \varepsilon_{\tau\tau} \end{pmatrix}, \tag{9}$$

where $\varepsilon_{\alpha\beta}$ is defined by

$$\varepsilon_{\alpha\beta} \equiv \sum_{f=e,u,d} \frac{N_f}{N_e} \varepsilon_{\alpha\beta}^f, \tag{10}$$

with N_f ($f = e, u, d$) representing the number density of the fermions f. Here we define the NSI parameters as $\varepsilon_{\alpha\beta}^f = \varepsilon_{\alpha\beta}^{ffL} + \varepsilon_{\alpha\beta}^{ffR}$. The present 90% confidence level bounds on the NSI parameters coming from non-oscillation experiments are compiled in Refs. [76,77]. Using the formula

$$\varepsilon_{\alpha\beta} \lesssim \left\{ \sum_P \left[\left(\varepsilon_{\alpha\beta}^{eP}\right)^2 + \left(3\varepsilon_{\alpha\beta}^{uP}\right)^2 + \left(3\varepsilon_{\alpha\beta}^{dP}\right)^2 \right] \right\}^{1/2} \tag{11}$$

for neutral Earth-like matter with an equal number of neutrons and protons, Ref. [77] gives the following bounds on $\varepsilon_{\alpha\beta}$:

$$\begin{pmatrix} |\varepsilon_{ee}| < 4 \times 10^0 & |\varepsilon_{e\mu}| < 3 \times 10^{-1} & |\varepsilon_{e\tau}| < 3 \times 10^0 \\ & |\varepsilon_{\mu\mu}| < 7 \times 10^{-2} & |\varepsilon_{\mu\tau}| < 3 \times 10^{-1} \\ & & |\varepsilon_{\tau\tau}| < 2 \times 10^1 \end{pmatrix}. \tag{12}$$

The bounds on the NSI parameters $\varepsilon_{\alpha\beta}^f$ from oscillation experiments are given in Table 2 of Ref. [73] for $f = d$. From Eq. (12) it is clear that the bounds on ε_{ee}, $\varepsilon_{e\tau}$, and $\varepsilon_{\tau\tau}$ are at least one order of

Table 10. Systematic uncertainties assumed for the sample normalization (in percentages) for a single detector at the T2HKK and T2HK experimental configurations. The "T2HK" column corresponds to the systematic errors of the Kamioka detector (for T2HK the numbers are same for both the detectors), and the "T2HKK at 1.5°" column corresponds to the systematic error of the Korean detector. (For the T2HKK setup, the systematic error of the Kamioka detector is given by the "T2HK" column and the systematic error of the Korean detector is given by the "T2HKK at 1.5°" column).

Setup	T2HKK at 1.5°	T2HK
ν_e events	3.84	4.71
$\bar{\nu}_e$ events	4.11	4.47
ν_μ events	3.83	4.13
$\bar{\nu}_\mu$ events	3.81	4.15

magnitude weaker compared to the other NSI parameters. Thus, in order to keep the number of parameter combinations to a manageable level, this section uses the following ansatz:

$$\mathcal{A} = \sqrt{2} G_\mathrm{F} N_e \begin{pmatrix} 1 + \varepsilon_{ee} & 0 & \varepsilon_{e\tau} \\ 0 & 0 & 0 \\ \varepsilon_{e\tau}^* & 0 & \varepsilon_{\tau\tau} \end{pmatrix}. \tag{13}$$

Therefore, the NSI parameters of interests are ε_{ee}, $|\varepsilon_{e\tau}|$, $\varepsilon_{\tau\tau}$, and $\arg(\varepsilon_{e\tau}) = \phi_{31}$. In the limit $\Delta m_{21}^2 \to 0$ it is known [88–90] that the oscillation probability depends only on $\delta_{\mathrm{CP}} + \phi_{31}$, and we therefore expect similar dependence on ϕ_{31} as on δ_{CP}.

For the simulation of the T2HKK experiment, we have taken the experimental configuration from the detector setup in Sect. 2 and consider the highest energy (or least off-axis) configuration at 1.5°. We also compare our results with the T2HK setup, that is the JD×2 configuration. We assume a 3 : 1 ratio of antineutrino and neutrino running. For this analysis we incorporate systematics by the method of pulls and considered four pull variables including a signal normalization, a background normalization, a signal tilt, and a background tilt. Namely, the numbers of signal (S_j) and background (B_j) events are scaled as $S_j \to S_j[1 + \sigma_\mathrm{s}\xi_\mathrm{s} + \sigma_\mathrm{s}^\mathrm{tilt}\xi_\mathrm{s}^\mathrm{tilt}(E_j - E_\mathrm{min})/(E_\mathrm{max} - E_\mathrm{min})]$, $B_j \to B_j[1 + \sigma_\mathrm{b}\xi_\mathrm{b} + \sigma_\mathrm{b}^\mathrm{tilt}\xi_\mathrm{b}^\mathrm{tilt}(E_j - E_\mathrm{min})/(E_\mathrm{max} - E_\mathrm{min})]$, where $\sigma_\mathrm{s}, \sigma_\mathrm{b}, \sigma_\mathrm{s}^\mathrm{tilt}, \sigma_\mathrm{b}^\mathrm{tilt}$ ($\xi_\mathrm{s}, \xi_\mathrm{b}, \xi_\mathrm{s}^\mathrm{tilt}, \xi_\mathrm{b}^\mathrm{tilt}$) are the systematic errors (the pull variables) for a signal normalization, a background normalization, a signal tilt, and a background tilt, respectively; E_max and E_min are the maximum and minimum energies; and E_j is the energy of the jth bin. Hence, we understand that the normalization errors affect the scaling of the events, whereas the tilt errors affect their energy dependence. Throughout the analysis we have fixed the tilt error to 10%. A total normalization error for each detector location and event sample is used as listed in Table 10; the magnitudes of these errors are taken from Table 6. The same normalization error for signal and background are used, and all systematics are considered to be uncorrelated. Unlike the PMNS-driven oscillation sensitivities described in the previous sections, this analysis has been performed using the GLoBES [82,83] package with the MonteCUBES [84] NSI probability engine.

7.2. Constraining NSI parameters

First we discuss the ability of the T2HKK experiment to constrain the magnitudes of the NSI parameters ε_{ee}, $|\varepsilon_{e\tau}|$, and $\varepsilon_{\tau\tau}$. For this purpose we assume that the values of these parameters are zero and present our results as limits in the ε_{ee}–$|\varepsilon_{e\tau}|$ plane. The assumed true value of ϕ_{31} is zero and it has been marginalized over in the presentation of the results. The PMNS oscillation parameters
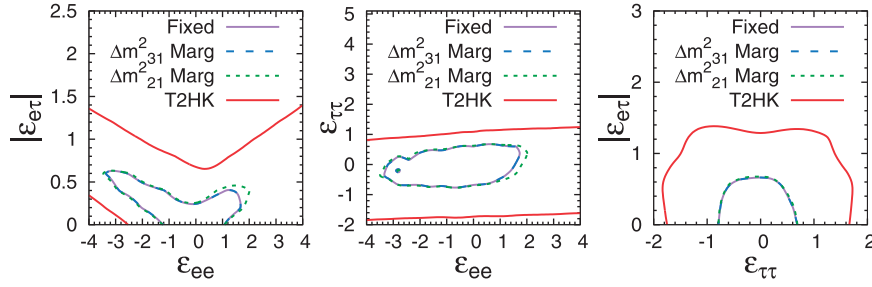
Fig. 44. Ability of T2HKK to constrain the magnitude of the NSI parameters at 3σ for $\theta_{23} = 45°$ and $\delta_{CP} = 270°$ with the normal hierarchy. The red lines show the comparison for two detectors at the Kamioka site. The other lines show the effect of the uncertainty on the value of the mass splittings.

δ_{CP} and θ_{23} are marginalized over as well, whereas θ_{13}, θ_{12}, Δm_{21}^2, and Δm_{31}^2 have been kept fixed close to their globally preferred values [85–87] and are not varied unless otherwise mentioned.

In Fig. 44, we present the sensitivities with PMNS parameters held at their currently favored values: $\theta_{23} = 45°$ and $\delta_{CP} = 270°$. In the left, middle, and right panels the 3σ allowed region is given in the ε_{ee}–$|\varepsilon_{e\tau}|$, ε_{ee}–$\varepsilon_{\tau\tau}$, and $\varepsilon_{\tau\tau}$–$|\varepsilon_{e\tau}|$ planes, respectively. In each panel the NSI parameters that are not plotted have been marginalized over. Here, and elsewhere unless otherwise noted, the marginalization is made over the ranges -4 to $+4$ for ε_{ee}, 0 to 2 for $|\varepsilon_{e\tau}|$, and -1 to $+1$ for $\varepsilon_{\tau\tau}$. We have additionally checked that the χ^2 minima do indeed always appear within these chosen ranges of $\varepsilon_{\alpha\beta}$. The purple curve in each panel shows the allowed region when Δm_{21}^2 and Δm_{31}^2 are kept fixed in the test spectrum. The green dotted curves and blue dashed curves show the effect of marginalizing over these parameters. It is clear that the uncertainty in Δm_{31}^2 has no effect on the sensitivity, whereas the allowed region increases slightly when we marginalize over Δm_{21}^2.

To demonstrate how the sensitivity is improved by using a Korean detector, we also show the equivalent result for the JD×2 configuration in Fig. 44 (red curves). It can be seen that this configuration provides significantly weaker constraints. Indeed, in this case it is necessary to extend the marginalization range of $\varepsilon_{\tau\tau}$ out to ±4 since there is still a significant posterior probability outside the original region. From all three panels, we note that the sensitivity of the KD+JD (T2HKK) configuration is far better than the equivalent JD×2 configuration, let alone the baseline single-tank design. This is essentially the same effect as seen in the standard PMNS oscillation model, with the longer baselines and the higher energies both enhancing the matter effect.

Next, we study the capability of T2HKK to constrain the NSI parameters assuming different values of θ_{23} and δ_{CP}. Figure 45 shows how changes in these parameters within their current allowed regions affect T2HKK's constraints in the ε_{ee}–$|\varepsilon_{e\tau}|$ plane. The left, middle, and right panels show $\delta_{CP} = 90°$, $180°$, and $270°$, respectively. In each panel, the purple, blue, and green curves correspond to $\theta_{23} = 41°$, $45°$, and $49°$, respectively. From the figure we note that the sensitivity is best for $\delta_{CP} = 180°$ and worst for $\delta_{CP} = 270°$. The sensitivity for $\theta_{23} = 45°$ is the weakest in comparison to the other two tested values.

Even at $O(1000)$ km, there will be over a thousand events in the data samples at a Korean detector, such that the statistical error on the event rate is a few percent. As a result, systematic errors are expected to play an important role, so we next study their impact on T2HKK's ability to constrain the magnitude of the NSI parameters. To do this, we again examine the same ε_{ee}–$|\varepsilon_{e\tau}|$ space as in Fig. 45, but for four different values of the systematic errors. In these plots a systematic error of $N\%$ implies a normalization error of $N\%$ applied to both signal and background events, both electron and
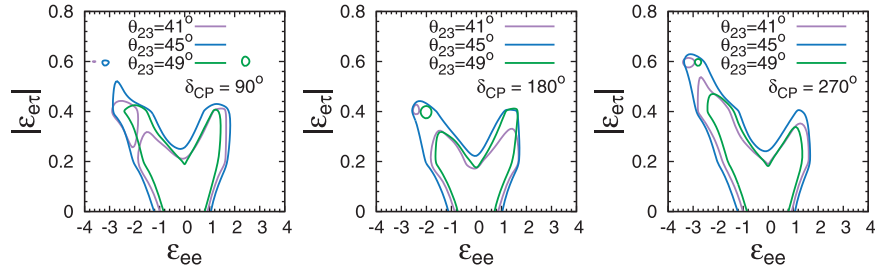
Fig. 45. Ability of T2HKK to constrain the magnitude of the NSI parameters at 3σ for different true values of θ_{23} and δ_{CP} with the normal hierarchy.
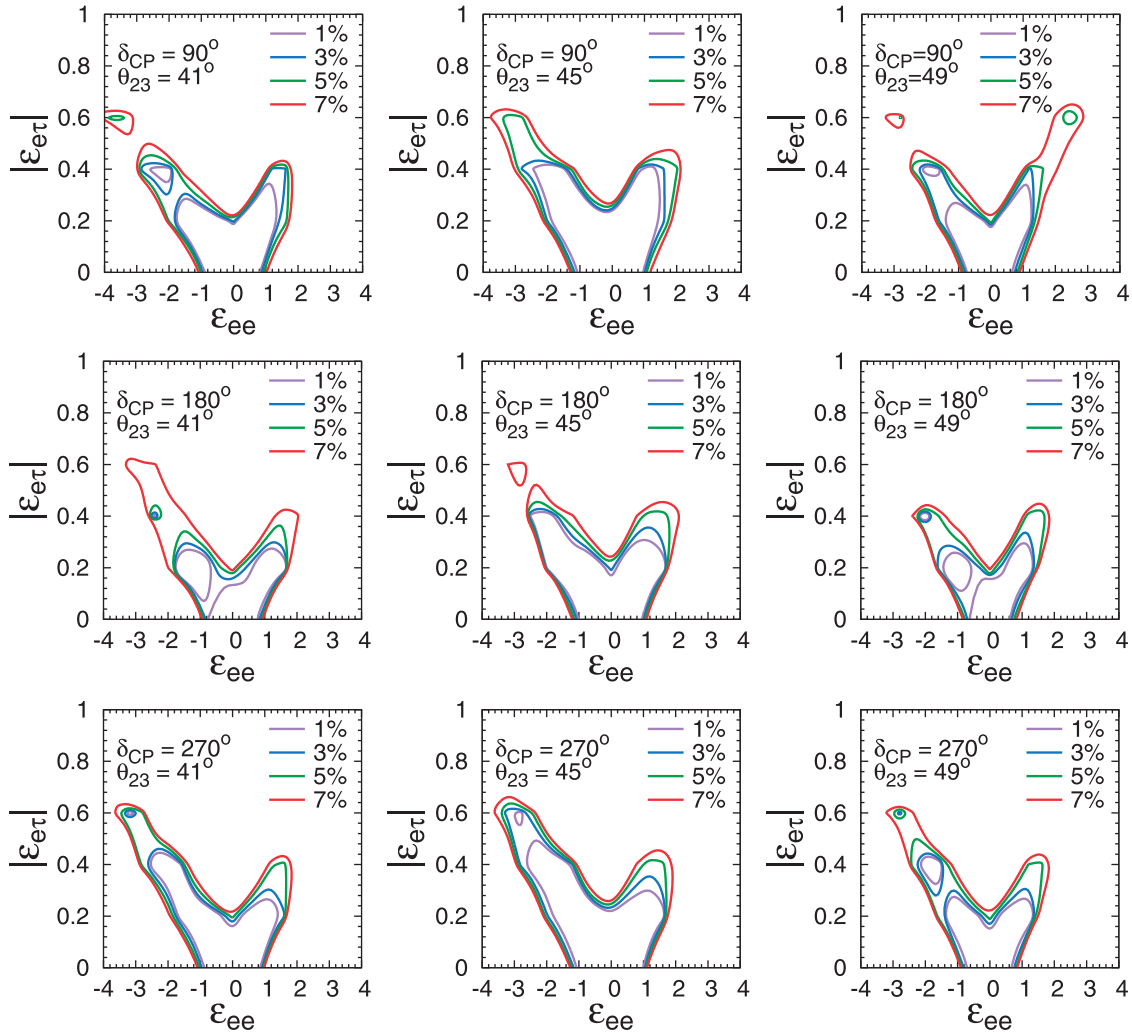

Fig. 46. Ability of T2HKK to constrain the magnitude of the NSI parameters at 3σ for different values of the PMNS parameters with the normal hierarchy. The columns correspond to (from left to right) $\theta_{23} = 41°$, $45°$, and $49°$, and the rows are for (from top to bottom) $\delta_{CP} = 90°$, $180°$, and $270°$.

muon events, and both neutrinos and antineutrinos. The dependence can be seen in Fig. 46. Here, rows correspond to (from left to right) $\delta_{CP} = 90°$, $180°$, and $270°$. In each row the first, second, and third panels correspond to $\theta_{23} = 41°$, $45°$, and $49°$, respectively. In all cases, we can see that the limits on the axes (i.e. with one of the two parameters held at zero) are not substantially affected
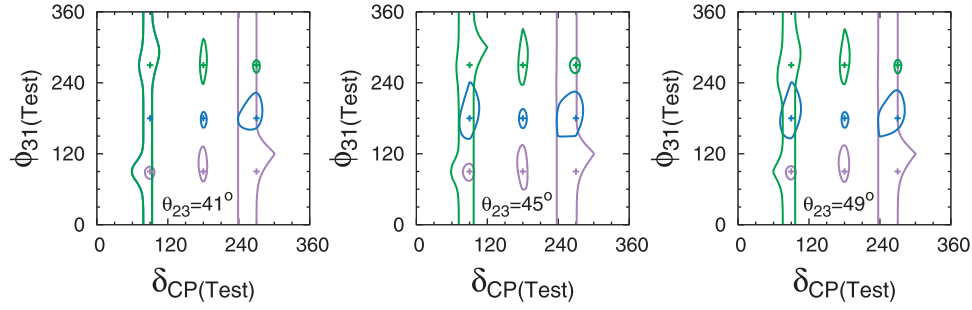
Fig. 47. Ability of T2HKK to constrain the two CP phases at 90% confidence level assuming the normal hierarchy. The left, middle, and right panels correspond to $\theta_{23} = 41°$, $45°$, and $49°$, respectively, and the purple, blue, and green contours correspond to ϕ_{31} (true) $= 90°$, $180°$, and $270°$, respectively. The $+$ signs in each panel correspond to the true values of (δ_{CP}, ϕ_{31}).

by systematic uncertainties, but that the ability to rule out correlated changes in $|\varepsilon_{ee}|$ and $|\varepsilon_{e\tau}|$ are impacted by such a systematic uncertainty.

7.3.   Constraining the CP phases

Assuming the NSI parameters are non-zero, there is an additional source of CP violation from the argument of the off-diagonal $\varepsilon_{e\tau}$ parameter. This would produce observable effects similar to those from the δ_{CP} parameter of the PMNS formalism, so we next consider constraints in the δ_{CP}–ϕ_{31} plane, with varying true values of θ_{23}, δ_{CP}, and ϕ_{31}. Here, the values of ε_{ee}, $|\varepsilon_{e\tau}|$, and $\varepsilon_{\tau\tau}$ are assumed to be 0.8, 0.2, and 0.0, respectively. These three parameters, as well as θ_{23}, are marginalized over in the analysis. As before, other PMNS parameters are held at their global best-fit values. Figure 47 shows the resulting allowed regions for T2HKK, with the left, middle, and right panels showing results assuming $\theta_{23} = 41°$, $45°$, and $49°$, respectively. The purple, blue, and green contours show the ϕ_{31} (true) $= 90°$, $180°$, and $270°$ cases, respectively. From the panels it is clear that the best sensitivity comes when $\phi_{31} \simeq \delta_{CP}$, and that the overall sensitivity is not significantly affected by the true value of θ_{23}. On the other hand, for the (δ_{CP}, ϕ_{31}) combinations $(90°, 270°)$ and $(270°, 90°)$ ϕ_{31} is entirely unconstrained.

Sensitivity to constraining the CP phases benefits explicitly from having two detectors at different baselines in the T2HKK configuration. To illustrate this, Fig. 48 shows the contribution of each detector separately assuming $\theta_{23} = 45°$, $\delta_{CP} = 270°$, and $\phi_{31} = 180°$. The purple contour shows the contribution from the detector in Kamioka, the blue contour shows that from the Korean detector, and the red is their combined sensitivity. For comparison, the orange contour illustrates the expectation for two detectors in Kamioka. That there is not much difference between the contours with one and two detectors in Kamioka illustrates that the increase in sensitivity seen in the T2HKK configuration comes mainly from its second baseline.

It is important to recognize that the combination of a detector in Kamioka, which has higher statistics, with a detector in Korea, which has a larger baseline, resolves parameter degeneracies and therefore allows for simultaneous measurement of the NSI and CP parameters. This is illustrated by the green contour, which shows the capability a single detector in Kamioka assuming that the NSI parameters ε_{ee}, $|\varepsilon_{e\tau}|$, and $\varepsilon_{\tau\tau}$ are non-zero, but known. First, this demonstrates that a single measurement at the first PMNS oscillation maximum is seriously limited by degeneracies in the extended model that cannot be untangled. Secondly, although the green contour shows a precise measurement, there is a degeneracy between the two available CP parameters shown by the correlated
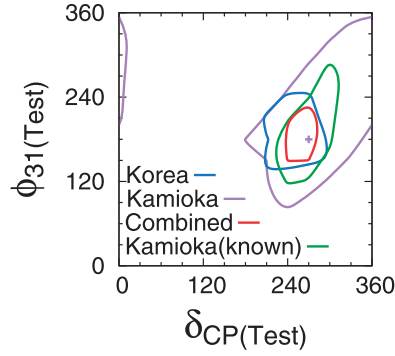
Fig. 48. Contribution of different detectors to constraints on the CP phases at 90% confidence level assuming $\theta_{23} = 45°$, $\phi_{31} = 180°$, and $\delta_{CP} = 270°$ with the normal hierarchy. See the text for a full explanation.

nature of the allowed region. The degeneracy is lifted by measurements at the Korean detector. Indeed, the T2HKK configuration, shown in red, yields a more precise measurement even though the NSI parameters are considered unknown in the analysis. In this sense an analysis that allows for the possibility of deviations from the PMNS model can benefit much more from the extra information obtained using multiple baselines than it would from simply improving the available statistics for a single-baseline measurement.

As before, we study how our systematic uncertainties affect our ability to constrain the CP phases. Figure 49 shows the expected sensitivity under four systematic error assumptions, 1%, 3%, 5%, and 7%, using the same procedure as in Fig. 46. The first, second, and third rows are for $\phi_{31} = 90°$, $180°$, and $270°$, respectively. In each row, the left, middle, and right panels correspond to $\theta_{23} = 41°$, $45°$, and $49°$, respectively. For $\delta_{CP} = 270°$ and $\phi_{31} = 90°$, it is possible to have a small closed contour in ϕ_{31} for small systematic error assumptions. As the systematic error is increased from 1%, it becomes impossible to constrain ϕ_{31} regardless of the assumed value of θ_{23}. For $\phi_{31} = 180°$ the sensitivity improves gradually when the systematic uncertainty is reduced from 7% to 1% for all values of θ_{23}. For $\phi_{31} = 270°$, the sensitivities evolve in a similar way to the $\phi_{31} = 90°$ case, but do not reach a closed ϕ_{31} interval for $\delta_{CP} = 90°$.

The above analyses have assumed a normal ordering and the 1.5° off-axis detector configuration at T2HKK, but here we discuss briefly the cases of an inverted ordering and other off-axis angles. For an inverted ordering we find that the sensitivity to constrain the NSI parameters and the phases is slightly weaker compared to the normal ordering. For example, T2HKK can constrain ε_{ee} in the region $-3.2 < \varepsilon_{ee} < 1.4$ assuming the normal ordering, whereas the bound for inverted ordering is $-3.2 < \varepsilon_{ee} < 1.8$ assuming $\theta_{23} = 45°$, $\delta_{CP} = 270°$.

Among the three T2HKK off-axis detector configurations, 1.5°, 2.0°, and 2.5°, we find that the best sensitivity is obtained for 1.5°. Indeed, the bounds on ε_{ee} are $-3.6 < \varepsilon_{ee} < 1.8$ and $-4 < \varepsilon_{ee} < 2.2$ for 2.5° and 2.0° off-axis configurations of T2HKK, respectively, assuming the normal ordering, $\theta_{23} = 45°$, and $\delta_{CP} = 270°$. This is in line with naive expectation, since the NSI parameters induce larger oscillation effects at higher energies. The 1.5° configuration further benefits from having the largest number of events among the configurations and a comparatively broad flux to provide more access to the neutrino energy spectrum [68]. For similar reasons, the sensitivity of the 2.0° configuration is better than that of the 2.5° one.

From the discussions above, we can conclude that the proposed long-baseline T2HKK experiment would have good sensitivity to NSI in neutrino propagation and can be expected to place stronger
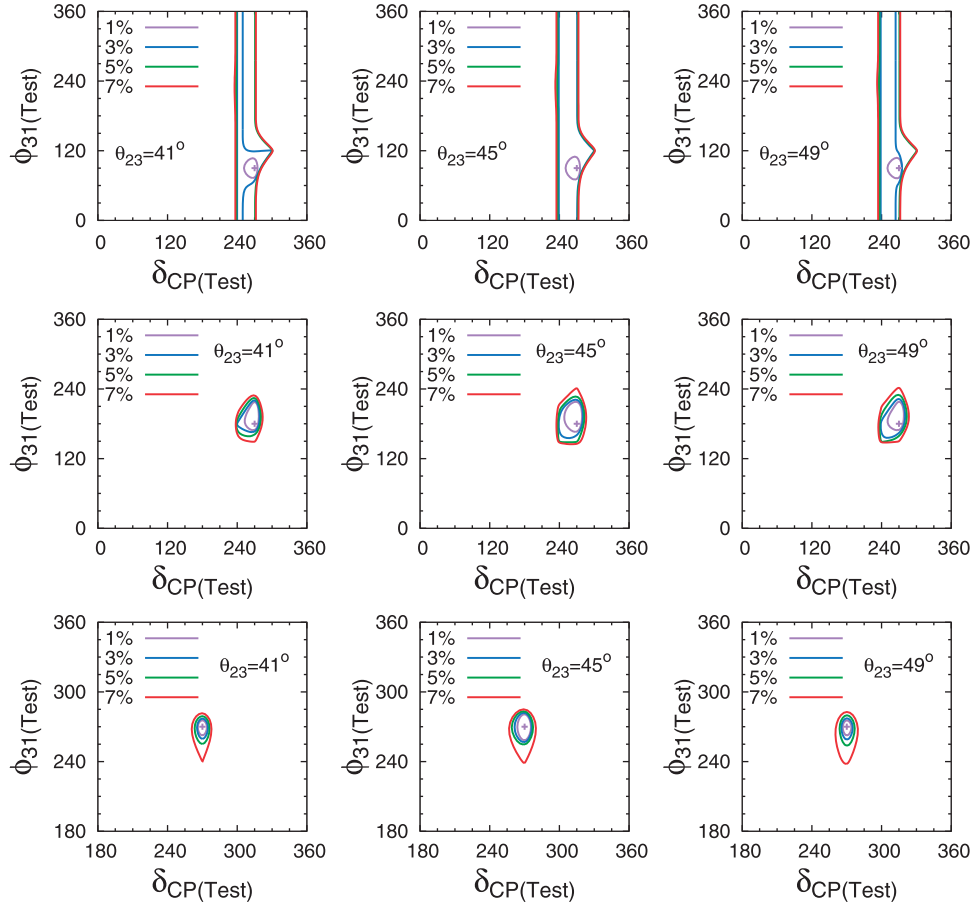
Fig. 49. Ability of T2HKK to constrain the CP phases at 90% confidence level with systematic uncertainties of 1%, 3%, 5%, and 7%, shown by the purple, blue, green, and red curves, respectively. The columns correspond to $\theta_{23} = 41°$, 45°, and 49°. The rows are for $\phi_{31} = 90°$, 180°, and 270°. The + signs correspond to the true values of (δ_{CP}, ϕ_{31}). The normal hierarchy is assumed.

bounds than with the two HK detectors in Kamioka (the T2HK setup). In addition, the sensitivity to constrain the NSI amplitudes does not vary much with the assumed values of θ_{23} and δ_{CP}. The achievable precision on the phases does depend upon the true values of δ_{CP} and ϕ_{31}, and for particular combinations it can be much harder to determine the value of ϕ_{31}. However, the unique two-detector configuration of the T2HKK setup is more powerful than a single detector, and would be extremely helpful in measuring the neutrino CP phases if NSI exist in nature. In studying the effect of systematics, it is found that T2HKK is not insensitive to the magnitude of the systematic errors, but that while the overall measurement is improved by reduction of the systematic uncertainties, the systematics are most important when considering sensitivity to specific degenerate parameter combinations.

8.   Summary and conclusion

The design of the future Hyper-K experiment is to build two identical water-Cherenkov detectors of 260 kt per detector in stages: one at the Tochibora mine in Japan at a 2.5° off-axis angle and a baseline of 295 km from the J-PARC neutrino target, and the other perhaps in Korea. The second detector improves physics sensitivities, from beam neutrino physics to astroparticle physics, due to increased statistics. In particular, searches for proton decay provide a strong motivation for having two detectors. According to our sensitivity studies, by locating the second detector in Korea the physics sensitivities

are further improved due to the longer baseline ($\sim$1100 km) and the possibility of a larger overburden (1000 m) at the candidate sites. These sites cover a range of possible off-axis angles to the J-PARC beam, between 1° and 3°, depending on the site. With the longer baseline in Korea both the first and second oscillation maxima of the PMNS neutrino appearance probability are reachable. The longer baseline of the Korean sites enhances the CP-violating component of the oscillation probability, and resolves parameter combinations between the neutrino mass ordering and CP-violating phase that would be nearly degenerate when measuring only at the Japanese site with beam neutrinos. This is a unique opportunity afforded by the J-PARC neutrino beam. By adding atmospheric neutrinos, neutrino mass ordering determination is improved at both the Japan and Korean sites.

Assuming a relatively simplistic systematic uncertainty model based on T2K systematic error evaluations [39], sensitivity studies of the long-baseline program of T2HKK have been performed. These have compared different configurations of Hyper-K detector(s) in Japan and Korea for ten years of operation without staging and with 1.3 MW beam power for $\nu : \overline{\nu} = 1 : 3$. In general, the configuration with one detector in Japan and one in Korea at a smaller off-axis angle gives better sensitivity overall than two detectors in Japan. Based on this systematic error model, the benefits of a smaller off-axis angle seem to outweigh the extra uncertainties of using a higher beam energy. Overall, the Mt. Bisul site, with its 1088 km baseline, 1.3° off-axis angle, and 1084 m overburden, is the leading candidate location. Although the smaller off-axis angle introduces more π^0-production high-energy tail of the beam flux, the large value of θ_{13} makes this less important and the sensitivity to the CP phase is improved over the nominal Hyper-K design.

According to our sensitivity studies, the precision at which δ_{CP} can be measured improves from 22° (17°) for one detector (two detectors) in Japan, to at worst 14° for T2HKK assuming CP is maximally violated. The coverage fraction for establishing CP violation at $5\,\sigma$ improves from 47% (55%) to 60% if the mass ordering is known from independent measurements, and the improvement is much larger otherwise. The significance of a CP violation discovery is improved relative to having two detectors in Japan for $0 < \sin \delta_{CP} < 1$, though the improvement is marginal for values near 1 unless the mass ordering is still unknown at the time of the experiment. The significance at which the wrong mass ordering can be rejected for any value of δ_{CP} improves from $0.7\,\sigma$ ($1\,\sigma$) for the nominal Hyper-K design (two detectors in Japan) to $5.5\,\sigma$ at T2HKK using beam neutrino data alone. In contrast, relative to two detectors in Japan the sensitivity of T2HKK to the atmospheric mixing parameters is weaker due to the reduction in statistics over the longer baseline to Korea. The addition of atmospheric neutrinos improves the sensitivity overall, but is particularly useful for resolving the octant degeneracy.

T2HKK is also expected to have improved sensitivity to non-standard interactions in neutrino propagation. Indeed, according to our study the sensitivity to the NSI parameters, ϵ_{ee}, $\epsilon_{e\tau}$, and $\epsilon_{\tau\tau}$, is enhanced relative to Hyper-K configurations with only Japanese detectors, especially with the 1.5° off-axis site in Korea, due to the larger matter effects along its baseline.

With $\sim$1000 m overburdens, sensitivities to solar-neutrino and SRN physics are further enhanced at the Korean candidate sites compared to the Tochibora mine ($\sim$650 m overburden) due to a much lower muon flux and spallation background rate. Using a simple MC, the expected significance of a supernova relic neutrino search for ten years of operation is $5.2\,\sigma$ ($4.2\,\sigma$) with the Korean (Tochibora) sites.

In this paper we have demonstrated that the second detector in Korea provides enhanced sensitivity to Hyper-K's physics goals in broad physics programs.

Appendix.   Construction details for bi-probability plots

Most common constructions of bi-probability plots show a single pair of ellipses, for a given value of L and E and assumed oscillation parameters. This common practice is an over-simplification; although long-baseline oscillation experiments have negligible variation in the baseline, the neutrino energy typically ranges over at least a factor of two, and often more. For the first generation of ν_e-appearance experiments (that is to say, T2K and NOνA) that use a narrow-band beam peaking near the energy of the first oscillation maximum this is tolerable, since the first period of the oscillation runs from half the peak energy up to infinity. When considering these experiments there are two obvious "fixes": Either use one energy (typically the peak energy) as a stand-in for the entire spectrum of measured neutrinos, or integrate the probability over the expected (without oscillations) spectrum of events.

The latter method corresponds to an (idealized) rate-only measurement, and provided backgrounds are accounted for could be compared to the data in the form of number of neutrino and antineutrino events. But this is not often done, as integrating over the full spectrum (much of which has lower appearance probabilities) significantly reduces the sensitivity of the experiment. On the other hand, the former method does not have any problems with averaging, but the number of events for which the ellipses are a good approximation is a small fraction of the total. This makes it difficult to summarize the overall sensitivity of an experiment in a correct way.

For experiments where the event spectrum is broad compared to the oscillation (wide-band beams such as DUNE, and second-maxima experiments such as T2HKK), approximating things as a single pair of measurements is even less suitable. Part of the point of such experiments is that they can make measurements at independent energies and see the different δ_{CP} and mass ordering dependencies.

Plotting a continuum of ellipses is not practical, so to give a sense of how the energy affects the measurement of δ_{CP} some representative energies have to be chosen. The plots in Sect. 3.1.1 use three representative energies. This is still far from a complete summary of a real measurement, but it provides a better illustration of what the configuration can measure.

A.1.   Choice of representative energies

The energies used to summarize the interaction spectrum are chosen based on a procedure that takes into account the interaction rates of neutrinos but is independent of the oscillation probabilities. First, the interaction rate (i.e. flux $\times$ cross section) spectrum is calculated, in the absence of oscillations. For water-Cherenkov detectors such as Hyper-K and the proposed ESSnuSB the quasi-elastic spectrum is

used as their analyses use primarily quasi-elastic events. For other experiments that can use any kind of neutrino interaction, the inclusive CC cross section is more appropriate. Note that for ESSnuSB and any experiment that uses inclusive CC cross sections, the cross section grows roughly linearly with energy, so the interaction rate spectrum is often substantially harder than the corresponding flux.

From the interaction-rate spectrum, the blue ellipses represent the peak energy, E_P, the value which is typically taken as representative in simpler bi-probability plots. This divides the interaction spectrum in two, with a fraction f of events below (and a fraction $1 - f$ above) E_P. The green ellipses are drawn for the median energy of the lower f events, while the red are the median energy of the upper $1 - f$ events. In this way, 50% of the events lie between the energies represented by the green and red ellipses. This method of identifying a peak and central 50% of the spectrum is also used in Fig. 3, where a band covering the central 75% of events is defined in a similar way.

The fact that measurements with a detector at Kamioka can be reasonably approximated as being "rate-only" is evident in Fig. 9. Although the ellipses differ in size and eccentricity, the separation between the two mass orderings, and the dependence of the appearance probabilities on the value of δ, is similar for all three energies. The most important difference is only apparent on closer inspection: the $\delta = 0$ CP-conserving point generates either higher or lower appearance probabilities than the $\delta = \pi$ point. Which point provides the larger appearance probability depends on both the mass ordering and whether the neutrino energy is above or below the energy of the oscillation maximum. For other configurations (Figs. 10, 11, and 12) the location, size, and orientation of the ellipses is dramatically different.

A.2. Statistical sensitivity

The gray ellipses give an indication of the statistical power of the measurement made in each configuration. They use a simplified background model to estimate a fractional error $\sqrt{(S + B)}/S$ from the number of signal (S) and background (B) events expected in the central 25% of the events around the peak energy (i.e. 1/4 of the total unoscillated flux). The number of signal events is scaled according to the appearance probabilities at the center of the ellipse, while the background is assumed to be independent. Five ellipses are drawn, to show how the sensitivity will vary with the actual oscillation probability. This is a somewhat arbitrary measure—not least because the shape and location of the bi-probability ellipse can vary over even this narrower energy range—but it enables some comparison between the statistical power of measurements with different baselines and fluxes, and using different run lengths.

References

[1] K. Abe *et al.* (Hyper-Kamiokande Working Group), arXiv:1412.4673 (2015); K. Abe *et al.* [Hyper-Kamiokande Proto-Collaboration], PTEP **2015**, 053C02 (2015) [arXiv:1502.05199 [hep-ex]].
[2] Y. Fukuda *et al.* (Super-Kamiokande Collaboration), Phys. Rev. Lett. **81**, 1562 (1998).
[3] S. B. Kim, in Proceedings of the KOSEF-JSPS Joint Seminar on New Developments in Neutrino Physics, Seoul, Korea, 2000 (Korea Institute for Advanced Study, Seoul, 2000), p. 182.
[4] K. Hagiwara, Nucl. Phys. Proc. Suppl. **137**, 84 (2004) [hep-ph/0410229].
[5] M. Ishitsuka, T. Kajita, H. Minakata and H. Nunokawa, Phys. Rev. D **72**, 033003 (2005).
[6] T. Kajita, H. Minakata, S. Nakayama, and H. Nunokawa, Phys. Rev. D **75**, 013006 (2007).
[7] F. Dufour, T. Kajita, E. Kearns and K. Okumura, Phys. Rev. D **81**, 093001 (2010).
[8] K. Hagiwara, N. Okamura, K. Senda, Phys. Lett. B **637**, 266 (2006), Erratum: Phys. Lett. B **641**, 491 (2006).

[9] K. Hagiwara, N. Okamura, K. Senda, Phys. Rev. D **76**, 093002 (2007).

[10] T. Kajita and H. Minakata, "Highlights in the T2KK Workshops in 2005 and 2006", http://www-rccn.icrr.u-tokyo.ac.jp/workshop/T2KK07/proceedings/t2kk-pdf/003-014.pdf; T. Kajita, S.B. Kim, A. Rubbia, arXiv:0808.0650 (2008); 3rd International Workshop on a Far Detector in Korea for the J-PARC Neutrino Beam 30 Sep - 1 Oct 2007. Tokyo, Japan PROCEEDINGS. Edited by T. Kajita, S.B. Kim. Tokyo, Univ. Acad. Pr., 2008. 173p.

[11] K. Abe et al. [T2K Collaboration], Phys. Rev. Lett. **107**, 041801 (2011) [arXiv:1106.2822 [hep-ex]].

[12] Y. Abe et al. (Double Chooz Collaboration), Phys. Rev. Lett. **108**, 131801 (2012).

[13] F. P. An et al. (Daya Bay Collaboration), Phys. Rev. Lett. **108**, 171803 (2012).

[14] J. K. Ahn et al. (RENO Collaboration), Phys. Rev. Lett. **108**, 191802 (2012).

[15] K. Abe et al. [T2K Collaboration], Phys. Rev. Lett. **112**, 061802 (2014). [arXiv:1311.4750 [hep-ex]]

[16] M. Hartz (for the T2K Collaboration) "T2K neutrino oscillation results with data up to 2017 summer", *KEK Colloquium* available at https://www.t2k.org/docs/talk/282

[17] Y. Abe et al. (Double Chooz Collaboration), JHEP **1410**, 86 (2014).

[18] F. P. An et al. (Daya Bay Collaboration), Phys. Rev. Lett. **115**, 111802 (2015).

[19] J. Choi et al. (RENO Collaboration), Phys. Rev. Lett. **116**, 211802 (2016).

[20] E. Baussan et al. (ESSnuSB Collaboration), Nucl. Phys. B **885**, 127 (2014). [arXiv:1309.7022 [hep-ex]].

[21] E. Wildner et al. (ESSnuSB Collaboration), Adv. High Energy Phys. **2016**, 8640493 (2016) [arXiv:1510.00493 [physics.ins-det]].

[22] A. Timmons, Adv. High Energy Phys. **2016**, 7064960 (2016).

[23] K. K. Maan, H. Duyang, S. R. Mishra and V. Bhatnagar, arXiv:1511.00287 [hep-ex].

[24] Dune Collaboration, "Conceptual Design Report", http://lss.fnal.gov/archive/design/fermilab-design-2016-02.pdf

[25] K. Abe et al. [Hyper-Kamiokande Proto-Collaboration], "Hyper-Kamiokande Design Report" KEK-PREPRINT-2016-21, ICRR-REPORT-701-2016-1.

[26] K. Abe et al. [T2K Collaboration], Nucl. Instrum. Meth. A **659**, 106 (2011) [arXiv:1106.1238 [physics.ins-det]].

[27] A. Blondel and M. Zito, "Near Detectors based on gas TPCs for neutrino long baseline experiments" CERN-SPSC-2017-002 ; SPSC-EOI-015 ; http://cds.cern.ch/record/2240188.

[28] S. Bhadra et al. [nuPRISM Collaboration], arXiv:1412.3086 [physics.ins-det]; C. Andreopoulos et al., arXiv:1606.08114 [physics.ins-det].

[29] I. Girardia, S. T. Petcov, and A. V. Titov Nucl. Phys. B **894**, 733 (2015).

[30] H. Minakata and H. Nunokawa, JHEP **0110** (2001) 001 [hep-ph/0108085].

[31] H. Nunokawa, S. J. Parke and J. W. F. Valle, Prog. Part. Nucl. Phys. **60**, 338 (2008) [arXiv:0710.0554 [hep-ph]].

[32] P. B. Denton, H. Minakata and S. J. Parke, J. High Energ. Phys. (2016) 2016: 51, https://doi.org/10.1007/JHEP06(2016)051, [arXiv:1604.08167 [hep-ph]].

[33] P. B. Denton, H. Minakata and S. J. Parke, [arXiv:1801.06514 [hep-ph]].

[34] A. Ioannisian and S. Pokorski, [arXiv:1801.10488 [hep-ph]].

[35] Y. Hayato, Acta Phys. Polon. B **40**, 2477 (2009).

[36] http://www.phy.duke.edu/~raw22/public/Prob3++/

[37] K. Hagiwara, N. Okamura and K.I. Senda, JHEP **1109**, 082 (2011) [arXiv:1107.5857 [hep-ph]].

[38] C. Patrignani et al. [Particle Data Group], Chin. Phys. C **40**, no. 10, 100001 (2016).

[39] K. Abe et al. [T2K Collaboration], Phys. Rev. D **91**, 072010 (2015) [arXiv:1502.01550 [hep-ex]].

[40] K. Abe et al. [T2K Collaboration], arXiv:1707.01048 [hep-ex].

[41] J. Nieves, I. Ruiz Simo and M. J. Vicente Vacas, Phys. Rev. C **83**, 045501 (2011) [arXiv:1102.2777 [hep-ph]].

[42] R. Gran, J. Nieves, F. Sanchez and M. J. Vicente Vacas, Phys. Rev. D **88**, no. 11, 113007 (2013) [arXiv:1307.8105 [hep-ph]].

[43] M. Day and K. S. McFarland, Phys. Rev. D **86**, 053003 (2012) [arXiv:1206.6745 [hep-ph]].

[44] A. Himmel [Super-Kamiokande Collaboration], AIP Conf. Proc. **1604**, 345 (2014) [arXiv:1310.6677 [hep-ex]].

[45] T. T. Böhlen et al., Nucl. Data Sheets **120**, 211 (2014).

[46] A. Ferrari, P. R. Sala, A. Fasso and J. Ranft, CERN-2005-010, SLAC-R-773, INFN-TC-05-11.

[47]　P. Antonioli, C. Ghetti, E. V. Korolkova, V. A. Kudryavtsev and G. Sartorelli, Astropart. Phys. **7**, 357 (1997) [hep-ph/9705408].
[48]　V. A. Kudryavtsev, Comput. Phys. Commun. **180**, 339 (2009) [arXiv:0810.4635 [physics.comp-ph]].
[49]　A. Tang, G. Horton-Smith, V. A. Kudryavtsev and A. Tonazzo, Phys. Rev. D **74**, 053007 (2006) [hep-ph/0604078].
[50]　ALOS World 3D: http://www.eorc.jaxa.jp/ALOS/en/aw3d/index_e.htm
[51]　L. Wolfenstein, Phys. Rev. D **17**, 2369 (1978).
[52]　S. P. Mikheev and A. Y. Smirnov, Sov. J. Nucl. Phys. **42**, 913 (1985); Yad. Fiz. **42**, 1441 (1985).
[53]　S. P. Mikheev and A. Y. Smirnov, Nuovo Cim. C **9**, 17 (1986).
[54]　W. McDonough and S. Sun, Chem. Geol. **120**, 223 (1995).
[55]　S. Ando, K. Sato and T. Totani, Astropart. Phys. **18**, 307 (2003) [astro-ph/0202450].
[56]　C. Rott, A. Taketa and D. Bose, Scientific Reports 5, Article number: 15225 (2015) [arXiv:1502.04930 [physics.geo-ph]].
[57]　W. Winter, Nucl. Phys. B **908**, 250 (2016) [arXiv:1511.05154 [hep-ph]].
[58]　A. S. Dighe and A. Y. Smirnov, Phys. Rev. D **62**, 033007 (2000) [hep-ph/9907423].
[59]　A. Mirizzi, G. G. Raffelt and P. D. Serpico, JCAP **0605**, 012 (2006) [astro-ph/0604300].
[60]　E. Borriello, S. Chakraborty, A. Mirizzi, P. D. Serpico and I. Tamborra, Phys. Rev. D **86**, 083004 (2012) [arXiv:1207.5049 [hep-ph]].
[61]　K. Choi et al. [Super-Kamiokande Collaboration], Phys. Rev. Lett. **114**, 141301 (2015) [arXiv:1503.04858 [hep-ex]].
[62]　C. Rott, J. Siegal-Gaskins and J. F. Beacom, Phys. Rev. D **88**, 055005 (2013) [arXiv:1208.0827 [astro-ph.HE]].
[63]　N. Bernal, J. Martin-Albo and S. Palomares-Ruiz, JCAP **1308**, 011 (2013) [arXiv:1208.0834 [hep-ph]].
[64]　C. Rott, S. In, J. Kumar and D. Yaylali, JCAP **1511**, 039 (2015) [arXiv:1510.00170 [hep-ph]].
[65]　J. F. Beacom and M. R. Vagins, Phys. Rev. Lett. **93**, 171101 (2004) [hep-ph/0309300].
[66]　N. C. Ribeiro, H. Nunokawa, T. Kajita, S. Nakayama, P. Ko and H. Minakata, Phys. Rev. D **77**, 073007 (2008) [arXiv:0712.4314 [hep-ph]].
[67]　A. M. Dziewonski and D. L. Anderson, Phys. Earth Planet. Interiors **25**, 297 (1981).
[68]　S. Fukasawa, M. Ghosh and O. Yasuda, Phys. Rev. D **95**, no. 5, 055005 (2017) [arXiv:1611.06141 [hep-ph]].
[69]　M. Ghosh and O. Yasuda, Phys. Rev. D **96**, no. 1, 013001 (2017) [arXiv:1702.06482 [hep-ph]].
[70]　M. M. Guzzo, A. Masiero and S. T. Petcov, Phys. Lett. B **260**, 154 (1991).
[71]　E. Roulet, Phys. Rev. D **44**, R935 (1991).
[72]　T. Ohlsson, Rept. Prog. Phys. **76**, 044201 (2013) [arXiv:1209.2710 [hep-ph]].
[73]　O. G. Miranda and H. Nunokawa, New J. Phys. **17**, no. 9, 095002 (2015) [arXiv:1505.06254 [hep-ph]].
[74]　J. Salvado, O. Mena, S. Palomares-Ruiz and N. Rius, JHEP **1701**, 141 (2017) [arXiv:1609.03450 [hep-ph]].
[75]　M. G. Aartsen et al. [IceCube Collaboration], arXiv:1709.07079 [hep-ex].
[76]　S. Davidson, C. Pena-Garay, N. Rius and A. Santamaria, JHEP **0303**, 011 (2003) [hep-ph/0302093].
[77]　C. Biggio, M. Blennow and E. Fernandez-Martinez, JHEP **0908**, 090 (2009) [arXiv:0907.0097 [hep-ph]].
[78]　A. Friedland, C. Lunardini and M. Maltoni, Phys. Rev. D **70**, 111301 (2004) [hep-ph/0408264].
[79]　A. Friedland and C. Lunardini, Phys. Rev. D **72**, 053009 (2005) [hep-ph/0506143].
[80]　S. Fukasawa and O. Yasuda, Adv. High Energy Phys. **2015**, 820941 (2015) [arXiv:1503.08056 [hep-ph]].
[81]　K. Abe et al. [Hyper-Kamiokande proto- Collaboration], arXiv:1611.06118 [hep-ex].
[82]　P. Huber, M. Lindner and W. Winter, Comput. Phys. Commun. **167**, 195 (2005) [hep-ph/0407333].
[83]　P. Huber, J. Kopp, M. Lindner, M. Rolinec and W. Winter, Comput. Phys. Commun. **177**, 432 (2007) [hep-ph/0701187].
[84]　M. Blennow and E. Fernandez-Martinez, Comput. Phys. Commun. **181**, 227 (2010) [arXiv:0903.3985 [hep-ph]].
[85]　D. V. Forero, M. Tortola and J. W. F. Valle, Phys. Rev. D **90**, no. 9, 093006 (2014) [arXiv:1405.7540 [hep-ph]].
[86]　I. Esteban, M. C. Gonzalez-Garcia, M. Maltoni, I. Martinez-Soler and T. Schwetz, JHEP **1701**, 087 (2017) [arXiv:1611.01514 [hep-ph]].

[87] F. Capozzi, G. L. Fogli, E. Lisi, A. Marrone, D. Montanino and A. Palazzo, Phys. Rev. D **89**, 093018 (2014) [arXiv:1312.2878 [hep-ph]].
[88] T. Ota, J. Sato and N. a. Yamashita, Phys. Rev. D **65**, 093015 (2002) [hep-ph/0112329].
[89] J. Kopp, M. Lindner and T. Ota, Phys. Rev. D **76**, 013001 (2007) [hep-ph/0702269 [HEP-PH]].
[90] O. Yasuda, arXiv:0704.1531 [hep-ph].